CZECH TECHNICAL
UNIVERSITY IN PRAGUE

FACULTY OF ELECTRICAL
ENGINEERING

TEXTILE-BASED STRUCTURES IN ELECTRONIC AND COMMUNICATION ENGINEERING

HABILITATION THESIS

LUKÁŠ VOJTĚCH
DECEMBER 2017

Motto:

Telecommunications engineering is an engineering discipline that brings together all electrical engineering disciplines including computer engineering with systems engineering to enhance telecommunication systems.

Burnham, Gerald O.; et al. (October 2001). "The First Telecommunications Engineering Program in the United States" (PDF). Journal of Engineering Education. American Society for Engineering Education. 90 (4): 653–657. Retrieved September 22, 2012.

Abstract

EN - This thesis deals with the search for and formulation of a theoretical approach to modelling the electrical conductivity of woven textiles and the experimental validation of the approach by measurements performed on woven textile samples. Drawing on these results, the thesis goes on to determine the electromagnetic shielding efficiency of nonhomogeneous 3D structures using modified approaches and succeeds in finding a new analytical description of the electromagnetic shielding efficiency of electrically conductive woven textiles. The proposed description applies to selected types of conductive woven textiles. The author's basic observation is that woven textiles are structurally similar to metallic grids. The proposed modelling method was analytically validated for the different conductivity values of the yarns used; experimental validation was performed as well. This led to the identification of a set of usable conductivity values for yarns, for which these approaches are valid within a given error. In view of the new approaches to modelling the electrical conductivity and electromagnetic shielding efficiency of conductive textiles presented in this thesis, it is believed that these findings will significantly contribute to the body of interdisciplinary research and applications at the boundary between electrical engineering and materials science. The thesis describes the experiments performed and the development of applications of the proposed materials that span various branches of electronics and communications technologies and demonstrate application potential. The example and experiments presented here will certainly help the reader appreciate the scope and application potential of these materials, especially in the context of interdisciplinary cooperation. The thesis is also meant to serve as learning material for students and to be used for teaching purposes and scientific education in general.

CZ - Tato habilitační práce se věnuje nejprve nalezení a odvození teoretického postupu modelování elektrické vodivosti tkaných textilií. Tento návrh je následně experimentálně ověřen, pomocí měření na vyrobených vzorcích. S využitím těchto výsledků práce pokračuje využitím modifikovaných postupů odvození elektromagnetické stínící účinnosti nehomogenních 3D struktur, kdy se podařilo dospět k novému způsobu analytického popisu elektromagnetické stínící účinnosti elektricky vodivých tkaných textilií. Navržený popis platí pro vybrané typy elektricky vodivých textilií, realizovaných technologií tkaní. Základním využitým pozorováním, je podobnost struktur tkaných textilií a mřížkových struktur na bázi kovových prvků. Navržený postup modelování je analyticky ověřen pro různé hodnoty elektrické vodivosti použitých přízí, zároveň je provedeno i ověření v experimentu. Výsledkem je nalezení oboru hodnot použitelných elektrických vodivostí přízí, pro které tyto postupy platí s danou chybou.

Z pohledu v této práci publikovaných nových postupů modelování elektrické vodivosti i elektromagnetické stínící účinnosti elektricky vodivých tkaných textilií, se jedná o soubor nových poznatků, které významně přispívají k rozvoji mezioborových znalostí a aplikací na rozhraní elektrotechniky a materiálového inženýrství. V práci jsou uvedeny také realizované experimenty i výsledky výzkumu a vývoje aplikací navrhovaných typů materiálů, které pokrývají různé oblasti elektroniky a komunikační techniky, s potenciálem jejich užití v praxi. Publikované příklady a experimenty jistě pomohou čtenáři lépe pochopit rozsah a potenciál aplikací těchto materiálů, zejména v kontextu mezioborové spolupráce. Práce si zároveň klade za cíl působit i jako didaktická podpora a umožnit další využití textu pro výukové a vědecké účely.

Keywords:

Electrically conductive textile; Electrical conductivity; Electromagnetic shielding efficiency; Communication engineering; Interdisciplinary research and application;

Acknowledgements

I would like to thank the head of the department, prof. Ing. Boris Šimák, CSc., and my colleagues for creating an excellent working environment at the Department of Telecommunications Engineering. I'd also like to thank to my dear colleague Ing. Bc. Marek Neruda, Ph.D. for his invaluable comments and great collaboration which makes work a pleasure for me and for all members of the team. I'd also like to thank my students who are my inspiration and who give me motivation to continue my work.

Dedication

EN - I'd like to dedicate this thesis to my grandparents Jarmila and Miroslav, Věra and Vlastimil, and my parents Jitka and Milan who instilled in me the most important things in life. All I am I owe to them...

Věnování

CZ - Rád bych tuto habilitační práci věnoval svým prarodičům Jarmile a Miroslavovi, Věře a Vlastimilovi a také mým rodičům Jitce a Milanovi - tedy těm, kteří mě do života vybavili tím nejdůležtějším. Zejména jim vděčím za to, kým jsem…

Contents

List of Figures

List of Tables

Abbreviations

ASK	Amplitude Shift Keying
AT	Attention
BAN	Body Area Network
BER	Bit Error Rate
BLE	Bluetooth Low Energy
CI	Confidence Interval
CSN	Czech Standard
CTU	Czech Technical University
DI	Distilled
DUT	Device Under Test
DVM	Digital Voltmeter Method
ECG	Electrocardiogram
EMC	Electromagnetic Compatibility
EMI	Electromagnetic Interference
EMR	Electromagnetic Reliability
EN	European Standard
EOS	Electrical Overstress
ESD	Electrostatic Discharge
ESE	Electromagnetic Shielding Efficiency
EU	European Union
FEE	Faculty of Electrical Engineering
GPS	Global Positioning System
GSM	Global System for Mobile Communications
HV	High Voltage

ILS	Instrument Landing System
IoT	Internet of Things
ISO	International Organization for Standardization
IT	Information technology
MS	Mobile Station
NFC	Near Field Communication
OCN	On-Chip Networks
PAN	Polyacrylonitrile
PEC	Performance (EMC) Criteria
PED	Portable Electronic Device
PES	Polyester
PP	Polypropylene
PVDF	Polyvinylidene Difluoride
PWM	Pulse Width Modulation
QoS	Quality of Service
RFID	Radio Frequency IDentification
RH	Relative Humidity
SNR	Signal-to-Noise Ratio
TEM	Transverse Electromagnetic Mode
VHF	Very High Frequency
VOR	VHF Omni Directional Radio Range
WHO	World Health Organization
WLAN	Wireless Local Area Network

1. Introduction

Since its beginnings as a discipline, telecommunications engineering has fostered interdisciplinary cooperation and applications. It was established as a program of study in 1910/1911 at the then imperial Czech Technical University in Prague with Ing. Jaroslav Klika's appointment as associate professor. A telecommunications technology pioneer, Mr. Klika started teaching courses on "rail operations safety" and "telegraphy and telephony". As well as railway engineering, the construction engineer Jaroslav Klika also dealt with problems relating to signal transmission in long-distance telegraph and telephone lines. The significant problem of telegraph signal distortion had to be studied and experiments had to be carried out before the transmission parameters of the telegraph lines used could be adjusted. As time went on, telecommunications engineering began to intersect with other scientific disciplines and have a more significant impact on people's lives, becoming, to some degree, a systems science.

Telecommunications technology underwent rapid development during the 20th century and continues to evolve in the 21st. In the 1970s, problems with interference affecting the useful life of equipment, particularly telecommunications devices used in industry and elsewhere, called for an immediate solution. Doc. Svoboda and Ing. Vondrák, my colleagues at the Department of Telecommunication Engineering, pioneered a new discipline in the Czechoslovakia, namely Electromagnetic Compatibility (EMC). The wide range of interdisciplinary applications and interrelationships in EMC attests to the very broad scope of telecommunications engineering which intersects with most branches of electrical engineering.

The year 1974, which is now considered a watershed, marked the entry into operation of the first ATM company network abroad. This year is also considered to have marked the dawn of a new era of technological evolution, namely the Internet of Things (IoT). A boom in this field only came forty years later.

At the end of the 20th century, information technologies seemed to have reached the peak of their development. The focus of investment switched from hardware to services. This change in philosophy formed the basis of a new approach to Information technology (IT) development and operations and, more importantly, IT services.

The development of new types of applications and services created new requirements on hardware components, new types of materials, sensors and actuators. The use of non-traditional approaches, methods and interdisciplinary knowledge became increasingly important. Understanding the relationships between

technologies and between various disciplines has become the key to innovation and finding original solutions.

With the advent of new technologies, “telecommunications engineering” gradually transformed into “communications engineering”, as short-distance communications technologies became increasingly important. Promising technologies within Internet of Things (IoT) and other fields include Radio Frequency IDentification (RFID) and its subtype Near Field Communication (NFC), Bluetooth Low Energy (BLE), Body Area Network (BAN), On-Chip Networks (OCN) and others.

The author of the present habilitation thesis has maintained a long-term focus on new developments in communications technologies in both his R&D and teaching activities and has built on the successful legacy of his predecessors. For the last 10 years, he has focused, in his scientific work, on automatic identification, particularly contactless RFID, the design of related telecommunication devices and their EMC parameters. The current problems and challenges of these fields are closely related to research in IoT and the vision of Industry 4.0. The author’s activities in RFID and IoT have always included a dissemination component. The author has actively promoted new technologies and approaches, including the results achieved by the Faculty of Electrical Engineering (FEE) Czech Technical University (CTU) in Prague, at scientific conferences and in periodicals including national media.

The present habilitation thesis is a contribution to the development of new opportunities and their future realization. The development of new types of electrically conductive textile-based materials and their applications and non-traditional combinations with communications technologies seem to be particularly promising. Examples of interesting applications include electrically heated planar structures, conductive textile structures and bus bars, textile sensors and electrodes, antenna structures, electromagnetic shielding elements and others.

The author’s R&D output presented in this habilitation thesis and his other scientific publications currently includes 14 papers in indexed journals, 3 chapters in a book published in English, more than 60 papers presented at significant conferences, 11 utility models, 1 patent and 6 patent applications. This body of published results can help the scientific community achieve progress in research and development and has potential to be applied in industry as well as in undergraduate, graduate and doctoral education.

The research results presented suggest that electrically conductive textile materials must be divided into several groups and examined within those. The criterion for the division is volume conductivity which must also be reflected in the model we choose. This is because of the effects of the different ways electric current

is conducted in the textiles depending on their structure. For this reason, the thesis deals with the search for and formulation of a theoretical approach to modelling the electrical conductivity of woven textiles and the experimental validation of the approach by measurements performed on woven textile samples.

Drawing on these results, the thesis goes on to determine the electromagnetic shielding efficiency of nonhomogeneous 3D structures using modified approaches and succeeds in finding a new analytical description of the electromagnetic shielding efficiency of electrically conductive woven textiles. The proposed description applies to selected types of conductive woven textiles. The author's basic observation is that woven textiles are structurally similar to metallic grids. The proposed modelling method was analytically validated for the different conductivity values of the yarns used; experimental validation was performed as well. This led to the identification of a set of usable conductivity values for yarns, for which these approaches are valid within a given error.

In view of the new approaches to modelling the electrical conductivity and electromagnetic shielding efficiency of conductive textiles presented in this thesis, it is believed that these findings will significantly contribute to the body of interdisciplinary research and applications at the boundary between electrical engineering and materials science.

The thesis describes the experiments performed and the development of applications of the proposed materials that span various branches of electronics and communications technologies and demonstrate application potential. The example and experiments presented here will certainly help the reader appreciate the scope and application potential of these materials, especially in the context of interdisciplinary cooperation.

The thesis is also meant to serve as learning material for students and to be used for teaching purposes. Relying just on standard teaching methods, it is often very difficult to show how particular topics are connected and what their interdisciplinary dimensions are. One of the aims of the thesis is to contribute to good teaching practice by providing an example of how to incorporate published procedures and derivations, which are often not properly checked. In particular, the conditions of validity of relationships, propositions and derivations must be tested and thought. This is an important consideration not only in engineering education but in scientific education in general.

The team led by the author of this thesis has been successful in the long term in exploring and exploiting non-traditional spaces between disciplines within both education and research and scientific activities. This has led to extensive

collaboration with industrial and research partners and across various departments of the Faculty of Electrical Engineering, CTU in Prague. The interdisciplinary RFID locator project was recognized in 2015 by the CTU's leadership with the Rector's Award for the application of scientific, research and creative work in practice. The EUREKA "Electromagnetic Reliability (EMR) of Electronic Systems for Electro Mobility" project was awarded the 2014 CATRENE Innovation Award by the EUREKA Cluster for Micro- and Nano-Electronics.

The habilitation thesis builds on more than eight years of research in the modelling, measurement and industrial applications of electrically conductive textiles, among other topics. It is based on two research and development projects supported by the Ministry of Industry and Trade of the Czech Republic, namely the 2008-2010 FI-IM5/202 (BE-TEX) "Humans and Equipment Protection Against High-Frequency Electromagnetic Radiation – Research and Development of New Textiles" and the 2012-2015 FR-TI4/202 (KOMPOZITEX) "Composite Textile Materials for Protection of Humans and Devices Against the Effects of Electromagnetic and Electrostatic Fields" projects. The work was also supported by the international LF13005 – "RFID Technology in Logistic Networks of Automotive Industry" (2013-2016, MSM/LF) project and the award-winning EUREKA LF13011 – "Electromagnetic Reliability (EMR) of Electronic Systems for Electro Mobility" (2013-2015, MSM/LF) project.

The results are being applied in ongoing scientific and teaching activities as well as industrial applications relating to the design of manufacturing processes and preparation for the production of conductive technical textiles with electromagnetic shielding capability. This work is undertaken by the companies VÚB a.s. Ústí nad Orlicí and Nyklíček a spol. s r.o. Nové Město nad Metují. New applications of heated textile elements will be dealt with in the new EUREKA E!11158 U Health "Auto-ID and Internet of Things Technologies to Enhance Health Care Quality" project.

The interdisciplinary nature of the work is conductive to strengthening collaboration between the departments of the FEE CTU in Prague. Recently, selected research results were used as the starting point for a new joint project of FEE CTU in Prague and the company HE3DA s.r.o. focused on the development of new types of lithium batteries and the control for these.

2. State of the Art

Modern trends in the development of new and rapidly applicable electrical and telecommunications engineering technology are increasingly focused on environmentally friendly elements and interdisciplinary cooperation. The result is a new "green" electrical engineering which the European Union (EU) expects to put in practice by 2020 under the Horizon 2020 framework program [1]. The goals of this program include the practical application of modern components and circuit structures and environmentally friendly (hence "green") electronics [2]. These activities are not just about technologies and materials; non-traditional applications and innovative solutions also play an important role. The interdisciplinary nature of the work allows for combinations of non-traditional technologies and knowledge transfer between both related and distant fields. Non-traditional relationships are established between such distant sectors as electrical engineering and the textile industry.

For example, a survey of the current state of the development of electrode and battery separators reveals that one of the promising areas of development [3] are new types of textile fibres (e.g. linear fabrics). Planar electrically conductive fabrics have been used for many years in protective clothing to distribute the electric charge evenly on the fabric surface. With a proper conductive structure, i.e., if the desired electrical conductivity is achieved, such materials ensure protection against Electrostatic Discharge (ESD) [4]. Recently, we have seen advances in increasing the electrical conductivity of materials, while the application focus shifted to the implementation of flexible electrically conductive elements or electromagnetic shielding [5].

Applications of these materials are based on manipulating the material's conductivity parameters. Pure textile materials such as cotton or polyester-based textiles are characterized by a very low conductivity. They are called insulating materials. A small portion of the conductive elements in the textile material become antistatic or static dissipative, making the material suitable for use in ESD protective clothing [6]. Moderately conductive materials are another group of textiles that are described in standard [7]. Highly conductive textile materials are the last group, which is used, for instance, in shielding applications.

Conductivity can be both modelled and measured. Modelling is mostly focused on products made of conductive textile materials such as textile antennas, sensors, etc. [8], [9], [10] and on electromagnetic shielding principles [11], [12], [13]. The authors describe the effects of parameters such as thickness [14], material structure [8], [11],

[15] or dimensions [9]. The conductivity value is mostly seen as an input parameter for the model and is itself not modelled in much detail.

Nevertheless, highly conductive textile materials can be modelled as resistors. Modelling the electrical properties of 1×1 rib knitted with stainless steel fibres is presented in [16]. A simplified resistance circuit network is proposed and verified by a resistance measurement using an Agilent Digital multimeter. The paper also describes the resistance calculation for a finite grid of resistors. The same calculation principle is applied to intrinsically conductive knitted fabrics made with stainless steel multi-filament yarns in [17]. The paper goes on to discuss the calculation of the contact resistance of overlapping yarns, which is experimentally verified for two hooked yarns as a first-order exponential equation. This calculation principle, i.e., the calculation of a grid of resistors based on Kirchhoff's circuit laws, is also applied to woven textile materials in [10]. The paper describes the calculation of the resistance of highly conductive woven textile materials, which is inspired by the measurement methods specified in the European Standard (EN) 1149-1 [6]. Resistance is measured using an ohmmeter or electrometer and circular electrodes and resistivity is calculated based on the dimensions of the electrodes [6]. Modelling the resistance of antistatic textile materials according to EN 1149-1 is discussed in [18]. The placement of points with the same potential on circular electrode's resistor grid is presented in detail. The research is extended to include a model of the resistance of a rectangular grid of resistors; the verification of this model by measurement is presented in [19]. We conclude that the surface resistance and bulk resistance of highly conductive textile materials are equal. An analytical calculation of a circular grid of resistors is investigated by our team in [4].

The presented models rely on the assumption that a conductive textile material, in a specific knitted and woven fabric, is composed of an ideal model of conductive yarn, i.e., a homogenous conductive cylinder with constant resistance along its entire length. This assumption makes it possible to use a constant value of the resistor in the electrical circuit. Highly conductive fibres are considered by the authors of the papers in order to take advantage of this simplification. Some of the models also incorporate the contact resistance of overlapping yarns [17]. This is assumed to be equal to zero in [10], [18], [19], [4], which is verified by measurement. No limit for the conductivity values of textile materials is determined; it is only assumed that these values are high. The present thesis is, therefore, partially focused on determining the limit conductivity values for the purpose of modelling.

A model can also help drive down production costs. The current process of determining conductivity is based purely on “post production” resistance measurements, as described in several standards, as opposed to pre-production engineering.

Electrical conductivity is the basic parameter characterizing particular types of electrically conductive fabrics and classes of applications of such materials.

Conductive textile applications include EMC solutions. EMC is an important sub-discipline of telecommunications engineering. Electromagnetic Shielding Efficiency, also known as Electromagnetic Shielding Effectiveness and Shielding Effectiveness, (ESE) is another important electrical parameter, which characterizes the ability of an electrically conductive fabric to block incident electromagnetic waves.

Shielding is a well-known principle preventing the undesirable effects of electromagnetic interference. The methods of determining the shielding efficiency of a material are described in many standards. Shielding enclosures, i.e., units whose electromagnetic emission and susceptibility need to be determined free from any interference from other sources, were measured based on the MIL-STD 285 [20] standard, later replaced by IEEE Std 299-2006 [21]. The electromagnetic shielding efficiency of planar materials is measured based on ASTM D4935-10 in the frequency range between 30 MHz and 1.5 GHz [22]. This frequency range can be extended by using a smaller coaxial apparatus [23] or extrapolating the measurement data [24]. In [25], the authors provided a comprehensive overview of the types of cable shielding in use with a focus on several methods of determining the shielding efficiency of cables, for example the absorbing clamp test method, wire injection test method, close field probe test method, reverberation chamber test method, and anechoic chamber (far field) test method. Furthermore, the paper presents a comparison of these methods. In general, electromagnetic shielding efficiency is determined by measuring voltage or power with and without the shielding.

In [26], the World Health Organization (WHO) discusses the importance of electromagnetic shielding for human health. During the 20th century, environmental exposure to man-made electromagnetic fields was steadily increasing because of the rapid development of communication and electrical devices. Take for example electric and hybrid vehicles, which are electrical devices with potential for global adoption. As well as the common 12 V DC electrical system, these vehicles utilize the so-called high voltage (HV) system which consists mainly of an AC motor, drive inverter and propulsion battery which are connected together by shielded cables. The total output power can reach 100 kW with the terminal voltages of the batteries reaching 800 V. Electric vehicles typically use three-phase motors. The three-phase system is controlled by pulse width modulation (PWM) which switches a battery with a voltage of several 100V [27]. The PWM signal causes electromagnetic interference in the cables and stator windings.

In [28], the authors discuss two shielding designs: separately shielded cables and cables with one shield for all three phases. Based on simulation and measurement data, they conclude that the separately shielded cables are less efficient.

The electromagnetic shielding efficiency of a vehicle seen as a shielding enclosure is discussed in [29]. The authors conclude that the addition of a metal shielding film, in this case a Permalloy and copper film, can significantly reduce the impact of the electromagnetic pulse.

The low-frequency shielding behaviour of shielded high-voltage cables in electric vehicles is analysed in [30]. The authors discuss the flat and triangular structure of the cables and their distance from the ground. They contend that both configurations simulated (i.e., the distance between the cables and the distance between the cable and the ground) exceed the ICNIRP limits [31] if the cables are not close enough to each other. The authors also conclude that the shielded cables cannot ensure a significant reduction in the strength of the magnetic field in the cable due to the special operational mode of electric vehicles.

Just as with electrically conductive textiles, the manufacture of textiles for electromagnetic shielding applications has heretofore not benefited from the use of any design methods. Implementing such design methods into the process of preparation for production or using such procedures to drive production optimization or raw material cost savings can produce significant production efficiencies. The potential for new applications of these materials in further technical fields is another benefit.

In the present thesis, is proposed a process of modelling electrical conductivity in woven textiles and then is verified the proposed approach experimentally. This is followed by an analysis of the potential for exploiting the structural similarity between woven textiles and selected ventilation grille types, which are standard components of technological installations, in modelling the electromagnetic shielding efficiency of these textiles.

The results of the research project discussed below indicate the need to divide electrically conductive textiles into several groups based on, above all, their electrical conductivity values and the corresponding methods of conductivity modelling. Using the procedures under study, is set forth, in the next section of the thesis, a way of modelling the electromagnetic shielding efficiency of a general type of electrically conductive woven textiles.

3. Electrically Conductive Technical Textile Materials

This chapter presents some of the applications of the highly conductive textile materials, the definition of these materials because of the definition in standards lacks, a survey of standardized and experimental measurement techniques of resistance of these materials and the modelling principles which are focused on the structure of the conductive textile material. Modelling principle of highly conductive textile materials for two and three electrode systems is presented. Resistance measurement of the yarn and fabric is described in deep detail and the conductivity of the fabric is evaluated. Comparison of measurement and modelling results show both models are able to determine the order of the volume resistivity and conductivity of the highly conductive textile materials.

3.1. Conductivity Assessment of Electrically Conductive Textile Materials

The current process of determining the conductivity value is based on resistance measurement, as described in several standards.

The standards differ in the range of the resistance values measured, in the specification of the sample measured, in the load of the sample or in the way the sample is connected to the measuring instruments. The DC resistance or conductance of insulating materials can be measured according to [32]. The measurement principle for moderately conductive materials is described in [7]. The process of measuring the surface resistance of static dissipative planar materials is described in [32], [33]. The determination of electrical resistance of floor coverings is described in [34]. The process of measuring the surface resistivity and vertical resistance of protective clothing is described in [6] and [35], respectively. The standard test method for determining the volume resistivity of rubber is specified in [36]. The authors of this paper are not aware of any standardized test methods for determining the resistivity and conductivity of highly conductive textile materials. There only resources available are the research papers mentioned below and a standard that describes a test method for the determination of the linear electric resistance of conductive tracks intended for application in textiles, e.g. yarns, printed or coated tracks, ropes, ribbons, and webbing [37]. However, this standard is not intended to be used as a guideline for the determination of volume or surface resistivity and does not, therefore, include any limitation of resistivity values. There's a mere mention that the standard is to be followed for materials showing ohmic behavior and for conductive tracks where electrical contact between the measurement electrodes and the conductive track is possible. Therefore, it can be used for highly conductive, moderately conductive and possibly some insulating textile materials, giving a resistance value per unit of length.

This chapter is focused on, among other things, the process of measuring the resistance of highly conductive textile materials with respect to textile heterogeneity and simplicity of the test procedure and it also describes the process of determining the conductivity value.

In its Glossary [38], the EOS/ESD Association, Inc. (EOS stands for electrical overstress) defines several basic terms such as the ranges of conductivity values for various materials. Insulation materials are characterized by a surface or volume resistance equal to or greater than 1×10^{11} Ω. Static dissipative material is defined as a material that has a surface resistivity of at least 1×10^{5} Ω /square or volume resistivity of 1×10^{4} Ω.cm but less than 1×10^{12} Ω /square for surface resistivity or 1×10^{11} Ω.cm for volume resistivity. (Note: Ω /square is not an SI unit; however, it is used extensively in material engineering. It is based on the fact that the resistance value measured between two parallel electrodes representing the opposite sides of a square does not change with the area of the square). Conductive material has a surface resistance of less than 1×10^{4} Ω or volume resistance of less than 1×10^{4} Ω and surface resistivity of less than 1×10^{5} Ω /square or volume resistivity of less than 1×10^{4} Ω.cm. Moderately conductive materials are characterized by volume resistivity values in the range of 1 to 10^{7} Ω.cm in [7], [39]. Highly conductive materials are defined neither in the standards [6], [7], [39], [33], [34], [35], [36] nor in the glossary [38]. However, a highly conductive material can be defined as a material that has a volume resistivity of less than 1 Ω.cm. This definition is based on the range of volume resistivity values for moderately conductive materials.

Based on the test fixtures specified in the standards presented, four basic groups of methods of determining the resistance of textile materials can be distinguished. The first group uses a two-electrode system [39], [40]. These methods are affected by a systematic error caused by contact resistance and the resistance of the measuring wires. The second group includes methods that use a three-electrode system. These are described in the standards [6], [39], [35] and can be used to examine high-resistance materials. The third group includes methods that use a four-electrode system such as the van der Pauw method [41] and the method proposed by Wener [42]. These methods eliminate the effect of contact resistance by measuring the voltage drop between two electrodes. The remaining two electrodes are supplied with power from a precision current source. These methods can be used only for the measurement of samples that are isotropic and homogenous, free of holes and flat, with a uniform thickness [41] or rectangular bar-shaped [42]. These techniques are not primarily designed for textile materials; however, several research papers attest that the van der Pauw method can be used [43], [44], [45], [46]. The last group comprises methods that use more than four contacts such as the Montgomery technique, which requires at least six contacts [47], [48]. The electrodes

are attached in the four corners of the sample's side, the current and voltage measurement is performed, all connections are rotated by 90° and the measurement is repeated. Optionally, a different sample or a different sample side is examined. The technique is used for determining the resistances of anisotropic materials.

Many papers present attempts to verify the suitability of the aforementioned measurement techniques for the study of textile materials. However, what is most important is the conductivity value with regard to the measurement technique used. Papers that discuss highly conductive textile materials are mentioned as well.

The equipment used for the measurement of current–voltage curves is presented in [49]. The paper describes the process of measuring the resistance of a conductive thin layer on a textile material. The authors confirm that standard methods of conductivity measurement involving ring electrodes are not suitable for highly conductive samples. Therefore, two parallel bars with an offset of 0.03 m, width of 0.04 m and pressed with a weight of 10 kg onto the samples for optimum contact are used. The resistance values obtained are in the range between 40 and 50 Ω when using conductive solder strips. A four-point probe technique is used to measure 0.05 x 0.05 m sized coated fabrics in [50]. The authors designed a test fixture consisting of four brass-plated electrodes placed parallel to each other. The two outer electrodes are connected to a current source and the two inner electrodes measure the voltage drop in a 0.02 x 0.02 m sized sample. A 2 kg weight is placed on the probe and resistivity values are read after one minute [51]. The measurement is performed in both weft and warp directions and a mean value is calculated. The surface resistivity values obtained are in the range between 10 and 700 Ω/square. The use of the van der Pauw method for measuring the resistance of textile materials is described in [43], [44], [45], [46]. A flat sample of the Shieldex® conductive metallized nylon fabric with a surface resistance of less than 0.02 Ω /square and without isolated holes is used in [43], [52]. The paper concludes that electrode diameter values within the range between 0.002 and 0.008 m do not affect resistance measurement when a constant force (5 – 74 kPa) is applied. According to the recommendation in [53], the area of single contact should be at least an order of magnitude smaller than the area of the whole sample. The anisotropy of a woven fabric is confirmed by the difference between vertical and horizontal resistance values. The method is further extended by an uncertainty evaluation based on the Monte Carlo method in order to determine the suitability of the van der Pauw method for the textile object under study [44]. The use of the van der Pauw method for measuring the sheet resistance of polypyrrole-coated para-aramide woven fabrics is compared with a four-point collinear array probe measurement [45]. The term 'sheet resistance' is usually used in semiconductor applications to refer to thin films that are nominally uniform in thickness. Sheet resistance is calculated as the ratio of resistivity and thickness of the material [54],

[55]. The sheet resistance values obtained fall within the range between 300 and 400 Ω/square. The authors conclude that the values obtained using the van der Pauw method are on average 12% lower than those obtained using a four-point probe. This difference is attributed to the specificities of the two measurement methods. Conductive layers printed on a textile substrate are examined using the van der Pauw method in [46]. To interpret the data correctly, the authors present a mathematical analysis. Several woven textile materials with different types of weave and different yarn densities in the weft and warp directions are used. Parasitic contact resistance between two metal bars is discussed and the van der Pauw method is preferred. The anisotropy of the conducting layer is examined in y and x directions, i.e., warp and weft. The sheet resistance of electrically conductive screen-printed fabrics is examined using the collinear four-point probe technique and the van der Pauw method in [56]. The authors demonstrate theoretically and experimentally that no anisotropy can be detected using the collinear four-point probe technique. They also conclude that this technique measures the square root of the product of resistance measured in warp and weft directions. A study of gas sensing capabilities based on the monitoring of conductivity changes in polypyrrole-coated fabrics is described in [57]. The Montgomery method is used, although a detailed description of the technique is missing. Other techniques used for the characterization of highly conductive fabrics include methods based on transmission lines and waveguide cavities, which are designed for the characterization of textile materials in the high frequency range [58], [59]. Waveguide cavity measurement requires a good connection between the textile sample and the waveguide aperture [58]. The authors contend that the method is suitable for textile materials entirely composed of conductive fibers. Also described in [51] is a measurement technique involving a microstrip line resonator. This technique can also be used with conductive textile materials containing conductive fibers. The technique involves the precise preparation of samples to a specified size, placement of the sample in the resonator, Q factor calculation based on the load Q, S21 and S11 measurement, and surface resistance and conductivity derivation [58], [59].

The test methods presented require the use of coated fabrics (van der Pauw) or the precise preparation of the sample and test cell for measurements (microstrip resonator). Ring electrodes cannot be used with highly conductive textile samples. One method that is considered to be easily applied is the four-point probe method that involves the use of electrodes placed parallel to each other, as described for coated fabrics in [50].

This chapter focuses on the examination of highly conductive textile materials. First, the term ‘highly conductive material’ is defined as a material with a volume resistivity of less than 1 Ω.cm. This is in line with the definition of moderately

conductive materials in the standards [7], [39]. The chapter goes on to describe the modelling of highly conductive textile materials for two- and three-electrode systems. The measurement techniques are described in detail and compared with modelling results.

3.1.1. Modelling of Highly Electrically Conductive Fabrics

The structure of highly conductive fabrics can be compared to an electric circuit, as described in [10], [16], [17], [18], [19], [4]. Generally, the structure of a conductive textile material can be described as an RLC electric circuit, Fig. 1. The figure shows two weft yarns and two warp yarns that are interlaced. The contact resistance of the yarns is represented as R_c. The length resistance of the yarn is represented as R_l. Inductance L is formed by the conductive components in the yarn and the capacitance between yarns is C.

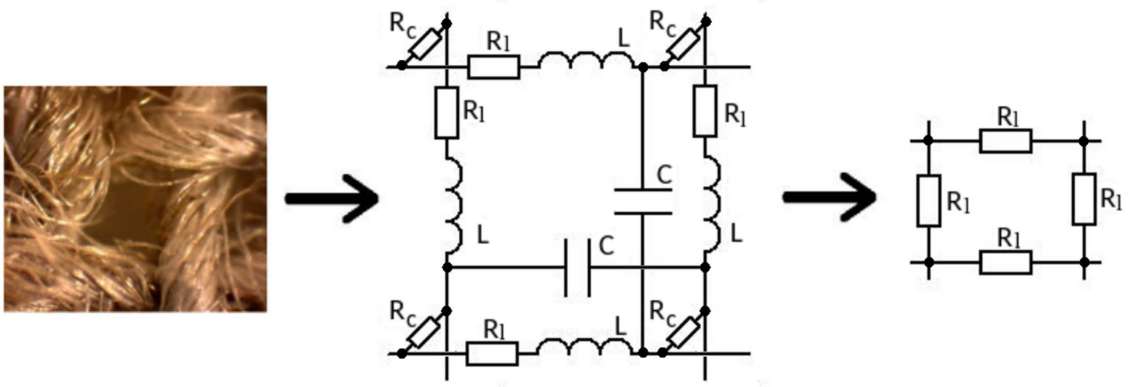

Fig. 1 Model of a conductive textile structure and its electrical interpretation.

Assuming that a textile material consists of highly conductive yarns, capacitance C and inductance L can be neglected for DC measurement methods. Moreover, contact resistance R_c can be considered to be zero as well because it is assumed that the contact resistance of the interlacing points is much lower than the length resistance of the fiber.

Additionally, the electric circuit can be simplified by using the same yarns in the weft and warp directions. This simplification enables the creation of a model of a conductive textile structure which is homogenous in terms of the yarns used. In fact, conductive yarn is basically a heterogeneous structure consisting of nonconductive and conductive fibers or components with a varying yarn diameter along the whole length. Therefore, yarn diameter is generally obtained by microscopic measurement and a mean is used as the diameter value [19]. However, this simplification eliminates the variation in the values of the resistors used in the

equivalent electric circuit. These resistors represent the value of the length resistance of the yarn between two interlacing points.

The above simplifications for highly conductive fabrics are summarized as follows:

- Capacitance *C* is neglected
- Inductance *L* is neglected
- Contact resistance R_c of interlacing points is neglected
- The same yarn in the weft and warp directions
- The same sett (number of yarns in 0.01 m) in the weft and warp directions

Consequently, an equivalent electric circuit only consists of the resistors representing the length resistance of the yarns, Fig. 2.

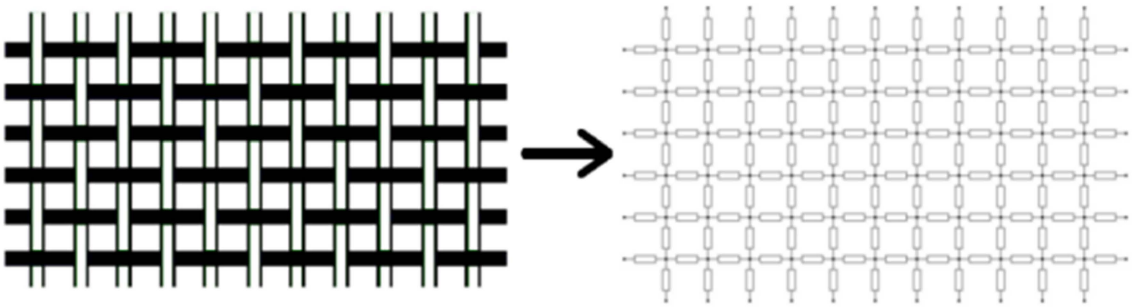

Fig. 2 Simplified equivalent electric model of a highly conductive fabric.

3.1.2. Electrical Conductivity and Electrical Resistivity in General

Electrical conductivity σ [S / m] is a measure of a material's ability to conduct an electric current. It is the reciprocal of electrical resistivity:

$$\sigma = \frac{1}{\rho} \quad [S/m], \tag{1}$$

where σ represents electrical conductivity and ρ denotes electrical resistivity.

Electrical resistivity is the property of a material with specific dimensions that describes the material's resistance. It is calculated as:

$$\rho = R\frac{A_c}{l_s} \quad [\Omega \cdot m], \tag{2}$$

where ρ stands for electrical resistivity, R denotes resistance, A_c is a cross-sectional area and l_s is the length of material.

Equation (2) is determined for most single-material conductors with a uniform cross section and electric current flow. A general definition of electrical resistivity, which takes into account the electric current flow in a material with an electric field inside, conforms to Ohm's law:

$$\rho = \frac{E}{J} \quad [\Omega \cdot m], \tag{3}$$

where ρ is electrical resistivity, E is the magnitude of the electric field, and J stands for the magnitude of the current density.

The SI unit of electrical resistivity (Ω·m) explains how an electrical resistivity value is obtained. Consider a cube with the dimensions 1 x 1 x 1 [m]. The opposite sides represent two contacts and the resistance between the two contacts is 1 Ω. This cube represents a material with an electrical resistivity of 1 Ω·m. Generally, electrical resistivity is calculated from the specific dimensions of a material, using the measured value of resistance.

Table I shows the typical electrical resistivity values of selected materials (insulators, semiconductors and conductors) [60].

Table I Electrical Resistivity Values of Materials [60]

Material	***ρ [Ω.m] (20 °C)***
Copper (conductor)	1.68×10^{-8}
Silver (conductor)	1.59×10^{-8}
Hard rubber (insulator)	10×10^{13}
Insulators	$10^{13} – 10^{16}$
Carbon (semiconductor)	3×10^{-5}
Germanium (semiconductor)	0.5
Silicon (semiconductor)	20 – 2300

Electrical resistivity is also called volume resistivity or specific electrical resistance. The standard [33] defines volume resistivity as the ratio of DC voltage per unit thickness to the amount of the current per unit area passing through a material. Other definitions can be found in [39], [61].

In [62], surface resistivity is defined as the electrical resistance between two parallel electrodes in contact with the sample's surface and separated by a distance equal to the contact length of the electrodes. Other definitions can be found in [33], [39].

3.1.3. Modelling of Resistivity for Two Electrode System

Based on the definitions of surface and volume resistivity presented above, it is possible to modify (2) as follows:

$$\rho_s = \frac{\frac{U}{L}}{\frac{I_s}{W}} = R_s \cdot \frac{W}{L} \quad [\Omega / square], \tag{4}$$

where ρ_S is surface resistivity, R_S is surface resistance, U stands for DC voltage, I_S denotes surface current, L is the distance between the electrodes, and W denotes the width of the sample.

$$\rho_v = R_v \cdot \frac{A_c}{L} \quad [\Omega \cdot cm], \tag{5}$$

where ρ_V is volume resistivity, R_V is volume resistance, A_c denotes the cross-sectional area of the sample and L denotes the distance between the electrodes.

Surface resistivity is calculated from the resistance value which is measured using, for instance, the test fixture depicted in Fig. 3. The test fixture used to determine volume resistivity consists of ring electrodes, which cannot be used for high conductivity materials. Therefore, only a setup for surface resistivity measurement is presented and further discussed in terms of its suitability for volume resistivity measurement.

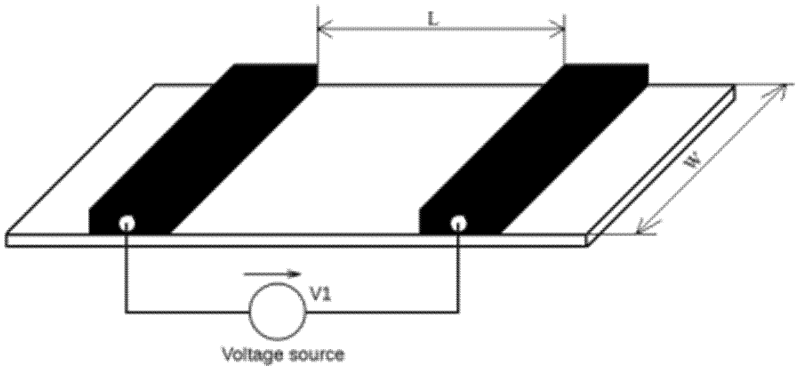

Fig. 3 Setup for surface resistivity measurement [62].

The definition and principle of measuring surface resistivity presented above are based on the measurement of the resistance between two parallel electrodes. The resistance value can be also determined by modelling a textile structure.

Considering the simplifications for highly conductive fabrics presented above, the structure can be visualized as in Fig. 4. Plain weave is chosen for its simple regular

structure, i.e., the warp and weft are aligned to form a simple crisscross pattern. This weave is usually used in apparel and upholstery fabrics and is also suitable for electromagnetic shielding applications.

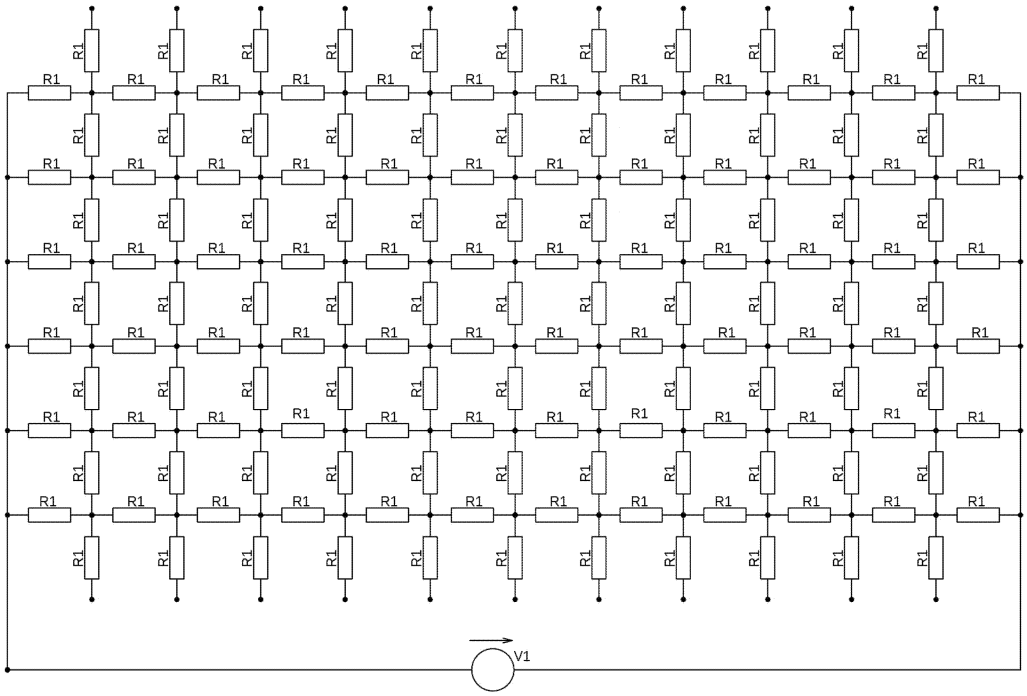

Fig. 4 Equivalent electric circuit for resistance measurement.

The rectangular orientation of the weft and warp yarns in the textile structure has to be taken into account in the design of the measurement technique. The test method described in [51] defines a procedure for parallel-plate electrodes. Electrical resistance is measured along both the length and width directions. Since the charge will follow the path of least resistance, only the lower reading by direction is recorded. However, one of the simplifications presented, namely that the same yarns are used in the weft and warp directions, allows us to consider only one direction.

An equivalent electric circuit, as shown in Fig. 4, can be simplified by considering equipotential points. The regularity of the equivalent circuit diagram and connected poles of power supply cause the same voltage drop in the nodes, which have the same “distance” from the connected power supply. Then, the resistors placed between these nodes are considered to be zero and the resulting resistance is calculated from the series-parallel connection of resistors shown in Fig. 5 as described in equation (6). This can be verified by placing a voltage probe in the individual nodes as described in detail in our previous research work [19].

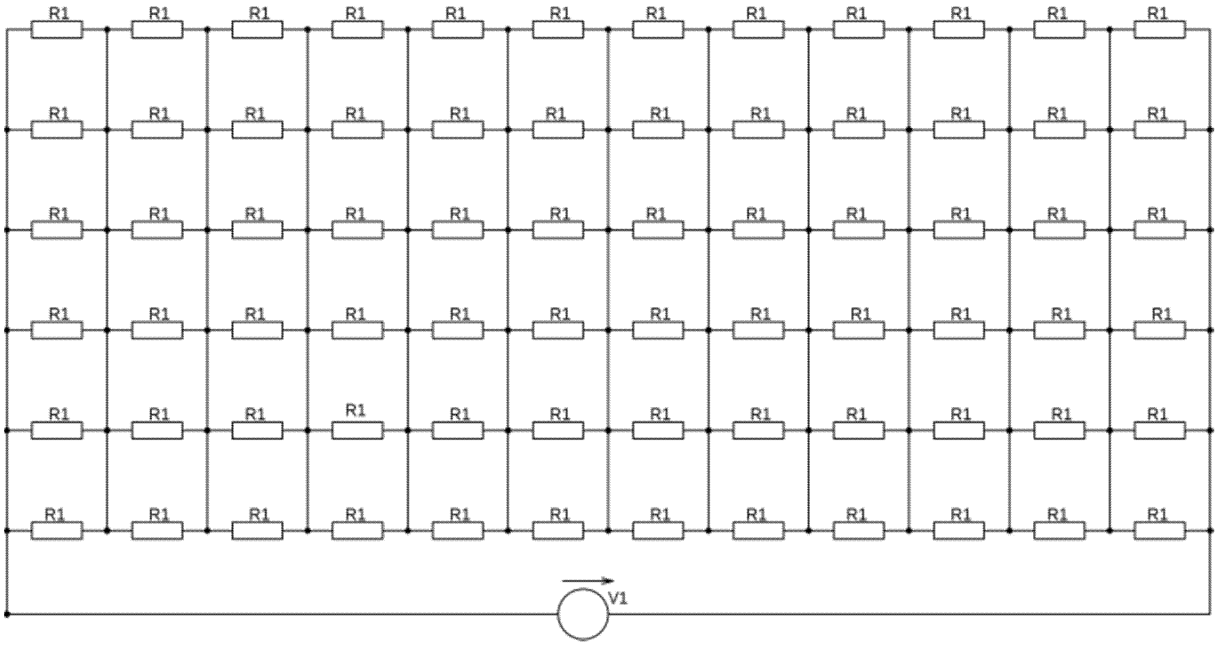

Fig. 5 Simplified equivalent electric circuit for resistance measurement.

$$R_{M2} = \sum_{v=1}^{u} \frac{R_1}{s} \quad v,u,s \in \{N\} \quad [\Omega], \tag{6}$$

where R_{M2} is the resulting modelled resistance, R_1 stands for the modelled resistor, v, u is the number of resistors in the series between electrodes, and s is the number of resistors directly connected to the electrode.

This simplification can be verified in simulation software by placing a voltage probe, or through measurement, as described in [19].

Equations (4) and (6) clearly show that surface resistivity is calculated from the dimensions of the electrodes, i.e., sample size, number of resistors in the sample (as determined by the sample's size and number of yarns in the warp and weft directions), and the length resistance of the yarn, which has to be either measured or calculated [63].

3.1.4. Surface and Volume Resistivity Derivation with Respect to Three Electrode System

For homogeneous materials [63], surface resistivity is derived from (3). However, this is also applicable to textile materials, as described in standards [6], [51]. The current density J and the calculation of electric field E are required.

Current density is often expressed as:

$$J = \frac{I}{S} \quad \left[A/m^2\right], \tag{7}$$

where J is current density, I denotes current and S means the surface area.

Surface current density J_S for a circular cross section is calculated as [63]:

$$J_s = \frac{I_s}{2\pi r} \quad [A/m], \tag{8}$$

where J_S is surface current density, I_S denotes surface current and r is the radius, which varies between r_1 and r_2, r_1 stands for the outer radius of the center electrode and r_2 is the inner radius of the outer ring electrode.

In fact, (8) represents the surface area of all sums of radii, which vary between r_1 to r_2, Fig. 6. It is assumed that all current flow between the electrodes passes along the surface area and does not penetrate the material's core. That is not the case in highly conductive materials where electrons also move in the material's core. So, the calculation is applicable to insulators and static dissipative materials, for example.

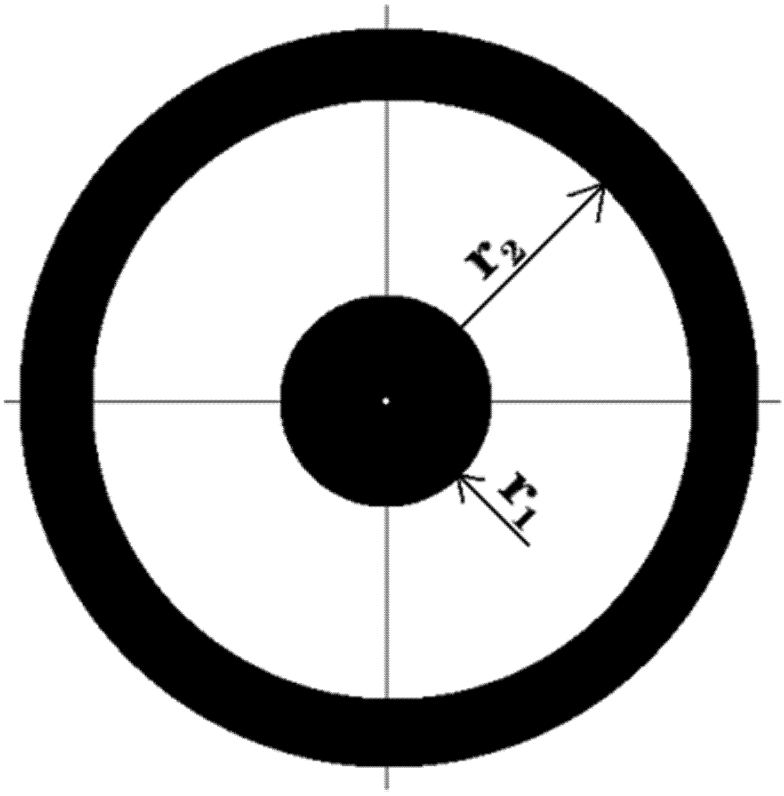

Fig. 6 Configuration of ring electrodes.

The electric field E between two concentric ring electrodes (this is also valid for surface currents) can be described as:

$$E = J_s \cdot \rho_s = \frac{I_s}{S} \cdot \rho_s = \frac{I_s \rho_s}{2\pi r} \quad \left[V \cdot m^{-1}\right], \tag{9}$$

where E denotes the electric field, J_S is surface current density, ρ_S means surface resistivity, I_S denotes surface current, S stands for the surface area and r indicates radius.

The integration of the electric field E from r_1 to r_2 results in the following calculation of voltage between circular electrodes:

$$U_{r1,r2} = \int_{r1}^{r2} E dr$$

$$U_{r1,r2} = \frac{I_s \rho_s}{2\pi} ln \frac{r2}{r1} \quad [V], \tag{10}$$

Surface current can be eliminated by applying basic Ohm's law:

$$R_s = \frac{U_{r1,r2}}{I_s} = \frac{\frac{I_s \rho_s}{2\pi} ln \frac{r2}{r1}}{I_s} = \frac{\rho_s}{2\pi} ln \frac{r2}{r1} \quad [\Omega], \tag{11}$$

And finally, the definition of surface resistivity for concentric ring electrodes is described as:

$$\rho_s = R_s \cdot \frac{2\pi}{ln \frac{r2}{r1}} = R_s \cdot k \quad [\Omega / square], \tag{12}$$

where ρ_S is surface resistivity, R_S means surface resistance, and k is the geometric coefficient of the electrodes.

The equation (12) is used in [6], [33] for resistance measurement and surface resistivity calculation.

In the measurement of volume resistivity we consider concentric ring electrodes placed on one side of the sample and another electrode placed on the other side of the sample [39]. Resistance is then measured between the inner electrode and the electrode on the other side of the sample. The voltage applied between these electrodes increases the electric field. Considering that the current I_V passes only between the electrodes, the electric field E and voltage U are calculated as follows:

$$E = J_v \cdot \rho_v = \frac{I_v}{S} \cdot \rho_v = \frac{I_v \rho_v}{\pi r^2} \quad \left[V \cdot m^{-1}\right], \tag{13}$$

$$U_{0,t_h} = \int_0^{t_h} E dt_h = \int_0^{t_h} \frac{I_v \rho_v}{\pi r^2} dt_h = \\ = \frac{I_v \rho_v}{\pi r^2} \int_0^{t_h} 1 dt_h = \frac{I_v \rho_v}{\pi r^2} \cdot t_h \quad [V] \quad , \tag{14}$$

where E denotes the electric field, J_V is volume current density, ρ_V means volume resistivity, I_V denotes volume current, S stands for the surface area, r is the radius of the inner electrode, U denotes voltage, and t_h is the distance between the electrodes.

Volume resistance is than calculated as follows:

$$R_v = \frac{U_{0,t_h}}{I_v} = \frac{\frac{I_v \rho_v}{\pi r^2} \cdot t_h}{I_v} = \\ = \rho_v \cdot \frac{t_h}{\pi r^2} = \rho_v \cdot \frac{4 t_h}{\pi D_1^2} \quad [\Omega] \quad , \tag{15}$$

where D_1 is the diameter of the inner electrode.

Volume resistivity is equal to:

$$\rho_v = R_v \cdot \frac{\pi D_1^2}{4 t_h} \quad [\Omega \cdot m] . \tag{16}$$

The equation (16) can be found in [64]. The standard [39] adds g parameter - the dimension of the gap between the electrodes to the diameter of the inner electrode D_1. According to the application notes for volume and surface resistivity measurement [65], the g parameter is typically excluded.

3.1.5. Modelling of Resistivity for Three Electrode System

The definition of volume and surface resistivity presented above shows that these parameters are obtained through the measurement of resistance and calculation, taking into account the electrodes' dimensions [6], [39].

Let's now consider the process of determining surface resistivity alone. Ring electrodes are placed on the surface of the textile sample and resistance is measured between the ring electrodes. Fig. 7 shows how such resistance can be modelled based on the simplifications presented earlier. We have a resistor network limited by electrodes. The picture is scaled to allow the visualization of the model proposed. In fact, the resistor network is much denser, in other words, it consists of more resistors than we can see in the figure. The number of resistors is calculated based on the density of the yarn in the weft and warp directions and the electrodes' dimensions.

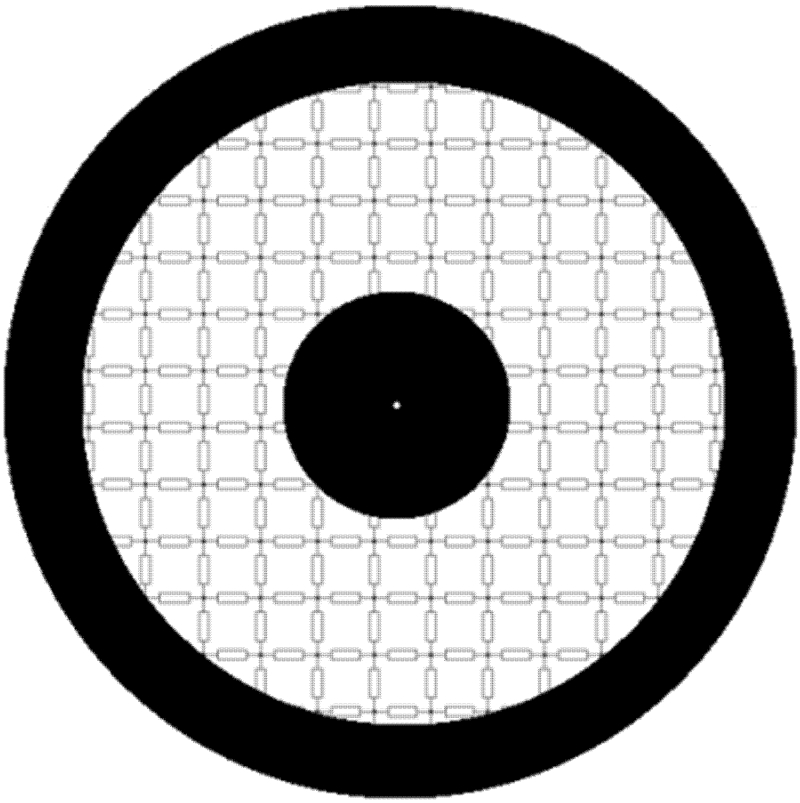

Fig. 7 Electrode placing on the surface of textile sample.

The inner and outer electrodes represent the contact points, to which the power supply is connected. A voltage source of the type described in the standards [6], [39] can be used. The circuit diagram is shown in Fig. 8. The diagram was created in Oregano, a Linux-based schematic capture and circuit simulation application [66]. Fig. 8 shows a resistor network corresponding to Fig. 7. The value of the resistors modelled is set to 1000 Ω, i.e., 1k in Fig. 8, which is in fact negligible. This is to simplify the circuit diagram. The resistors, which are only partially shown in Fig. 7, are modelled as portions of the 1k resistor modelled. Therefore, Fig. 8 shows the values of the resistors to be 10, 200, 700 (in Ω units). The value of each resistor is shown below its schematic symbol, regardless of the resistor's orientation. The circuit diagram is analyzed by voltage probes. Three such probes are depicted in Fig. 8. Several important results are summarized in Fig. 9.

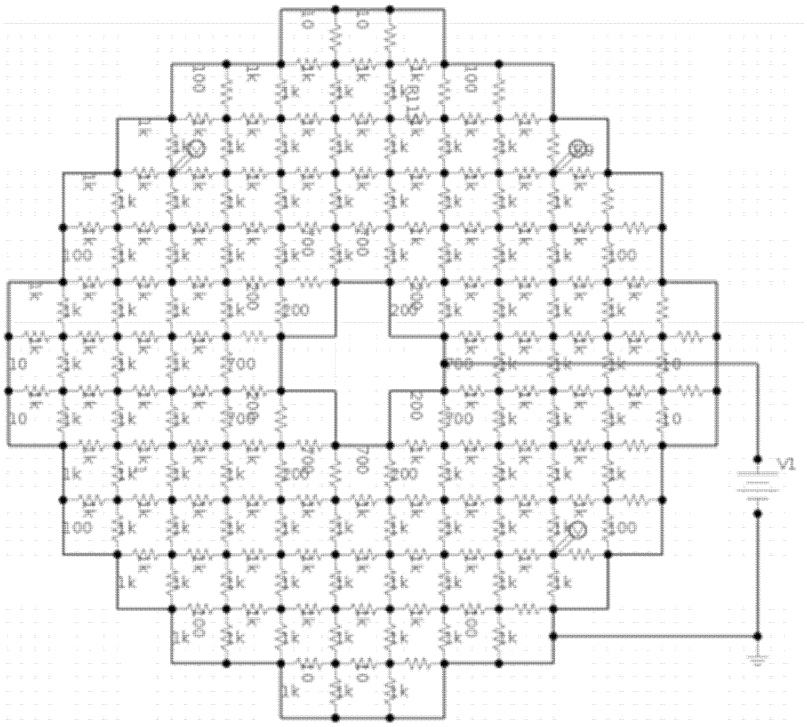

Fig. 8 Circuit diagram of the resistor network modelled in Oregano application [66].

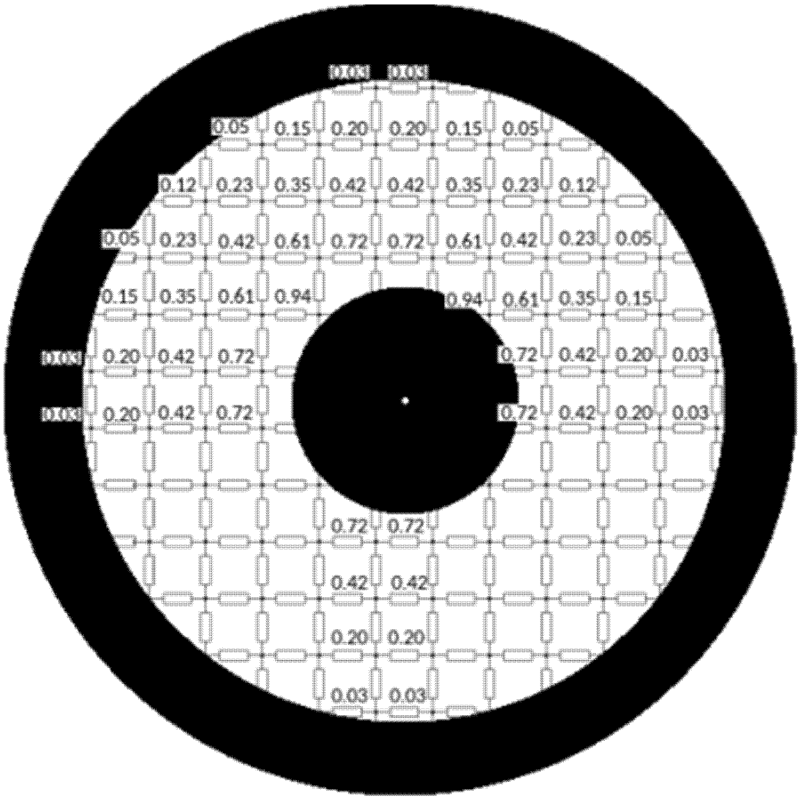

Fig. 9 Analysis of the resistor network by voltage probes.

The whole resistor network is symmetrical about its vertical and horizontal axes, provided that the yarn has the same density in the warp and weft directions and the fabric consists of one yarn only. This means that the model's resulting resistance can be calculated as a sum of four parallel-connected resistors *R*x, where *R*x is equal to the resulting resistance of one quadrant of the resistor network because nodes must have the same electric potential according to the basic law of physics. If the electric potential in two nodes connected by a conductor is the same, there is no voltage between them because no current can pass through the conductor that connects them. Therefore, these two points in a circuit can be disconnected or connected (merged into one point) without changing the total resistance of the circuit. The same voltage values indicate points with the same electric potential. Please note that in Fig. 9 the voltage value shown corresponds to the electric potential of the lower right node. The voltage values shown also indicate symmetry in one quadrant. Hence, *R*x is a parallel connection between two identical resistors. With these principles we conclude the discussion of the possibilities of circuit simplification which are also presented in our previous research work [10].

The *R*x value can be calculated using known electric circuit modelling methods. The basic method is an application of series and parallel resistor rules and Y-Δ transformation. However, these methods can be used for only a small number of resistors because the computational complexity increases with the number of resistors. Kirchhoff's circuit laws can be considered as well. The number of loops, or equations, significantly increases the computational demands. Impedance matrix, or Z-matrix, is another useful method, which arranges individual loops into rows of matrix, based on the loop current method. Each loop in the circuit diagram represents one equation and one row in the impedance matrix. Fig. 10 shows the 25 loops involved in the calculation of R_X as shown in Fig. 9. The R_1 resistors represent the uniform length resistance of the yarn. The R_2 value is a fraction of R_1. It is calculated based on yarn density and the electrodes' dimensions. It is a different value, lower than R_1 in Fig. 10.

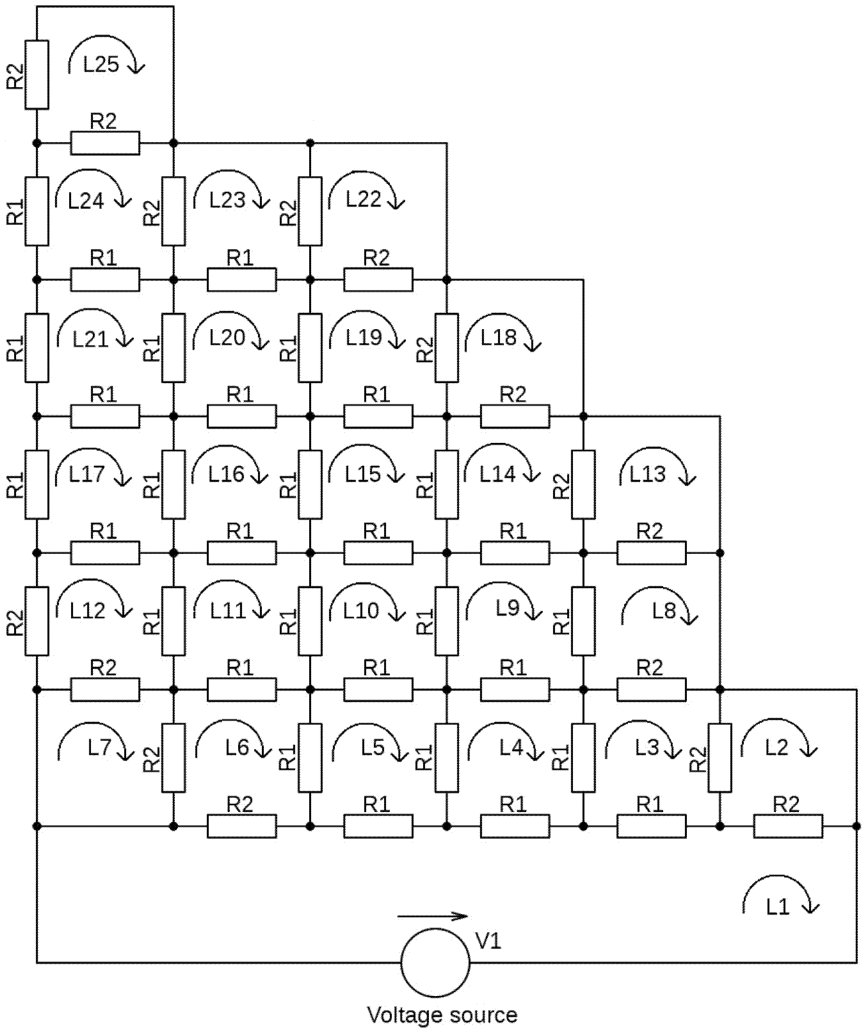

Fig. 10 Loops in a simplified circuit diagram.

The loop names and directions define the relevant equations. The same arrow direction in neighbouring loops indicates plus, while opposing directions indicates minus. All neighbouring loops have to be considered for all loops, or equations. The equation for the *L1* loop is then defined as follows:

$$\begin{aligned} U_{V1} &= R_2(I_1 - I_2) + R_1(I_1 - I_3) + R_1(I_1 - I_4) + \\ &+ R_1(I_1 - I_5) + R_2(I_1 - I_6) \end{aligned} \quad . \tag{17}$$

where U_{V1} means the power supply, R_1 and R_2 denote the length resistance of the yarn, I_1 is the current corresponding to the L_1 loop, I_2 is the current corresponding to the L_2 loop, etc.

An equation for another loop, e.g. L_{24}, can be described as follows:

$$\begin{aligned} U_{V1} &= R_2(I_1 - I_2) + R_1(I_1 - I_3) + R_1(I_1 - I_4) + \\ &+ R_1(I_1 - I_5) + R_2(I_1 - I_6) \end{aligned} \quad . \tag{18}$$

Equations (17) and (18) are written into the impedance matrix in the 1st and 24th rows (19). The voltage sources of the individual loops, or circuit equations, are placed on the left side of the matrix. The corresponding currents are placed on the right side. The position of each resistor value corresponds to an equation and the current, e.g. the equation for L_1 represents the first row in the matrix, and the sum of resistors for the I_1 current is found in the first column. Therefore, the impedance matrix consists of 25 rows and 25 columns. For instance, the resistance value – R_1 is a result of the L_{24} loop (18) and I_{21} current and hence, it is found in the 24th row (L_{24} loop) and 21st column (I_{21} current) of the impedance matrix. Because of its dimensions, the complete impedance matrix is not shown. However, the first three and the last two rows and columns are shown in (19).

$$\begin{bmatrix} U_{v1} \\ 0 \\ 0 \\ \dots \\ 0 \\ 0 \end{bmatrix} = \begin{bmatrix} 3R_1+2R_2 & -R_2 & -R_1 & \dots & \dots & \dots \\ -R_2 & 2R_2 & -R_2 & \dots & -R_1 & 0 \\ -R_1 & -R_2 & 2R_1+2R_2 & \dots & 0 & 0 \\ \dots & \dots & \dots & \dots & -R_2 & 0 \\ \dots & -R_1 & 0 & -R_2 & 2R_1+2R_2 & -R_2 \\ \dots & 0 & 0 & 0 & -R_2 & 2R_2 \end{bmatrix} \cdot \begin{bmatrix} I_1 \\ I_2 \\ I_3 \\ \dots \\ I_{24} \\ I_{25} \end{bmatrix} \quad (19)$$

.

The impedance matrix can normally be reformulated as:

$$\mathbf{U} = \mathbf{Z} \cdot \mathbf{I}. \quad (20)$$

The equation (20) applies to any of the independent loops L_1 – L_{25}. The impedance matrix ***Z*** is a regular, square matrix with no linearly dependent rows. The impedance matrix is square because it consists of the same number of rows, or equations, which correspond to the 25 loops in the circuit diagram, and columns, or resistor values, which correspond to 25 currents. The rows are not linearly dependent because every equation contains up to 6 currents, which differ by at least 24 zero values. The indexes of the currents are different for every equation and zero values are located in different columns in the impedance matrix. Hence, it is not possible to multiply a row of the matrix by a number to get another row. Consequently, (20) can be multiplied by the inverse matrix $\boldsymbol{Z}^{-1}$ from the left. The current ***I*** is then calculated as [67]:

$$\mathbf{I} = \mathbf{Z}^{-1} \cdot \mathbf{U}. \quad (21)$$

The current I_k in the k loop is calculated as:

$$I_k = 1/\Delta \cdot (\Delta_{1:k} \cdot U_1). \tag{22}$$

where I_k means the current in the k loop, Δ denotes the impedance matrix determinant, $\Delta_{1:k}$ is the algebraic complement of the impedance matrix, 1 in the parameter $\Delta_{1:k}$ stands for the omitted row in the impedance matrix and k in $\Delta_{1:k}$ stands for the omitted column k in this matrix, and U_1 is the power source.

The input impedance of one power source in the circuit diagram is equal to the modelled resistor R_x. It can be calculated from (22) as follows:

$$R_X = Z_{in} = U_1 / I_1 = \Delta / \Delta_{1:1}. \tag{23}$$

The equation (23) shows that the value of the resistor R_x is calculated as the ratio of the determinants of the matrix. In other words, the determinant of the whole impedance matrix is calculated. Then, the first row and first column of the impedance matrix are omitted and the determinant is calculated again. The value of the determinant can be calculated in MATLAB®. However, the impedance matrix presented (19) contains a number of zero values and for this reason, the Cholesky factorization is used [68].

3.1.6. Measurement of Highly Electrically Conductive Fabrics

Measuring Yarn Resistance

Yarn resistance can be measured using the test method described in [62]. The method is based on a two-electrode system with a movable probe. A test fixture of the type shown in Fig. 11 is fabricated. The distance between the stable electrode and the movable probe, or the second electrode, is set to 0.01, 0.05, 0.1, 0.15 or 0.3 m. Examining yarn with varying length ensures a more predictive value for the physical quantity being measured and a decrease in the test procedure's runtime compared to measuring resistance of yarn with constant length, and consequently, is better at dealing with material heterogeneities caused by the manufacturing process. A yarn sample is fixed at one end of the test fixture by the stable electrode and a load is applied at the opposite end. The weight of the load is chosen in accordance with the standard [69]. This ensures that the same tension is applied to all samples. The electrodes are made of brass and contain gold-plated contacts. The total weight of the electrode is 2 kg. This ensures good contact with the textile sample. Each sample is examined in five lengths, namely 0.3, 0.15, 0.1, 0.05 and 0.01 m, to eliminate the effects of yarn deformation caused by the electrodes' weight.

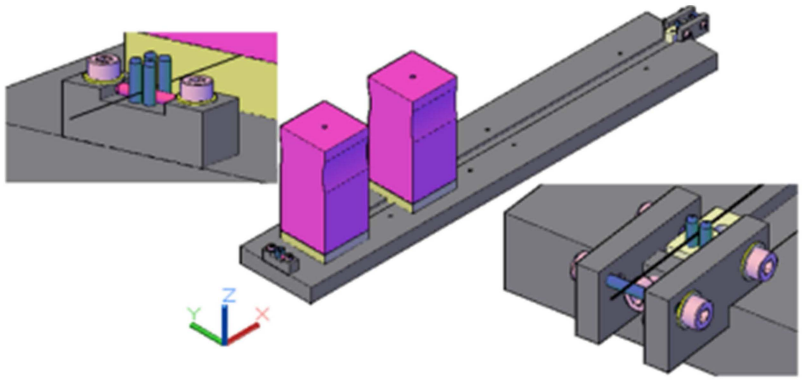

Fig. 11 3D model of a test fixture used for the measurement of yarn resistance.

Four yarn samples with different percentage of conductive content and different linear mass density are chosen, Table II. The samples are kept in a climate-controlled environment and measurement is performed at 40 % relative humidity (RH), 22 °C. The linear density of the yarn samples being measured is 29.5 tex (the unit of measurement indicating the linear mass density of fibres, yarns and threads) and 24 tex. For this reason, 15 g and 12 g weights are used, respectively. The resistance values are recorded using the Voltcraft® LCR 4080 meter.

Table II Yarn Specification

#	Composition	Linear density [tex]
1y	SilveR.STAT® 240 dtex/10F	24
2y	60% PES* / 40% SilveR.STAT® 3.3dtex	29.5
3y	40% PES / 60% SilveR.STAT® 1.7dtex	29.5
4y	60% PES / 40% SilveR.STAT® 1.7dtex	29.5

*** PES stands for Polyester**

The data are shown in Table III and Fig. 12. The results for electrodes with an offset of 0.01 m are not included here because of the enormous scatter attributable to the manufacture of these yarns. Preliminary tests showed that the standard deviation was up to 8 times higher and the variation coefficient was up to 10 times higher if the 0.01 m offset was included in the evaluation of the data. The measurement is repeated eight times in different sections of the yarn, and linear resistance, i.e., electrical resistance per unit of length, is calculated in [Ω/cm].

Table III Results of the Evaluation of Yarn Resistance

Sample	Average [Ω/cm]	Sample standard deviation [Ω/cm]	95% confidence interval
1y	3.74	0.82	0.28
2y	45.14	8.42	2.92
3y	89.74	15.12	5.24
4y	166.34	73.55	25.48

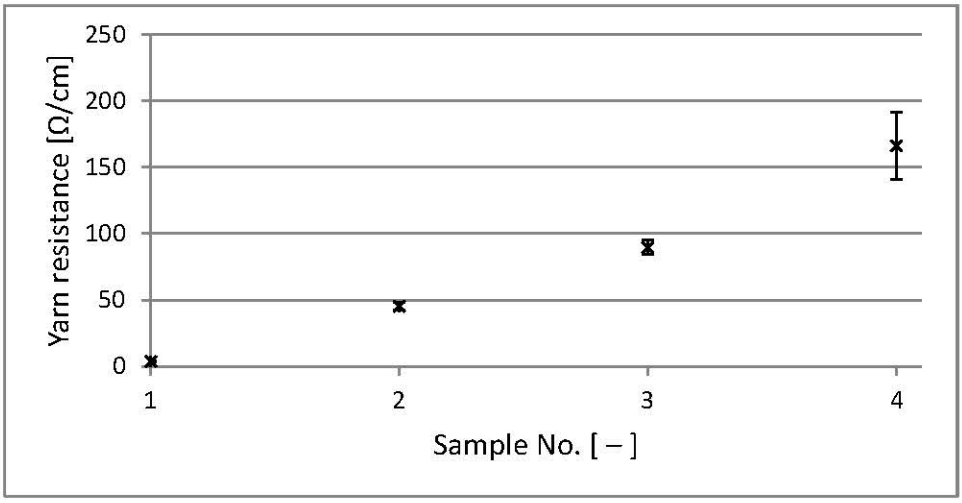

Fig. 12 Evaluation of the yarn resistance of #1y – 4y samples.

The effects of the yarns' composition on the resistance values recorded are clear from the measurement results. The more conductive a component, the lower is the resistance value recorded. The resistance value of the most conductive sample, #1y, which consists entirely of conductive material, is the lowest of all the samples examined, namely 3.74±0.82 Ω/cm. Samples #3y and #4y differ in the percentage of conductive content (60% and 40%, respectively). The resistance values recorded are 89.74±15.12 Ω/cm and 166.34±73.55 Ω/cm, respectively. Samples #2y and #4y differ in the type of the conductive component used. #2y contains a higher percentage of conductive content and its resistance value is, therefore, lower, namely 45.14 ±8.42 Ω/cm. The data also show that the lower the conductivity of a yarn sample, the greater is the 95% confidence interval.

Measuring Fabric Resistance

Using a four-point probe with electrodes placed in parallel is considered to be an easily applied method. The test fixture has a similar construction to that of the test fixture used for measuring yarn resistance, Fig. 13. The stable (A) and movable (B) electrodes are spaced 0.05, 0.1, 0.15 and 0.3 m apart. The test fixture is made to hold a 0.03 m-wide fabric sample. The length of this sample is 10 times its width when using the maximum electrode spacing. The total weight of each electrode (2 kg brass electrode plus gold-plated contacts) ensures good contact with the fabric sample. The stable (A) and movable (B) electrodes are voltage electrodes. The voltage supply is connected, and a voltage drop is measured between the two electrodes. A precision current source is connected to the two outermost electrodes (C), (D), i.e., metal clips. A fabric sample is attached to the outermost electrode (C)

and a load is applied at the end of the sample. The weight of the load is chosen in accordance with the standard [70]. The stable electrode (A) is fixed in its position and the movable electrode (B) is placed at a distance of 0.3, 0.15, 0.1 and 0.05 m in order to eliminate the effects of fabric deformation caused by the electrodes' weight. Resistance values are measured at these positions and the results are evaluated. Basically, it is recommended to examine 3 – 5 samples or to examine a sample at 3 – 5 different positions. This electrode configuration makes it possible to examine one 0.4x0.03 m-sized sample in four sections. Moreover, the evaluation of resistance values makes the determination of contact resistance simpler because resistance is dependent on distance. The linear approximation of this dependence produces a constant called *contact resistance* on the y-axis (resistance values are shown on the y-axis). This evaluation of the measuring technique also makes it easy to see the material's heterogeneity via the 95% confidence interval.

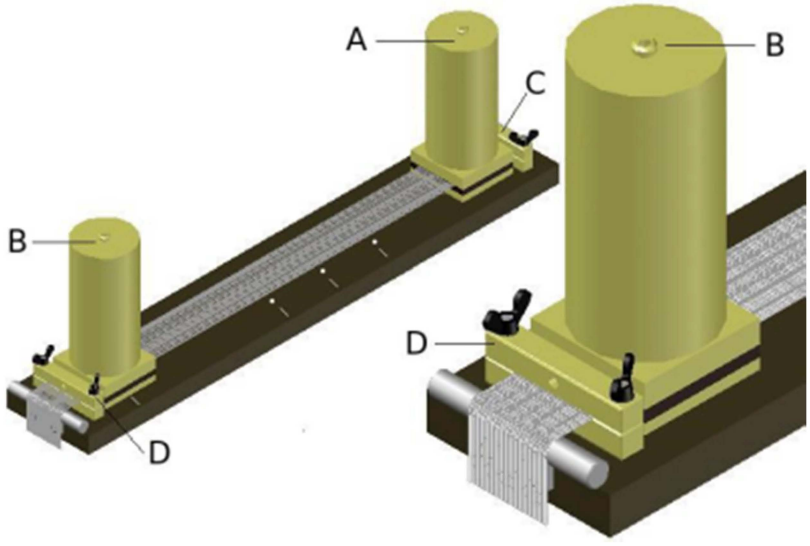

Fig. 13 3D model of a test fixture used for the measurement of fabric resistance.

Seven fabric samples were made from the yarns used in the previous measurement, Table IV. The samples are kept in a climate-controlled environment and measurement is performed at 40% RH, 22 °C. A 200 g weight is used to achieve the desired mass per unit area [71]. An Agilent B2911A Precision Source/Measure Unit and Agilent 34420A Nano Voltmeter are used. The Kelvin (4-wire) method and the Digital Voltmeter Method (DVM) comparison method involving the use of a METRA laboratory standard resistor calibrator (MANGANIN 0.1 Ω) are used for low resistance measurement [71], [72]. 150 resistance values are recorded at an interval of 3 s, the stability of the sample is checked (the values are stable within two significant digits and fluctuation is small), and the mean is calculated.

Table IV Fabric Specification

#	Composition	Fabric structure	Mass per unit area [g/m^2]	Warp/weft density d_w [t/cm]	Linear density [tex]
1	SilveR.STAT® 240dtex/10F	Plain weave	75	13/13	24
2	SilveR.STAT® 240dtex/10F	Plain weave	95	16/16	24
3	60% PES / 40% SilveR.STAT® 3.3dtex	Plain weave	92	13/13	29.5
4	60% PES / 40% SilveR.STAT® 3.3dtex	Plain weave	115	16/16	29.5
5	60% PES / 40% SilveR.STAT® 3.3dtex	Plain weave	135	19/19	29.5
6	40% PES / 60% SilveR.STAT® 1.7dtex	Plain weave	115	16/16	29.5
7	60% PES / 40% SilveR.STAT® 1.7dtex	Plain weave	117	16/16	29.5

The data are shown in Table V – Table XI, Fig. 14 – Fig. 20 and are summarized in Table XII. The results are characterized by a high value of the coefficient of determination R^2, i.e., $R^2 \geq 0.9995$, which means that the regression line perfectly fits the data and the samples are considered relevant and representative of the material. The values of the 95% confidence interval obtained by calculation indicate low variability in the resistance values recorded. The resistance values for the fabric samples are: #1 R_{F1}=0.073±0.004 Ω/cm, #2 R_{F2}=0.066±0.002 Ω/cm, #3 R_{F3}=0.68±0.01 Ω/cm, #4 R_{F4}=0.64±0.01 Ω/cm, #5 R_{F5}=0.47±0.01 Ω/cm, #6 R_{F6}=2.98±0.10 Ω/cm and #7 R_{F7}=19.2±0.8 Ω/cm. These values correspond to the resistance values for the yarns used, i.e., the more conductive a yarn, the more conductive is the fabric. We can also see that the greater the sett of a material, the lower is the resistance value, e.g. #1 and #2 differ in sett, being 13 and 16, respectively. The same can be said of #3, #4 and #5, which are characterized by a sett of 13, 16, and 19, respectively. The resistance values calculated for the particular electrode distances and expressed in Ω/cm vary because of the heterogeneity of the textile material. The regression line and its line equation indicate the contact resistance values through the y-intercept, i.e., the point where the line crosses the y-axis, and the linear resistance value, i.e., the slope of the regression line. The linear resistance value obtained from the slope of the regression line differs from the mean of the resistance values obtained by measurement because the mean model cannot explain any of the variance in the resistance values, it merely measures it. Additionally, the regression model also includes the forecasting of the electrode distance, Table XII. We can compare the two results to determine the percent deviation, which is at most 10%. Contact resistance is 0.070 Ω for #1, 0.031

Ω for #2, 0.145 Ω for #3, 0.214 Ω for #4, 0.1776 Ω for #5, 0.924 Ω for #6, and 15.755 Ω for #7. The contact resistance values are of the same order of magnitude as the linear resistance values. This means that the contact resistance of the connectors is minimized and the contact resistance between the samples and electrodes is as specified.

Table V Fabric Resistance - Sample 1

#	Distance [mm]	Average [Ω]	Average [Ω/cm]	Sample standard deviation [Ω/cm]	95% confidence interval
1	300	2.05E+00	6.83E-02	9.36E-04	1.50E-04
	150	1.07E+00	7.17E-02	8.23E-04	1.11E-04
	100	7.31E-01	7.31E-02	3.33E-04	1.18E-04
	50	3.93E-01	7.85E-02	3.41E-04	5.45E-05
			7.29E-02	3.69E-03	5.91E-04

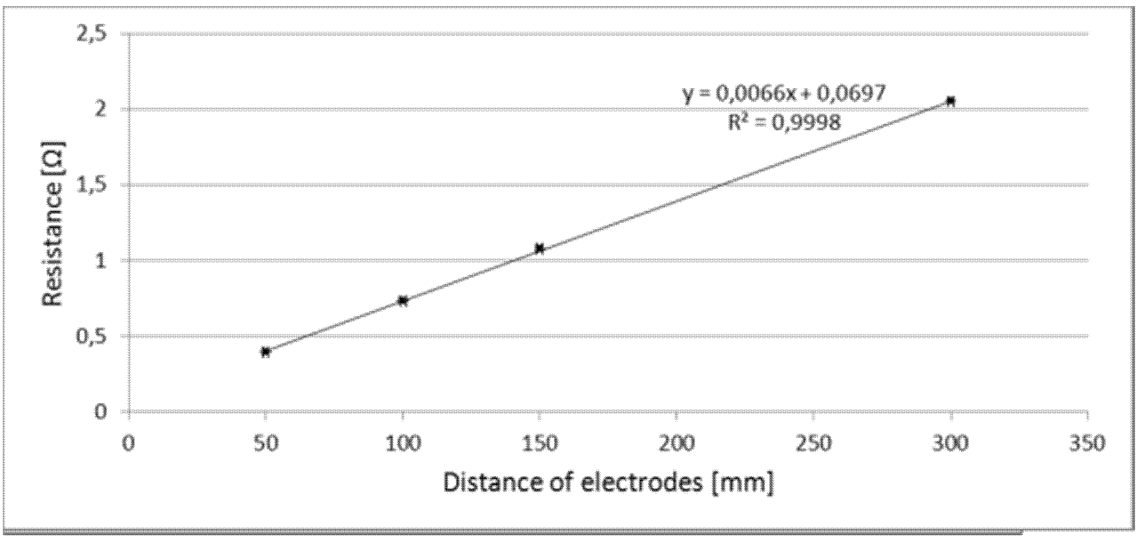

Fig. 14 Fabric resistance - sample 1.

Table VI Fabric Resistance - Sample 2

#	Distance [mm]	Average [Ω]	Average [Ω/cm]	Sample standard deviation [Ω/cm]	95% confidence interval
2	300	1.92E+00	6.40E-02	8.34E-04	1.34E-03
	150	9.81E-01	6.54E-02	4.38E-04	7.01E-05
	100	6.60E-01	6.60E-02	3.33E-04	5.33E-05
	50	3.44E-01	6.89E-02	3.33E-04	5.33E-05
			6.60E-02	1.77E-03	2.84E-04

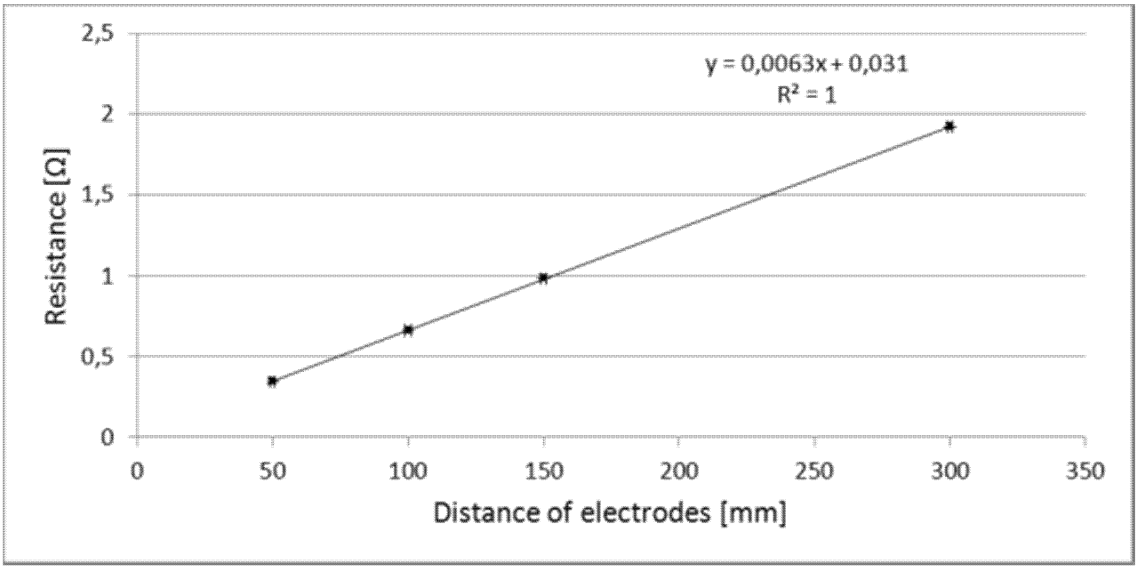

Fig. 15 Fabric resistance - sample 2.

Table VII Fabric Resistance - Sample 3

#	Distance [mm]	Average [Ω]	Average [Ω/cm]	Sample standard deviation [Ω/cm]	95% confidence interval
3	300	20.08E+00	6.69E-01	2.51E-02	4.02E-03
	150	10.40E+00	6.94E-01	7.18E-03	1.15E-03
	100	6.78E+00	6.79E-01	1.15E-02	1.84E-03
	50	3.36E+00	6.73E-01	4.47E-03	7.15E-04
			6.79E-01	9.29E-03	1.49E-03

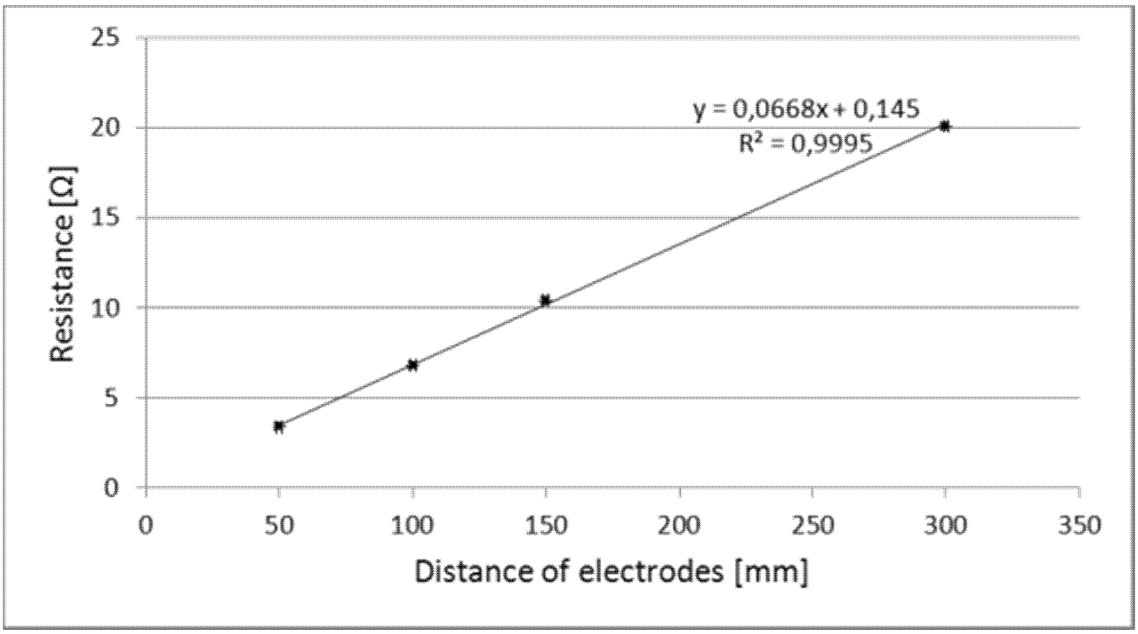

Fig. 16 Fabric resistance - sample 3.

Table VIII Fabric Resistance - Sample 4

#	Distance [mm]	Average [Ω]	Average [Ω/cm]	Sample standard deviation [Ω/cm]	95% confidence interval
4	300	18.83E+00	6.28E-01	2.54E-02	4.06E-03
	150	9.49E+00	6.33E-01	9.99E-03	1.60E-03
	100	6.44E+00	6.44E-01	5.77E-03	9.23E-04
	50	3.32E+00	6.63E-01	4.83E-03	7.74E-04
			6.42E-01	1.37E-02	2.19E-03

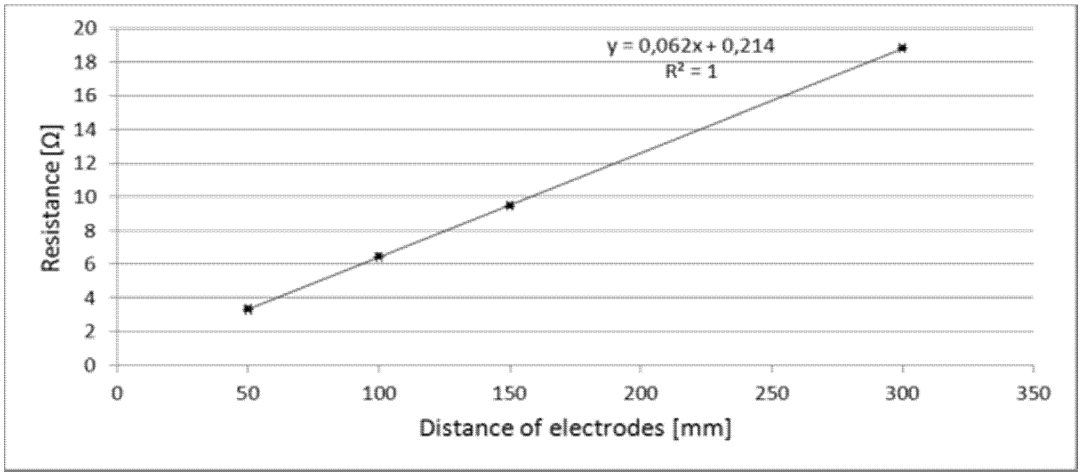

Fig. 17 Fabric resistance - sample 4.

Table IX Fabric Resistance - Sample 5

#	Distance [mm]	Average [Ω]	Average [Ω/cm]	Sample standard deviation [Ω/cm]	95% confidence interval
5	300	1.38E+01	4.61E-01	1.58E-02	2.53E-03
	150	6.98E+00	4.66E-01	2.37E-03	3.78E-04
	100	4.69E+00	4.69E-01	3.47E-03	5.54E-04
	50	2.49E+00	4.98E-01	3.12E-03	4.99E-04
			4.73E-01	1.44E-02	2.32E-03

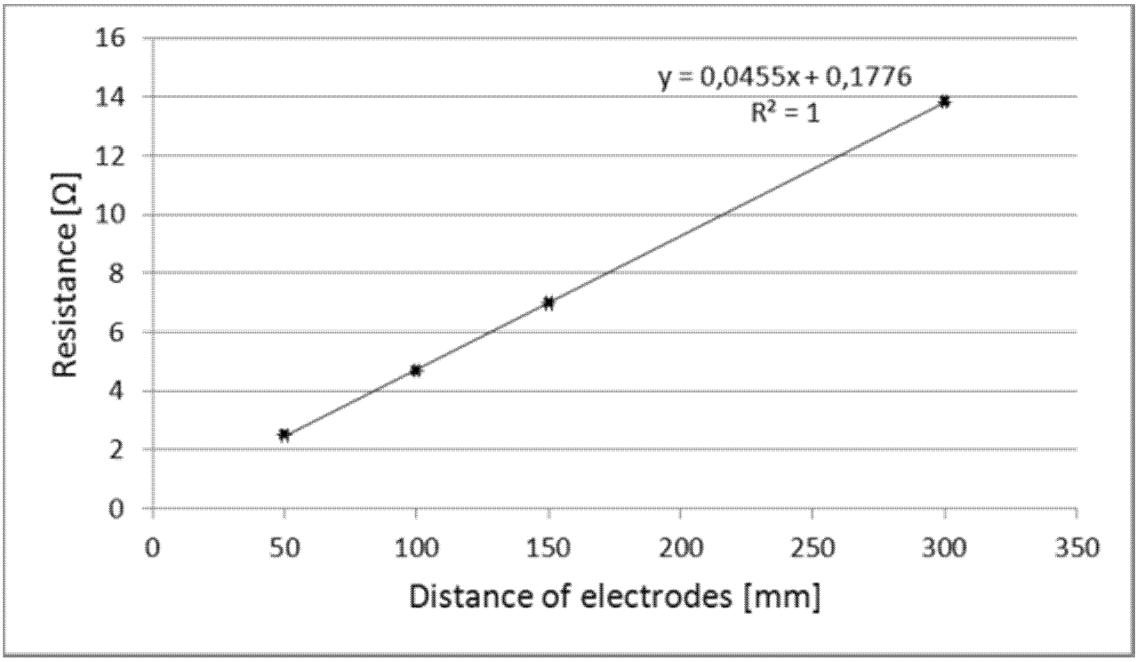

Fig. 18 Fabric resistance - sample 5.

Table X Fabric Resistance - Sample 6

#	Distance [mm]	Average [Ω]	Average [Ω/cm]	Sample standard deviation [Ω/cm]	95% confidence interval
6	300	8.74E+01	2.91E+00	1.19E-01	1.91E-02
	150	4.39E+01	2.93E+00	3.77E-02	6.03E-03
	100	2.93E+01	2.93E+00	3.53E-02	5.64E-03
	50	1.58E+01	3.15E+00	1.17E-02	1.88E-03
			2.98E+00	1.00E-01	1.61E-02

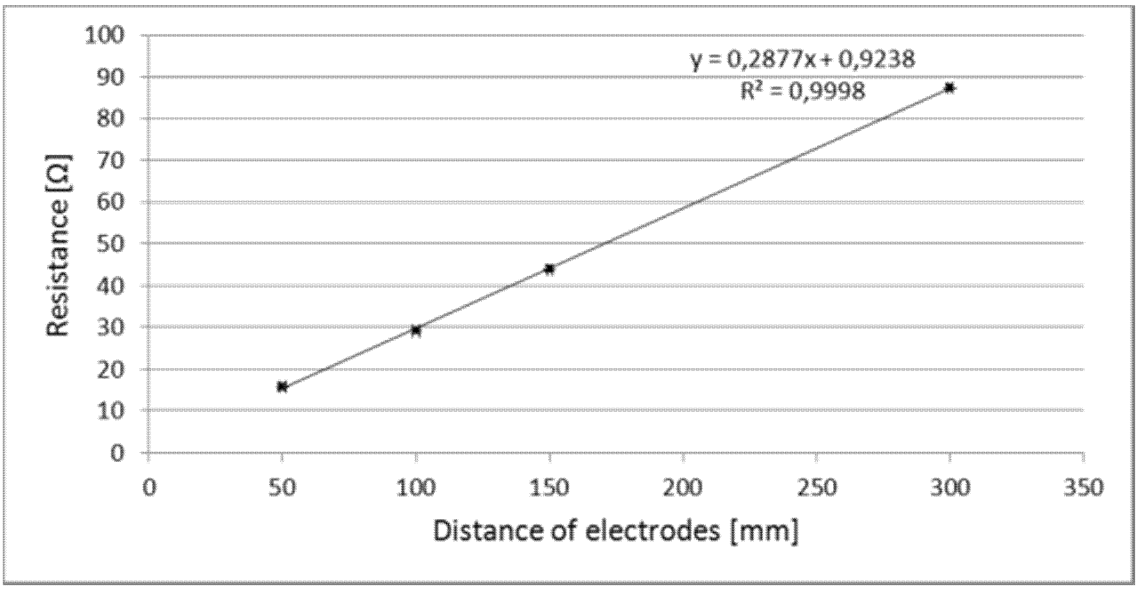

Fig. 19 Fabric resistance - sample 6.

Table XI Fabric Resistance - Sample 7

#	Distance [mm]	Average [Ω]	Average [Ω/cm]	Sample standard deviation [Ω/cm]	95% confidence interval
7	300	5.44E+02	1.81E+01	3.70 E+00	5.93E-01
	150	2.81E+02	1.87E+01	4.12E-01	6.59E-02
	100	1.95E+02	1.95E+01	7.56E-01	1.21E-01
	50	1.01E+02	2.02E+01	9.08E-02	1.45E-02
			1.92E+01	7.96E-01	1.27E-01

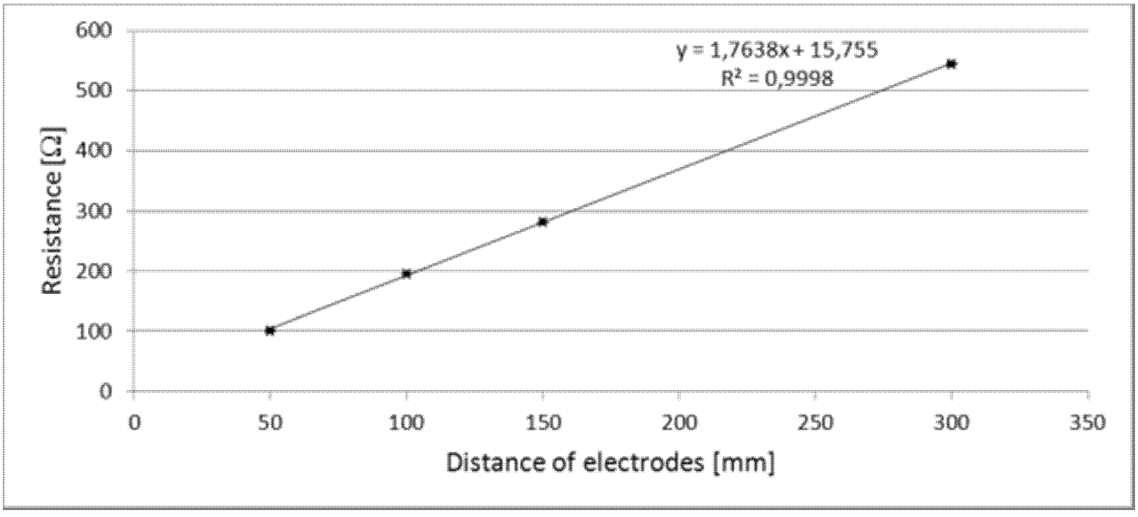

Fig. 20 Fabric resistance - sample 7.

Table XII Fabric Resistance - Sample 1 - 7

#	Average - mean model [Ω/cm]	Sample standard deviation [Ω/cm]	95% confidence interval	Average - regression model [Ω/cm]
1	7.29E-02	3.69E-03	5.91E-04	6.60E-02
2	6.60E-02	1.77E-03	2.84E-04	6.30E-02
3	6.79E-01	9.29E-03	1.49E-03	6.68E-01
4	6.42E-01	1.37E-02	2.19E-03	6.20E-01
5	4.73E-01	1.44E-02	2.32E-03	4.55E-01
6	2.98E+00	1.00E-01	1.61E-02	2.88E+00
7	1.92E+01	7.96E-01	1.27E-01	1.76E+01

3.1.7. Determination of Fabric Electrical Conductivity

Voltage electrodes are placed on the surface of a sample. In standard methods of determining volume resistivity, electrodes are placed on both sides of a sample [39], [61]. However, our previous research [19] showed that surface resistance values are equal to bulk resistance values for highly conductive fabrics, i.e., fabrics characterized by resistance values of several ohms for 30x30 and 30x100 mm-sized samples. This means that the conductivity of the samples is such that all the current penetrates the material's core.

Therefore, (5) can be used and the cross-sectional area of the sample has to be calculated. The width *W* of the sample is 0.03 m. The distance between the electrodes is considered to be 0.01 m, as we are using the linear resistance values obtained from the slope of the regression line. The thickness data, namely the mean values (pivot half-sums), pivot ranges and 95% confidence interval (CI), are shown in Table XIII. Thickness is measured using the MarCator 1086 digital indicator with a resolution of 1E-06 mm. Due to the sample size being $4 \leq n \leq 20$ measurement points, we use the statistical procedure proposed by Horn in [73]. This procedure is based on the depths that correspond to the samples' quartiles.

Table XIII Fabric Thickness

	Thickness [mm]		
#	**Pivot half sum P_L**	**Pivot range R_L**	**95% CI**
1	2.95E-01	5.00E-03	2.62E-03
2	3.00E-01	9.00E-03	4.71E-03
3	4.69E-01	1.50E-02	7.85E-03
4	5.37E-01	2.50E-02	1.31E-02
5	5.33E-01	2.00E-02	1.05E-02
6	4.76E-01	1.10E-02	5.75E-03
7	4.91E-01	3.00E-02	1.57E-02

Volume resistivity and fabric conductivity results are shown in Table XIV. The greatest conductivity value (ρ_V = 1.77E+04 S/m) is obtained for #2. This sample has the greatest conductive content and is characterized by a sett d_w = 16 t/cm (number of yarns in 1 cm). By contrast, the sett for #2 is d_w = 13 t/cm. Samples #3, #4 and #5 consist of the same yarns, the only difference being the sett value (d_w = 13, 16 and 19 t/cm, respectively). Hence, the conductivity value is expected to increase with the sett value. However, the conductivity value for #3 is greater than for #4, which is due to the thickness value being smaller for #3 than for #4. The conductivity value for #7 is σ=2.60±0.14 Ω.cm. This sample can be categorized as moderately conductive textile material because its volume resistivity value falls in the range between 1 and 10^7 Ω.cm as defined in [7], [39]. The conductivity value for #6 is σ=0.41±0.02 Ω.cm, which is very close to this limit.

Table XIV Fabric Volume Resistivity and Conductivity

	Volume resistivity ρ_{VF} [Ω.cm]		Conductivity σ_{VF} [S/m]	
#	**Average**	**Sample standard deviation**	**Average**	**Sample standard deviation**
1	5.83E-03	3.30E-04	1.71E+04	9.72E+02
2	5.66E-03	1.82E-04	1.77E+04	5.69E+02
3	9.39E-02	2.04E-03	1.07E+03	2.32E+01
4	9.98E-02	3.28E-03	1.00E+03	3.29E+01
5	7.28E-02	2.72E-03	1.37E+03	5.14E+01
6	4.10E-01	1.51E-02	2.44E+02	8.99E+00
7	2.60E+00	1.44E-01	3.85E+01	2.13E+00

3.1.8. Measurement and Modelling Results

A comparison of measurements involving a two-electrode resistivity model based on (6) requires the determination of the value of parameter R_1. Previous research showed that this parameter can be calculated as in [19]:

$$R_1 = \frac{R_l \cdot l_{R_1}}{l_R} = \frac{R_l}{l_R} \cdot \frac{W - t_w \cdot d}{t_w}. \tag{24}$$

where R_1 is the resistor modelled, R_l stands for the resistance of the fiber with a length l_R, l_{R1} denotes the length of R_1, t_w means the number of warp/weft threads, d denotes the yarn diameter, and W is the width of the fabric sample.

Yarn resistance, i.e., the R_l parameter for the length l_R = 0.01 m, is shown in Table III. The width of the sample is W = 0.03 m. The warp and weft density values d_w for all samples are given in Table IV. The densities recorded are 13, 16 and 19 t/cm for 39, 48 and 57 warp/weft threads t_w, respectively. The yarn diameter d is determined using an INTRACO MICRO RTL PC-2 microscope with an embedded Dino-Eye AM4023CT digital camera. Fig. 21 shows the diameter measurement for #2, the composition of the sample and twenty diameter values measured at different

positions on the yarn. Diameter is measured for every sample (#1 – #7), even though only four types of yarn (#1y – #4y) were used, Table II and Table IV. The yarn diameter *d* and the calculated values for the modelled resistor R_1 are summarized in Table XV. Diameter evaluation shows that the pivot half-sum values vary between samples with the same composition, i.e., between samples #1 and #2 and #3 – #5. This difference is attributable to the composition of the yarn as shown in Fig. 21 as well as to the small number of measurements – twenty values recorded per sample (#1 – #7). The diameter of yarn #1y (samples #1 and #2) is recorded sixty times and the mean is d_{1y}=0.245±0.035 mm. The diameter of #2y (samples #3 – #5, #3y (#6) and #4y (#7)) is also measured at sixty points of measurement and it is d_{2y} = 0.239±0.038 mm, d_{3y} = 0.220±0.029 mm, and d_{4y} = 0.240±0.046 mm. An evaluation of the R_1 values shows that resistance decreases with the increase of the sett value. This observation is in accordance with (24).

Table XV Resistor R_1 Evaluation

#	d [mm]					R_1 [Ω]
	Pivot half sum P_L	Pivot range R_L	95% CI	Average	Sample standard deviation	
1	2.63E-01	7.10E-02	2.39E-02	2.51E-01	2.52E-02	1.94E-01
2	2.44E-01	2.90E-02	9.77E-03			1.40E-01
3	2.35E-01	4.50E-02	1.52E-02	2.39E-01	3.81E-02	2.39E+00
4	2.40E-01	7.20E-02	2.43E-02			1.74E+00
5	2.38E-01	7.10E-02	2.39E-02			1.30E+00
6	2.20E-01	5.00E-02	1.69E-02	2.20E-01	2.87E-02	3.64E+00
7	2.20E-01	6.80E-02	2.29E-02	2.40E-01	4.59E-02	6.40E+00

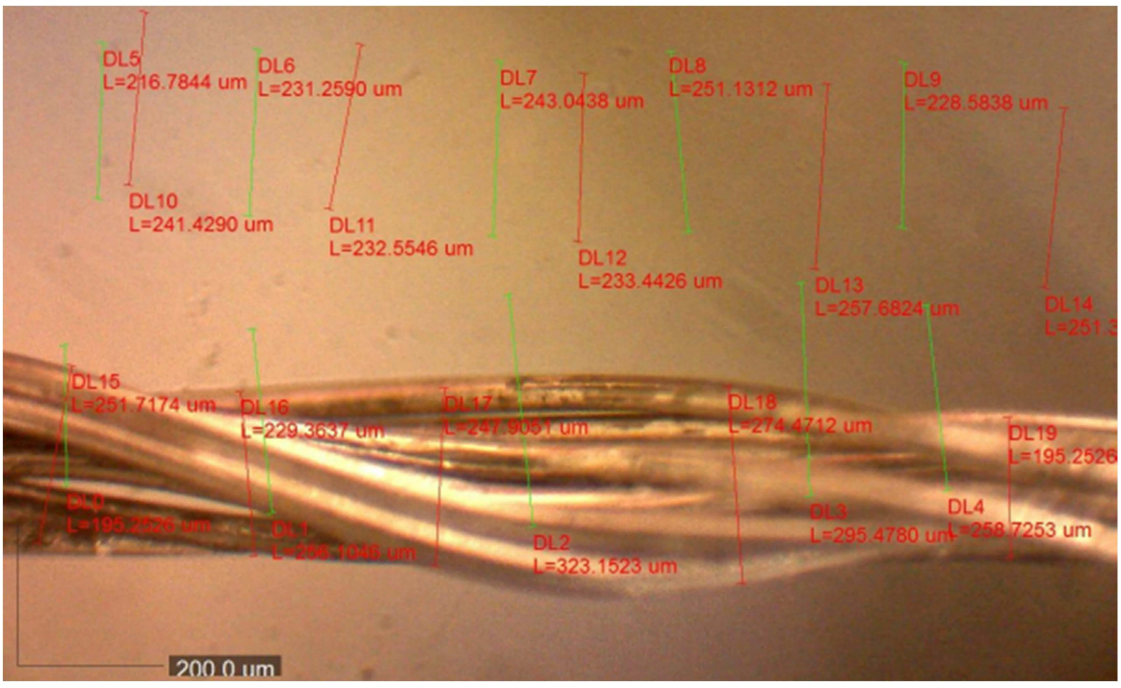

Fig. 21 Yarn diameter measurement in sample #2 and #1y.

Table XVI and Table XVII show a comparison for a two-electrode system of the resulting modelled resistance R_{M2} with volume resistivity ρ_{VM2} calculated according to (5) and conductivity σ_{VM2} calculated according to (1) and the measured resistance R_F with the recalculated volume resistivity ρ_{VF} (5) and conductivity σ_{VF} (1). Tab. XVII shows a comparison for a three-electrode system of the values of ρ_{VM2}, σ_{VM2}, ρ_{VF} and σ_{VF} and the volume resistivity ρ_{VM3} calculated according to (16) and conductivity σ_{VM3} (1). The resistance values R_{M2} are calculated according to (6) with respect to the results presented in Table XV. The resistance values R_F are analysed in Table V – Table XII and Fig. 14 – Fig. 20. The modelling and measurement results show that the values for samples #1 – #6 are of the same order of magnitude. The value for sample #7 differs in the order of magnitude because the sample is a moderately conductive textile material, as previously mentioned. The variation in the modelled and measured values for samples #1 – #6 is considered acceptable, considering the heterogeneous structure of the textile material as depicted in Fig. 22 and Fig. 23. The order of magnitude or the maximum order of magnitude of conductivity, resistivity and resistance are commonly indicated by the producers [74], [75], [76]. Hence, the three-electrode model can be considered valid and can be further extended in the weft and warp directions by different yarns with different sett values. It can also be concluded that the model is valid for highly conductive textile materials, i.e., materials with a volume resistivity of less than 1 Ω.cm.

Table XVI Comparison of Measured and Modelled Resistance for a Two-Electrode System

#	R_F [Ω/cm] Average - regression model	R_{M2} [Ω/cm]
1	6.60E-02	6.45E-02
2	6.30E-02	4.65E-02
3	6.68E-01	7.98E-01
4	6.20E-01	5.81E-01
5	4.55E-01	4.32E-01
6	2.88E+00	1.21E+00
7	1.76E+01	2.13E+00

Table XVII Comparison of Measured and Modelled Results

#	ρ_{VF} [Ω.cm]	ρ_{VM2} [Ω.cm]	ρ_{VM3} [Ω.cm]	σ_{VF} [S/m]	σ_{VM2} [S/m]	σ_{VM3} [S/m]
1	5.83E-03	5.70E-03	5.48E-03	1.71E+04	1.75E+04	1.82E+04
2	5.66E-03	4.18E-03	6.69E-03	1.77E+04	2.39E+04	1.50E+04
3	9.39E-02	1.12E-01	7.15E-02	1.07E+03	8.92E+02	1.40E+03
4	9.98E-02	9.35E-02	8.81E-02	1.00E+03	1.07E+03	1.14E+03
5	7.28E-02	6.91E-02	4.47E-02	1.37E+03	1.45E+03	2.24E+03
6	4.10E-01	1.73E-01	1.99E-01	2.44E+02	5.78E+02	5.02E+02
7	2.60E+00	3.14E-01	3.22E-01	3.85E+01	3.18E+02	3.10E+02

Fig. 22 Image of sample #3 consisting of yarn #2y.

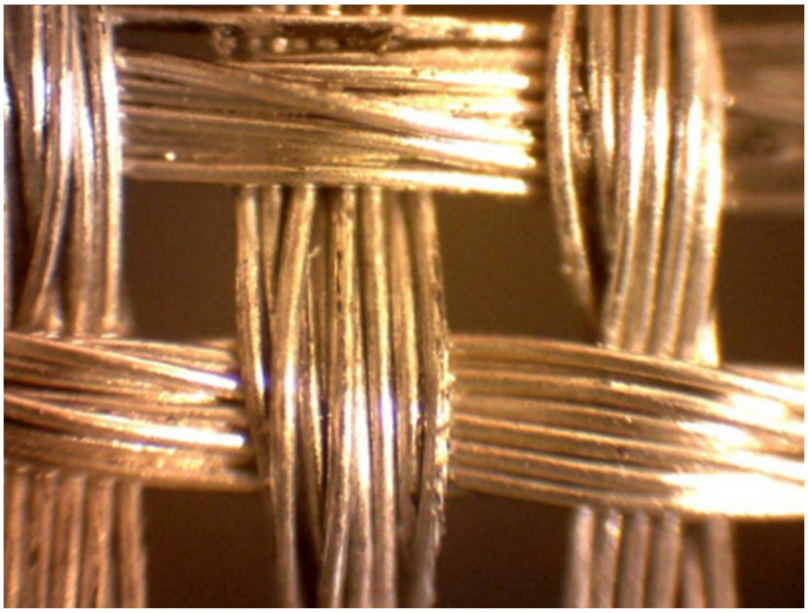

Fig. 23 Image of sample #2 consists of yarn #1y.

3.1.9. Conclusions for Modelling

Current standards lack a definition of highly conductive textile materials and hence, in this chapter presented definition is based on that of moderately conductive materials. A highly conductive textile material is a material that has a volume resistivity of less than 1 Ω.cm. There are no standard methods of determining volume resistivity and conductivity for highly conductive textile materials. There is only a standard that described the process of determining the resistance of conductive

tracks. For this reason, it was necessary to describe the measuring technique for determining resistance in particular detail. Volume resistivity and electrical conductivity were analysed, even though the relevant calculations are not available in the standards. The yarn resistance data show that the 95% confidence interval increases with a yarn's resistance. The resistance value for the yarns fall within the range between 3 and 166 Ω/cm. The fabric resistance data are characterized by a high value of the coefficient of determination $R^2 \geq 0.9995$, which means that the regression line perfectly fits the data and the variability of the resistance values as indicated by the 95% confidence interval, and by determination of contact resistance values. The resistance values for the fabric samples were in the range between 0.066 and 17.6 Ω/cm. The conductivity and volume resistivity of the fabrics were calculated based on the thickness of the samples and was in the range between 38.5 and 17700 S/m and 0.0057 and 2.6 Ω.cm, respectively. Sample #7, characterized by a volume resistivity of ρ = 2.6 Ω.cm, is considered as a moderately conductive textile material, and hence, the modelling results for this sample are not valid. The modelling and measurement results for samples #1 – #6 are of the same order of magnitude of resistance, volume resistivity and conductivity. This result is acceptable considering the heterogeneous structure of the textile material and the values commonly indicated by the producers. It is also proven that the three-electrode model is valid for highly conductive textile materials and can be, in future work, extended in the weft and warp directions by different yarns with different sett values.

3.2. Application - Electrically Conductive Textile Materials for Medical Applications

Electrically conductive textiles are fabrics that can lead an electric current. These materials can be used not only in sensor design but also in heating applications. This chapter discusses the design of a patient heating application that uses electrically conductive textile materials based on conductive fibres. The heating capability of a specific sample and an experimental technique are discussed. The results show that the sample can be heated up to 35 °C, at which point the subject lying on a bed with the material feels warmth all over the body.

3.2.1. State of the Art

In [77], the authors compare five carbon fibre materials using infrared imaging technology. They conclude that this technology can be used to determine the heat conduction performance of the chosen carbon fibre samples quickly and accurately. The company Gerster TechTex manufactures heatable textiles for floor heating applications as well as an electric blanket [78]. The textiles consist of a warp-knitted base structure with conductive carbon fibre loops for heating. The Bekinox® stainless-steel fibres are electrically conductive fibres designed for car seat heating, garments, gloves, etc. [79]. They come in insulated and non-insulated types. A metal conductive yarn is presented in [80]. The authors contend that carbon fibre can be partially broken, flexible printed circuit boards (PCB) have a limited bending angle, and stainless steel can be also partially broken in the layout process or by wear and tear. They further assert that a metal conductive yarn can be sewn into a non-conductive textile material and connected to a 5 – 12 VDC power supply. The same approach (conductive yarns sewn into textiles) has been adopted by the company SEFAR [81].

Electrically conductive textile materials are made by sewing conductive fibres into non-conductive textiles. Thus, we can choose to heat only a part of the textile material or create various heating patterns depending on the production method. There are more approaches to making textile materials heatable.

Previous research has shown that electrically conductive textile materials can be made from conductive fibres (blend of conductive and non-conductive fibres) [82] or using a coating process [83]. Our paper [83] contains a discussion of conductive textile materials for bed heating applications. The dimensions are those of a typical bed sheet, i.e., 190 x 100 cm (reduced to allow the attachment of a metal clip). In [83], we demonstrated that copper-coated polyester can be heated up to 39 °C at 5.5 VDC.

The present experiment focuses on the investigation of the heating capability of an electrically conductive textile material, namely copper-coated polyester. We used a sample with the shape and size of a bed sheet intended for hospital and home care use as part of the silver economy.

The chapter discusses the sample's resistance which determines whether the material can conduct an electric current, and can therefore be heated. The sample needs to be connected to a power supply using a good connection such as a metal clip, Velcro fastener or glue. The measurement data show that the sample can be heated up to 35 °C, at which point the patient lying on a bed covered with the material feels warmth all over the body.

3.2.2. Description of the Sample

The choice of conductive textile material was based on previous research [16]. It is copper-coated PES with the resistivity ρ = 0.0352 Ω/square (resistance per square area), warp/weft density dw = 60 t/cm, mass per unit area 80 g/m^2. A macro picture of the copper-coated polyester can be seen in Fig. 24. The regularity and uniformity of the structure clearly indicate that the sample is a woven textile made up of only one type of fibre. This is, however, not important because the conductive component (copper) is external to the textile, being applied on both sides.

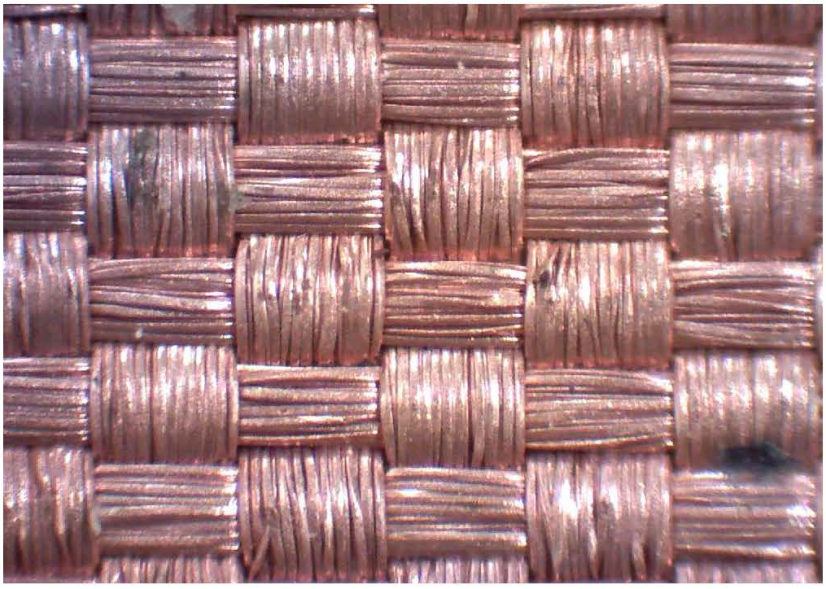

Fig. 24 Copper-coated polyester.

3.2.3. Sample Dimensions and Resistance Value

The dimensions of the sample are 190 x 100 cm and correspond to a twin bed (typically 190 x 99 cm). The difference in the width is negligible, considering that we're heating a human subject and 1% difference in the overall surface area cannot have any effect on the validation of the proposed concept.

The surface area is calculated as the product of length and width. However, two surfaces have to be considered because the material is surface copper-coated on both sides. The area of one surface is 1.9 m^2; the total surface area of the sample is 3.8 m^2.

The thickness of the sample ranges in the tenths of millimetres and can be accurately determined using a microscope or micrometre, e.g. Oxford Precision OXD-331-5010K. A comparison of the two methods is presented in [19] and shows that a micrometre measurement can be used. Furthermore, the heating ability of the sample depends on the resistance of the material, namely the resistance of the two electrically conductive surfaces. Therefore, the sample thickness is not important for the resistance evaluation.

Considering that the sample is characterized by the resistivity value ρ = 0.0352 Ω/square, dimensions of 190 x 100 cm and surface area 3.8 m2, the total resistance value of the sample can be calculated as follows:

$$R \approx \rho S = 0.135 \quad [\Omega]. \tag{25}$$

where R is the resistance of the sample, ρ means surface resistivity and S is the surface area.

3.2.4. Energy Required to Heat the Material

The power (voltage) supplied to the material, which is in contact with the human body, is limited due to safety concerns. It is typically 12 V for AC current; however, the maximum value is higher (25 VDC) at direct contact to active parts in especially dangerous areas [84].

3.2.5. Connection of the Textile Material

In order to energize the whole sample, the sample must be connected along its entire width. Moreover, as the textile is electrically conductive on both sides, each side and both ends need to be connected because of the use of a DC power source (positive and negative poles).

These requirements can be addressed by using a conductive metal clip, conductive glue or conductive Velcro fastener [85]. Velcro fastener is suitable because it is also made from a textile material and can easily be washed without changing its chemical properties. The use of conductive glue is debatable; however, glue can be used for concept verification in laboratory conditions instead of a conductive metal clip.

The connection of cables to the textile material is another area that must be addressed. We can use clips or a connector. A metal clip and screws, which hold both parts of the clip together, are used in the laboratory. This ensures that the

connection to the textile material is stable and free from any significant transition resistance.

The attachment of the metal clip to the textile is shown in Fig. 25. The clip goes around each end of the textile and provides a good connection between the electrically conductive textile material and the power supply cables, allowing the power to heat the textile sheet.

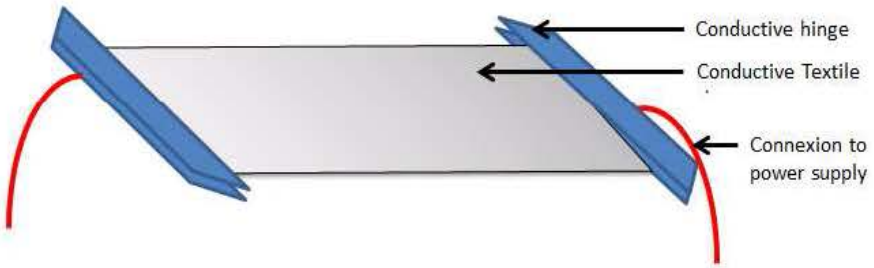

Fig. 25 Connection of the sample to the cables.

3.2.6. Experiment Setup

The temperature is measured by a Metex 3860D thermocouple and a MOBIR M4 thermographic camera. Voltage and current are supplied by a MAAS 1-15 VDC / 0 – 40 A, 600 W, HCS-3400 power supply. A human subject (patient) is asked to give a subjective thermal comfort assessment.

The thermocouple that is used to measure the temperature between the sample and the subject is placed between the sample and the subject's lower back. Infrared images are taken from a position above the scene.

The sample is placed on a hospital bed (single bed). A subject dressed in a T-shirt and trousers is lying on the bed, simulating a patient in hospital or home care. The subject's arms and hands are stretched along his body.

The experiment begins by energizing the sample. Power, temperature and infrared images are taken at eight individual measurement steps designated as ID 1 – 8. At each step, the subject's sensations are recorded.

3.2.7. Measurement Data and Discussion

At the beginning of the experiment, the temperature between the patient's back and the conductive textile sample was 31 °C. When the power supplied to the sample reached 150 W, the temperature increased from 31 °C to 32 °C. The first observation is that the increase in temperature is proportional to the power supplied, as explained in [81].

A summary of the measurement data is given in Fig. 26 and Table XVIII, showing all eight steps involving increases in power and the resulting changes in temperature. The corresponding infrared images are shown in Fig. 27 and Fig. 28. The summary also presents the subject's subjective observations. The intensity of the heat is represented as the number of red circles with different sizes, which are split into two groups based on the different sizes that the red circles can have.

The first two infrared images (#1 and #2 in Fig. 27) are almost identical. The area surrounding the bed appears black. The ambient temperature during the experiment is 22 ° C. The bed appears blue, slightly warmer than the surrounding area but colder than the subject lying on the bed whose body parts with the highest temperature such as the head and arms (he wears a T-shirt with short sleeves) range between purple and white.

At the time of the second picture (#2 in Fig. 27), the subject feels a very light warm sensation on his hips, legs and back. This may be because his body warms the sample or because of the contact with the sample.

The first temperature change in the sample is visible in the third image (#3 in Fig. 27). The sample now appears slightly purple. At this time, the temperature between the sample and the subject increased from 31 °C to 32 °C. The patient now feels more warmth on his hip, legs and back and his sensations are more distinct. He also feels warmth on his shoulders and hands but very slight.

The fourth picture (#4 in Fig. 27) shows that the sample is getting warmer (the temperature increased from 32 °C to 34° C, as shown in Fig. 26). We can also see that the subject is getting warmer too. Indeed, his body appears more white and yellow than in the previous image (particularly the lower back and the part of the shoulders and thighs that are in contact with the sample). His perceptions bear this out: he feels warmth on his hands, shoulders, back, hips and legs.

At the time of the fifth picture (#5 in Fig. 28), the temperature measured behind the subject's back is the same as in the previous step (#4, 34°C). The sample turns red and all the subject's body parts are warmer than at the time of the previous picture #4 (showing white in the infrared image) as a result of the contact with the sample. This can be due to blood circulation transferring heat to all body parts, so the temperature of the lower back does not change, while the rest of the body is getting warmer.

The rise in temperature is more visible in the sixth picture, #6 in Fig. 28. The subject now feels warmth on his head and feet and also feels enveloped in heat. This is represented by the red circle surrounding his body. Blood circulation has transported the heat to all his body parts. The temperature between the subject's back and the sample is 35 °C.

At the time of the seventh picture (#7 in Fig. 28), the temperature measured with the thermocouple is still 35 °C. The subject feels warmth on his feet and neck, which are not in direct contact with the bed sheet.

The last picture (#8 in Fig. 28) shows that the sample is warming the subject even more. The subject feels warmth all over his body (not only in the parts that are in contact with the sample). The temperature is 35 °C (same as before), but the subject's sensations take longer to develop.

These results show that a woven copper-coated polyester sheet can be used as a heated bed sheet. After reaching a temperature of 35 °C, the patient feels warmth in all his body parts and is enveloped in heat. Hence, 35 °C is the right temperature for this application because it produces the desired sensation of warmth in the patient. The sheet can be used to improve comfort for patients and general users alike.

The temperature of 35 °C is reached when the bed sheet is powered with 190 W. This seems to be a significant number, but it is only 0.01 W/cm² when taking the size of the bed sheet into consideration. With this power, there is no risk to the human body, as the contact is only indirect.

Table XVIII Measurement Data

ID	Temperature [°C]	Power [W]	Sensations
1	31	12	room temperature
2	31	50	+ warmth in hips, legs, back
3	32	150	+ warmth in hips, legs, back
4	34	180	+ warmth in hands, shoulders, back, hips and legs
5	34	180	+ more warmth
6	35	190	+ head and feet, + enveloped in heat
7	35	210	+ warmth in neck and feet
8	35	225	warmth all over the body

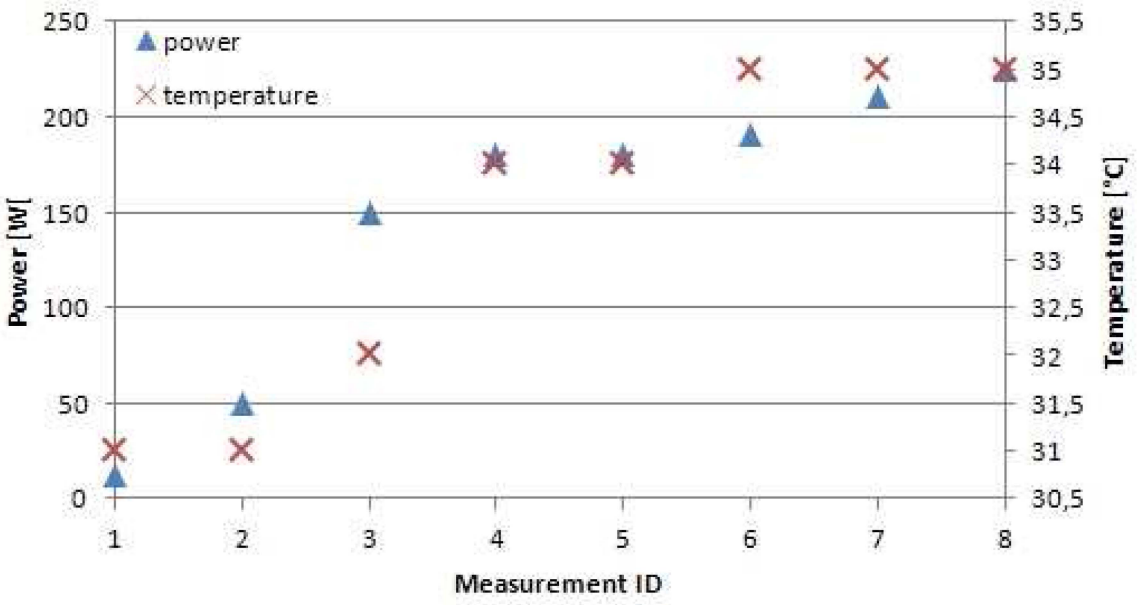

Fig. 26 Temperature and power changes at eight measurement steps.

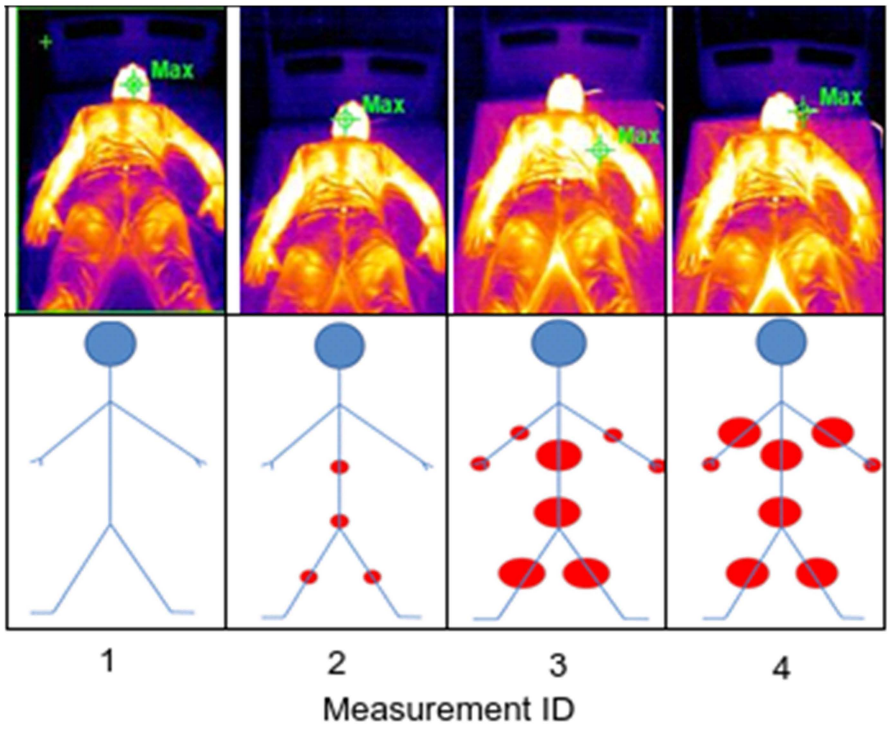

Fig. 27 Infrared images and interpretation of sensations for the first four steps.

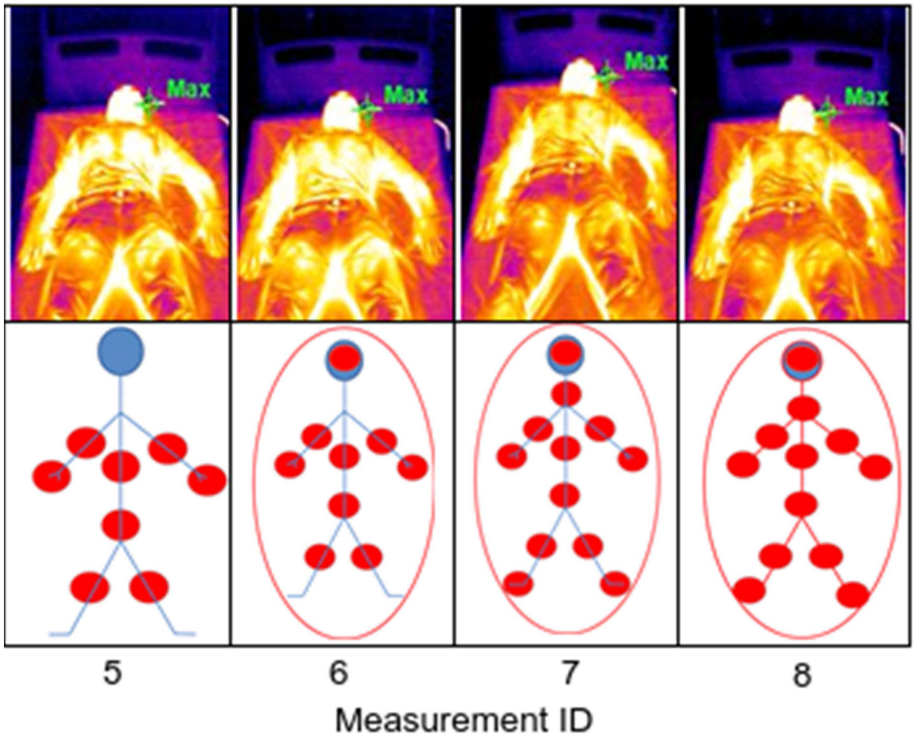

Fig. 28 Infrared images and interpretation of sensations for the last four steps.

3.2.8. Conclusions

The chapter describes an experiment in the design and measurement of a bed-sized sample of a heatable electrically conductive textile material, which can be used for patient warming applications in hospital and home care.

The sample material is copper-coated polyester with the resistivity value ρ = 0.0352 Ω/square. An electrical connection of the sample is proposed. A metal clip with screws is used in laboratory experiments. The sample is energized, and increases in temperature relative to power are recorded. Infrared images are taken at the individual measurement steps. At each step, the sensations of the subject lying on the heated textile are recorded.

The sample demonstrated good conductivity, as the temperature increased by several degrees of Celsius up to 35 °C, at which point the whole body of the subject was warm.

The chapter proves that electrically conductive coated textile materials can be confidently used for patient warming applications.

3.3. Application – "Self-drying" Planar Textile Materials with Electrically Conductive Structures

The chapter focuses on the design and simulation of the drying ability of highly conductive textile materials [82], [83]. Measurement data are presented and discussed.

3.3.1. State of the Art

One of the new features of smart fabrics is conducting electric current. This can be used in applications where "self-drying" is desired.

Textiles are dried in drying machines, several types of which exist. Hot and dry air enters the drum, absorbs the moisture and is led away from the machine, or cooled in a condensation chamber, by a water, air or heat pump. Another type of textile dryers uses microwave technology to extract moisture from the material's core [86].

The efficiency of the drying process can be improved by using suitable textile structures. Smart fabrics containing conductive elements can conduct an electric current. This ability depends, however, on the position or arrangement of the conductive element. This feature can be used for drying the textiles.

The chapter deals with the design and testing of "self-drying" textile materials.

3.3.2. Design of "Self-Drying" Textile Materials

The process of drying wet materials requires energy. It is important that we apply an appropriate amount of energy (voltage and current), ensuring user safety and avoiding damage to the textiles. If we feed too much power over a long period of time, we can even destroy the textile. A textile sample must contain at least 9% moisture at an air temperature of 20 °C and relative humidity of 50%; otherwise the fibres can suffer deformation [87].

For wearable textile materials, the choice of voltage is limited. In [88], the authors describe several environments in terms of their effects on the drying process. Wet, conductive environments and cramped spaces are considered as especially dangerous rooms. This classification designates safety extra-low voltage as 12 VAC and 25 VDC where there's direct contact with the active parts.

3.3.3. Description of the Equipment

The woven fabric sample contains 30% SilverStat / 30% Shieldex / 40% PES in the warp and 60% Shieldex / 40% PES in the weft direction. Its dimensions are 3x10 cm. The sample is placed between two electrodes as seen in Fig. 29. A HY3003D-2, Shenzhen Mastech DC power supply is used. The temperature of the sample is measured using an RC METEX M-3890D digital multimeter. A measurement probe is

attached to the sample and connected to the multimeter. Measurement data are recorded in the ScopeView 1.09 program. The sample is moistened by 15 drops of water. The electrical resistance of the sample is measured using an ESCORT ELC-3133A RLCG bridge.

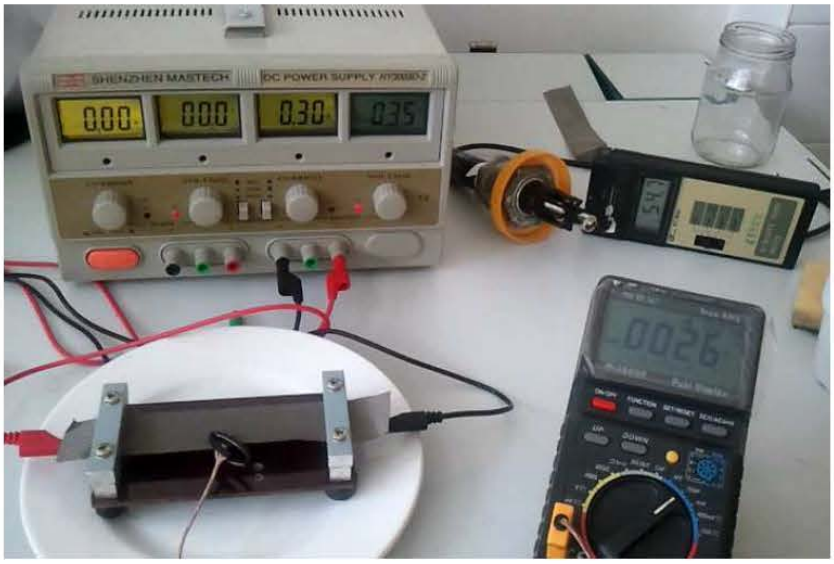

Fig. 29 Measurement setup.

3.3.4. Measurement Data and Discussion

The conductive textile material was moistened by 15 drops of water (approx. 1g). The temperature of the sample was measured at 4 different power levels, approx. 1 W, 2 W, 5 W and 10 W. The sample was replaced after each measurement with a new sample with the same size and properties. The variation of the sample's temperature in time is shown in Fig. 30 – Fig. 35.

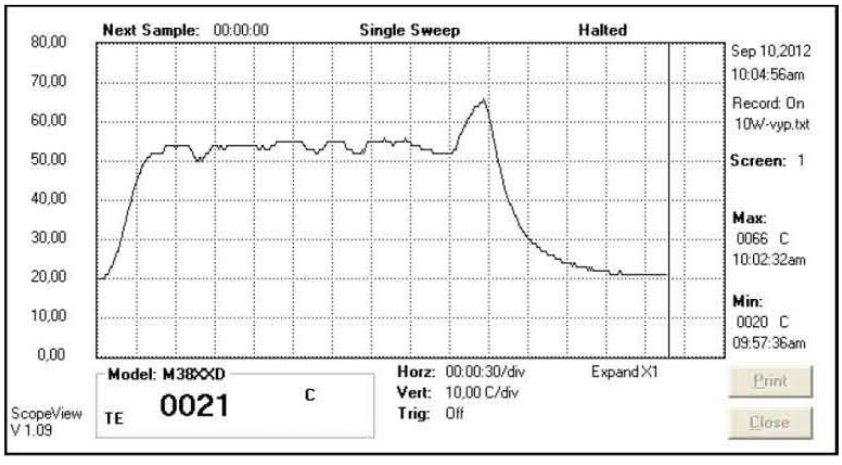

Fig. 30 Variation of the sample's temperature in time for P=10 W.

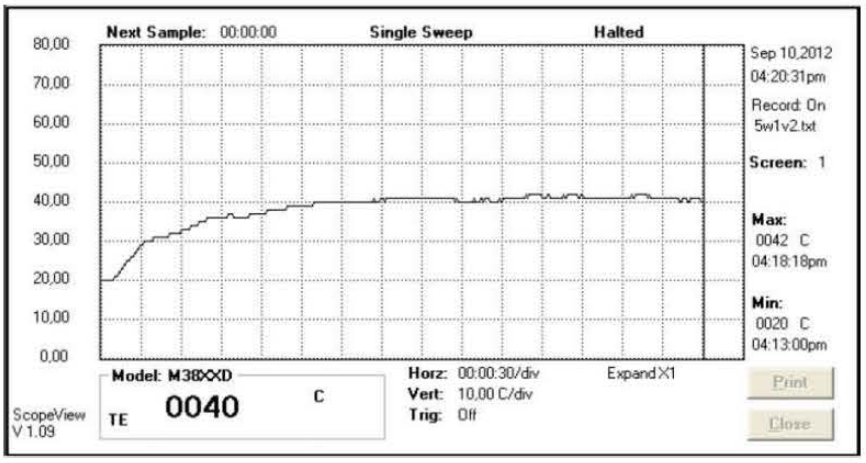

Fig. 31 Variation of the sample's temperature in time for P=5 W (first part).

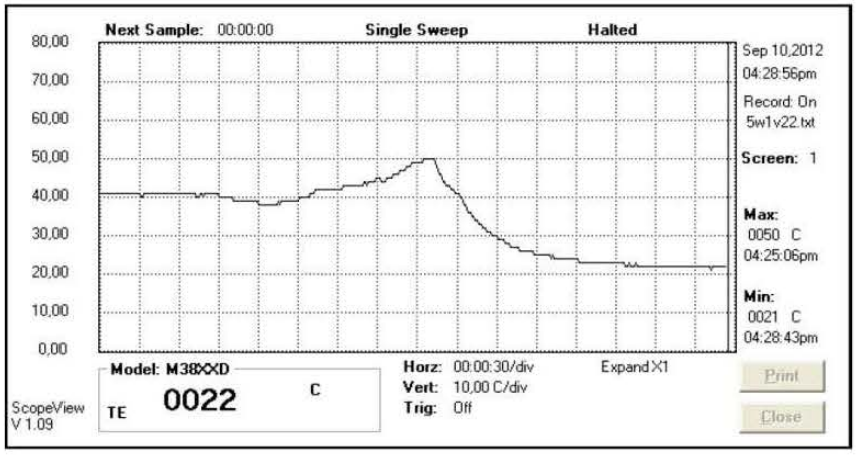

Fig. 32 Variation of the sample's temperature in time for P=5 W (2. part).

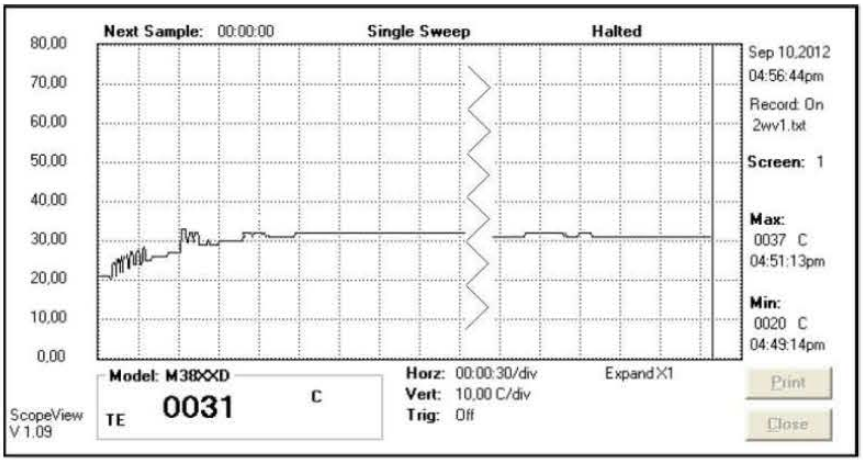

Fig. 33 Variation of the sample's temperature in time for P=2 W (first part).

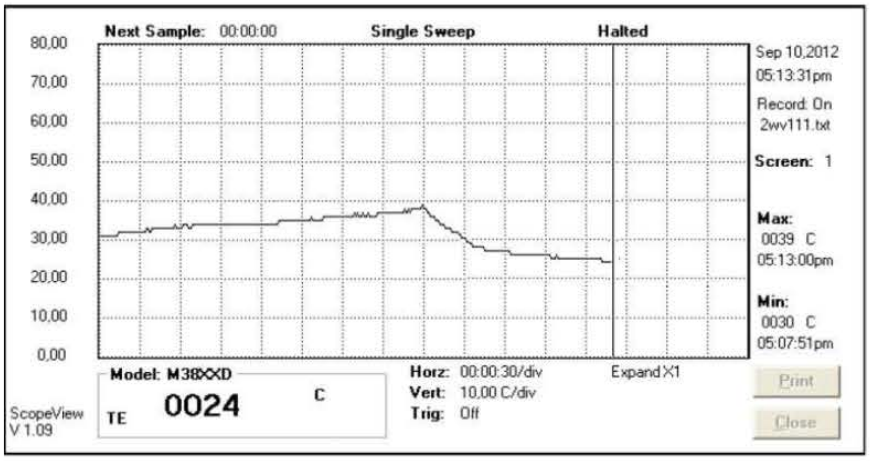

Fig. 34 Variation of the sample's temperature in time for P=2 W (2. part).

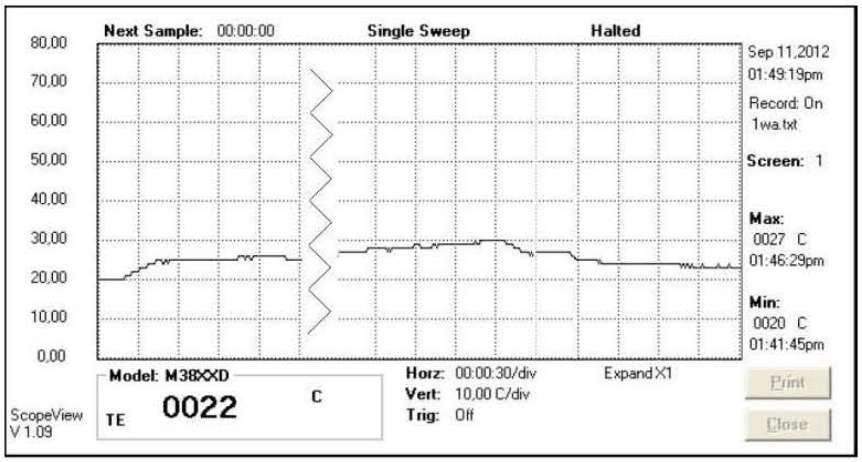

Fig. 35 Variation of the sample's temperature in time for P=1 W (image is adjusted for better visibility).

The measurement data show that the curve has the same shape for all power levels. The curve indicates several physical processes taking place. The first upward shift of the curve reflects the energy supplied from the DC power source to the wet textile. The almost horizontal part of the curve represents the evaporation process, in which energy is consumed to evaporate water (W=>Q). The temperature is maintained, as sample cools by evaporation. The second upward shift indicates that the textile material is dry and is now becoming hotter until it starts to burn. At the maximum point, the DC power source was switched off. The subsequent drop in temperature represents equilibration with the surroundings.

Table XIX Measurement Data I

Power Supplied [W]	Drying Time [min:s], [s]	Duration of the First Increase in Temperature [s]	Voltage [V]
1.05	33:44, 2024	42	0.3
2.27	20:20, 1220	81	3.6
5.43	10:28, 628	148	5.6
10.14	4:30, 270	63	7.8

Table XX Measurement Data II

Power Supplied [W]	Initial Temp. [°C]	Constant Temp. [°C]	Δ Temp. [°C]
1.05	20	27	7
2.27	21	32	11
5.43	20	41	21
10.14	20	54	34

Table XXI Sample Resistance

Measured Resistance [Ω]	Average Resistance [Ω]
3.668	3.672
3.671	
3.678	

It is clear from the measurement data that by the second increase in temperature the conductive textile material had been dry. If we continue drying it, it starts to twirl. It is therefore very important to determine the right time to switch off the power supply.

3.3.5. Conclusions

The chapter describes an experiment involving the description, design and measurement of a self-drying textile material. Conductive fibres in a woven fabric can conduct an electric current. This can be used for drying a wet material by applying energy to it. Determining the right amount of energy depends on the moisture content, the structure of the textile, application time and system setup. Two temperature increases can be observed. The first corresponds to the initial warming of the textile; the second indicates that the textile material is already dry. The power supply must be switched off at the right time to avoid damage to the textile.

3.4. Application - Monometallic Textile Electrodes for “Green” Batteries

This chapter focuses on the design and manufacture of monometallic textile electrodes for "green" batteries, i.e., the use of environmental technologies in eco-friendly electronics, particularly the new-generation electrochemical power sources [153]. The proposed technological processes were validated with samples and measurements in laboratory conditions with good results. These industrially applicable technologies were used for the application of a thick monometallic deposit as part of the preparation of the samples. This means that future mass production and deployment in electrical engineering applications are possible.

3.4.1. State of the Art

A basic requirement for any new developed electrode material is mass production readiness. This should be taken into account during the development of the electrodes and the technological processes for their manufacture. Other considerations include maintaining the required chemical resistance of the electrodes, a good ratio of effective electrode area to overall dimensions, and the weight of the electrodes.

The race to increase the efficiency of battery cells drives the search for materials with the maximum surface area possible. Nanotextiles appear to be the ideal electrode carrier, as the originally nonconductive fibre can be coated with an appropriate electrode metal. Currently, nanotextiles can be made with polymers with specified chemical resistance properties such as ELMARCO [89] nanotextiles, which are commercially available.

These nanotextiles cannot be combined with strongly alkaline electrolytes because they are made of polyvinylidene difluoride (PVDF), PVDF copolymers and polyacrylonitrile (PAN) [89], and as such are not resistant to 6M KOH electrolytes [90]. The development of new types of environmentally friendly electrochemical power sources must rely on eco-friendly metals (zinc, tin, copper) and strong alkaline electrolytes in gel form [91].

Polypropylene (PP), in particular, is highly resistant to alkaline and acidic chemicals. PP is widely used in chemical technologies and components. PP fibre-based textiles first need to be made conductive before they can be used as an electrode.

This can be achieved by several techniques:

- Metal powder coating;

- Physical vacuum deposition methods;
- Chemical coating;
- Electroplating.

3.4.2. Desired Properties and Performance of Electrodes

The primary objective of the present research was the design of sufficiently conductive “green” electrodes with a current carrying capacity for use in battery cells that meet the following requirements:

Chemical Resistance of the Substrate

This requirement is addressed by the use of textile materials based on PP which can resist the 6M KOH solution over a long period of time.

Maximum Substrate Surface Area

PP nonwoven fabrics seem to be the ideal textile choice, as they have a greater surface area than woven fabrics while having the same fabric density. The maximum possible surface-area-to-weight ratio can be achieved in electrodes applied on mechanically reinforced substrates (fibres needled or woven between layers) or heat reinforced substrates (fibres sintered into isles).

Chemical hardening is not a practical solution, as it could become a source of technological complications due to chemical pollution affecting both the manufacturing bath and the cells themselves.

Conductive Electrode Layer Material

Nickel, which is being phased out in the consumer industry due to environmental concerns, and tin, which is environmentally friendly and non-allergenic, appears to be the best material for strongly alkaline electrolytes. The formation of undesirable bimetals or intermetallic products relating to the deposition of metal layers containing only one metal must be avoided. This means that a monometallic electrode is preferred.

Electrical Load of the Metal Layer

Thickness values ranging in the tens of μm are considered due to, in particular, the current demands on battery charging and operation and also in order to avoid the loss of the electrode metal due to primary spontaneous dissolution.

Depth Profile of the Metal Layer

The surface area of the working part of the electrode depends not only on the fabric surface but also on the internal volume. It is assumed that the individual coated fibres of the fabric will be in contact with the battery electrolyte in the greatest possible depth profile. Consequently, our goal is to achieve maximum throwing power.

3.4.3. Technological Preparation of Monometallic Layers

An analysis of the above requirements and available technologies reveals that the required properties cannot be obtained using the procedures we have mentioned. The solution lies, however, in the combination of several procedures. The experiment entails depositing tin, because tin is a “greener” metal than nickel. Research is therefore primarily focused on developing a new type of alkaline battery cells based on this eco-friendly metal.

Fabric Pretreatment

The fabric needs to be washed or degreased first, as pre-treatments on the basis of synthetic and organic chemicals are commonly used in the textile industry. The starch that remains after the textile is pre-treated could affect the deposition of electroformed layers (e.g. internal stress of metals or formation of amorphous layers). Grease residues impair the quality of the vapour-deposited tin metal layers.

Washing the base material takes 15 minutes in a bath heated to 70 °C. The bath contains 1.5 % NaOH solution in distilled (DI) water. After the washing procedure, the material is rinsed in DI water for 10 minutes and dried with hot air.

Sample Preparation

The sample is placed onto a frame that supplies electric power and ensures the proper suspension and attachment of the textile sample. The frame is made of 2.5 mm^2 copper wire. Fig. 36 shows the preparation of the sample after the vacuum deposition of tin.

Vacuum Deposition

A sufficiently thick layer must be deposited on either one or both sides of the sample depending on the requirements on the sample electrode, Fig. 36. The metal evaporation tray should be full to ensure that an adequate layer of tin is deposited. This reduces spontaneous dissolution during the subsequent electroforming reinforcement of the layer.

Fig. 36 Sample of PP textile – vacuum deposition of tin.

Electroforming – Reinforcement of the Tin Layer

The electroformed tin metal layer, which reinforces the initial vapour-deposited tin film, is applied in an alkaline tinning bath, as the electrode will be operated in an alkaline environment. Furthermore, alkaline tinning baths have higher throwing power. Although the alkaline (battery cell) electrolyte will be based on KOH, a tinning bath with NaOH may be used. Both baths are prepared with Na_2SnO_3 or K_2SnO_3 and the appropriate hydroxide.

According to [92], the tinning bath consists of Na_2SnO_3 at a concentration of 105 g/l and 10 g/l NaOH in DI water. The normal anode/cathode area ratio is 1:1. The bath should be operated at a temperature of 70 °C.

The initial coating requires the placement of a plated electrode in a bath with a current density $J_{plating}$ = 1 A/dm2. The duration of the initial coating is $t_{plating}$ = 15 min.

The initial coating is followed by the first reinforcement of the layer at a current density $J_{reinforcement1}$ = 5 A/dm^2 for t = 55 min.

The second reinforcement occurs in different conditions, namely current density $J_{reinforcement2}$ = 20 A/dm^2, t = 30 min. Tin anodes are not covered with the standard yellow and green layer indicating anode polarization. Under the operating conditions described above these would turn dark grey and tin would be released to the bath in the form of divalent ions, resulting in a tough coating with a higher surface area compared to conventional decorative gloss paints based on tetravalent ions [4]. This is due to the smaller surface area of the anode compared to the cathode. Another effect is the generation of considerable amounts of oxygen in the electrolyte.

After the layers have been deposited, the sample is rinsed with DI water over the bath and washed under running water to remove the bath residues from the fabric. Then it's dried.

Once the sample has been carefully dried, the suspensions are removed with lever shears. The textile monometallic sample electrode is ready.

3.4.4. Samples

The proposed technological processes were validated in laboratory conditions with good results. Macro pictures of the electrodes can be seen in Fig. 37 – Fig. 40. Moreover, the electroforming procedures made it possible to coat the extending fibres not only from the front towards the anode, but also on the sides, which would be impossible in most electrolytes due to depth efficiency. On average, 0.72 g/cm^2 of tin was deposited on a unilateral electrode. Cyclic stress-strain tests of the conductive felt structure (3D structure) used as a collector and carrier of electrode materials in an alkaline battery showed good results and stability of the deposited monometallic layer. The main criteria for the evaluation of the collector included the generation of hydrogen under cyclic stress (the charging and discharging of a battery), successful application of an active material to the collector, and ultimately, comparison with other materials – nets, pocket electrodes etc.

Fig. 37 Monometallic tin felt electrode ready for filling (non-woven PP textile carrier prepared by needling).

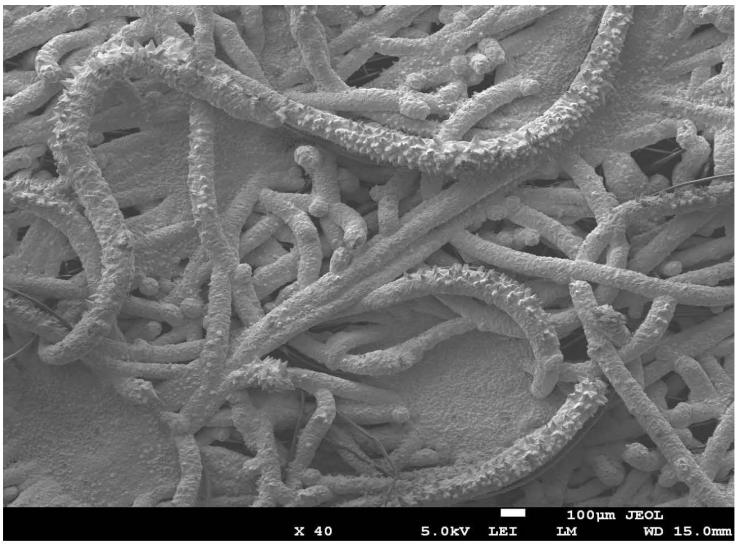

Fig. 38 Monometallic tin electrode on needled PP.

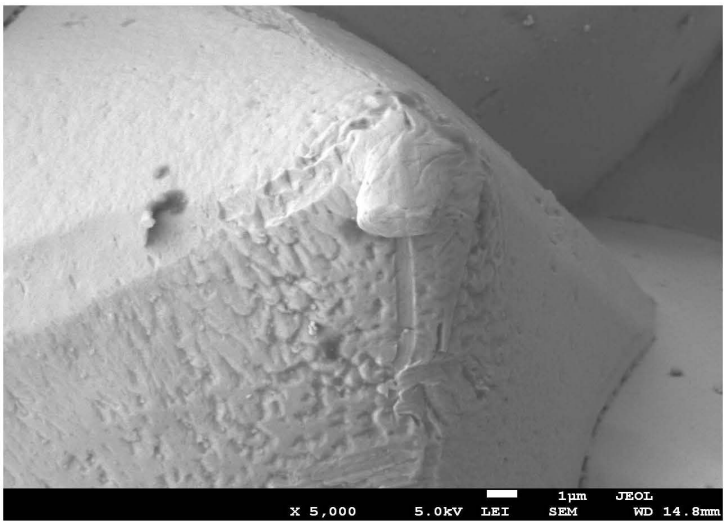

Fig. 39 Detail of the crystal surface of divalent tin in a monometallic tin electrode.

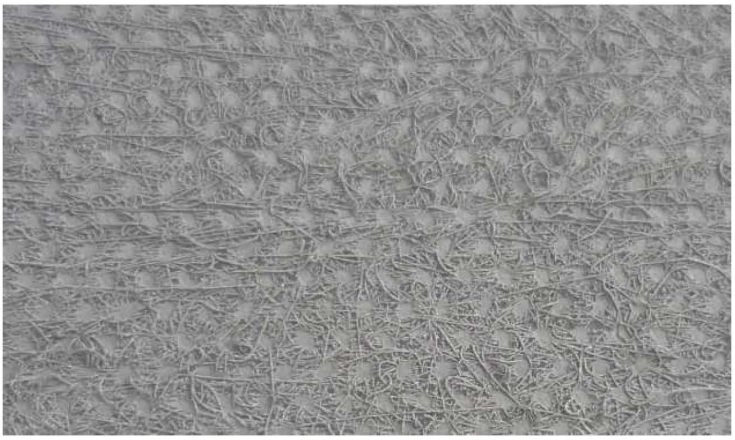

Fig. 40 Macro picture of a monometallic tin electrode on heat reinforced PP.

3.4.5. Measurement Data and Discussion

Several methods can be used to measure the effective surface area of electrodes. Most methods are based on optical (3D surface measurement) or electrochemical (electrical conductivity) principles. One of the optical methods is a surface area calculation based on processing images obtained by scanning at different angles [93]. However, low frequency conductometry is utilized more frequently [94]. This method is based on measuring the electrolyte conductance *G* between the two electrodes of the surface area *A* and the distance *l* between them. This method can be used either to measure the surface area of the electrodes using a calibrated and analysed electrode, or for comparative measurements. Comparative measurements were also used in the present research. All electrodes were set in an electrolysis beaker with water and resistance was measured under stable conditions described below, Fig. 41.

The comparative measurements were conducted with the following experimental setups:

- All-metal copper board electrodes were used. These electrodes were coated with tin in the same type of galvanic bath as the thick layers deposited onto the textile electrodes.
- The same type of electrolyte (i.e., DI water with a conductance of 15 µS) and the same temperature of 20 °C were used.
- The same test cell geometry, electrode distance and electrode dimensions were used.
- The resistance (conductance) between electrodes was measured with a measurement signal with a frequency of 100 Hz.

Fig. 41 Electrode testing setup.

Under these conditions, conductance can be calculated as follows:

$$G = \frac{1}{R} = \kappa \cdot \frac{A}{l} \quad [S]. \tag{26}$$

where G stands for conductance [S], R denotes resistance [Ω], κ means electric conductivity [S.cm-1], A is the (effective) surface area of the electrodes [cm2] and l denotes the distance between the electrodes [cm].

Table XXII Measurement Data

Base electrode material	Electrode resistance	Resistance value [kΩ]	Sample weight (0.1 dm^2) [g]
Cu//Sn	$R_{Cu//Sn}$	9.12	4.55
Needled PP//Sn	$R_{Needled\ PP//Sn}$	9.53	0.94
Heat reinforced PP//Sn	$R_{Heat\ reinforced\ PP//Sn}$	9.03	0.62

Table XXII contains the measurement data for the three different electrode base materials. The electrode $R_{Heat\ reinforced\ PP//Sn}$ has the lowest resistance value, i.e., the greatest specific conductance value and a greater effective surface area compared to the reference all-metal electrode $R_{Cu//Sn}$, as shown in (26). The greatest resistance value, i.e., the lowest specific conductance value and effective surface area, is observed in the electrode $R_{Needled\ PP//Sn}$.

3.4.6. Conclusions

The aim of the experiment was to design and validate a technological process of the preparation of monometallic layers of tin with maximum surface area deposited on a PP textile substrate, with intended application in “green” electrodes for electrochemical power sources. The chapter describes several procedures and presents results showing that the project’s goals were achieved. The proposed technologies are mass production-ready. During work on this experiment, a promising path for continued research in this area was identified. Laboratory tests were carried out on samples unilaterally or bilaterally coated on various types of PP substrates, with different reinforced fabrics, and different planar densities. The samples were also subjected to laboratory tests for cyclic stress-strain resistance in the measuring cell of an electrochemical cell between cycles of charging and discharging. A comparison of the conductance values measured in the experimental measuring cell shows that the electrode $R_{Heat\ reinforced\ PP//Sn}$ has a greater effective surface area than the reference all-metal electrode $R_{Cu//Sn}$, while $R_{Needled\ PP//Sn}$ has a smaller effective surface area than the reference electrode. The most important feature of the proposed textile electrodes is their ability to absorb liquid electrolyte or electrode paste, if they are used in a battery cell. The electrode $R_{Needled\ PP//Sn}$ is suitable in this respect, as the material shows the greatest electrolyte absorption capacity despite a less efficient surface area. Still, textile electrodes lead to improvements in the battery capacity/weight ratio.

Future research may focus on the application of orthogonal nanostructures on the coated fibres of the PP textile. The technology of nano-bar deposition appears to be a promising alternative to chemically deposited nanotubes, as it can produce a thick current-stressed layer.

3.5. Application - Wearable textile electrodes for ECG measurement

The electrocardiogram (ECG) is one of the most important gauges of a person's physiological health. Current ECG monitoring systems are either stationary or wearable. In either case, the experience is not comfortable for the person monitored because these systems are not part of standard clothing. Conventional stationary systems often use suction cup electrodes or adhesive electrodes. Wearable monitoring systems use metallic, textile or conductive polymeric electrodes or contactless sensing. Both solutions can cause discomfort and are ill-suited to long-term ECG monitoring of patients and athletes. The existing electric potential sensing methods cause discomfort when used for preventive ECG monitoring, especially the monitoring of stress in rescue workers, firefighters or soldiers. These factors limit the adoption of these methods.

One of the promising uses of ECG monitoring technology is the monitoring of persons working under great physical and mental stress, for example soldiers, firefighters, police officers and rescue workers in mines. Stress in these professions has a major impact on the quality of work and life [95]. High levels of stress have an impact on the rescue operation itself – they can increase the response time and the probability of making a mistake. That directly increases risks to health, life or property. It is, therefore, in the best interest of these organizations to react quickly to increased employee stress levels and to end or limit their exposure to stress.

The means of measuring ECG can be classified into two basic groups. The first includes ECG tests that are highly accurate and meet stringent Quality of Service (QoS) requirements. The second category includes ambulatory ECG monitoring devices designed specifically for athletes [96] or for long-term ECG monitoring during a specific patient examination period [97]. The second category also includes systems that optimise the dose of drugs affecting patient activity.

The current wearable ECG monitoring systems use several types of electrodes. Adhesive electrodes are commonly used in commercial Holter monitors. Many systems use textile electrodes embedded in clothing [98], [99], [100], [101]. Other approaches involve handheld electrodes [102] or contactless sensing [103].

This chapter deals with the development and testing of wearable textile electrodes for use in an ECG monitoring device ensuring high levels of comfort for the user [155]. The electrodes are made of an electrically conductive textile composite material that provides high levels of comfort to the user, while ensuring high-quality ECG results. As well as a carrier (a T-shirt with a flame retardant), the composite is integrated into embroidered sensing electrodes made from a polyester-

cotton mixture coated with silver nanoparticles. The electrodes provide great comfort and are antibacterial and anti-allergic (thanks to the use of silver nanoparticles).

3.5.1. Wearable Electronics

The development of electrically conductive textile materials integrated into various types of clothing has created a new area of applications called wearable electronics. Heated textile structures [82] or textile antenna structures integrated into clothing [4] have become feasible. A similar technology can be used to make wearable textile electrodes for ECG devices that can be part of standard clothing.

The electrodes should meet the following parameters:

- The use of a sufficiently conductive textile material with a specified conductivity and suitable composition [4] (providing high-quality electrical signal sensing)
- The use of a cotton-based fabric (soft to touch thanks to the use of cotton blend yarn)
- Integration into clothing (the system is easily applied and the electrode maintains a stable position)
- Standard maintenance (washing and ironing) possible
- Avoiding fabrics with a plated surface (non-cotton substrates cause skin irritation because of the use of synthetic fibres; the surface layer is made of copper, which oxidizes, or nickel, which is allergenic).
- Sufficient contact with the pectoral muscles (to ensure there is a sufficient difference in electrical potential between the electrodes).

3.5.2. Fabrication of a T-shirt with a Textile Electrode

To ensure the requirements above are met, the T-shirt was made from a knitted fabric with reduced flammability (such that is used in comfortable protective clothing for rescue workers and firefighters). Rectangular cut outs of the knitted electrically conductive fabric were sewn to the breast. The material is characterized by the following parameters:

- Yarn fineness: 29.5 tex
- Silverstat 60%, 40% PES
- Surface conductivity: 1.2 Ω/square, measured using the method in [19]

The knitted fabric is made from a composite yarn containing silver nanoparticles for electrical conductivity. The use of silver nanoparticles ensures that

the textile electrodes are corrosion-resistant, antibacterial and anti-allergic and that they keep their mechanical and electrical properties when exposed to sweat. The blended fabric is washable and ironable and the electrodes keep their surface conductivity even after many wash cycles.

The textile electrodes were rectangular in shape, with the dimensions 70x100 mm. They were placed so as to contact the upper chest right below the clavicles, Fig. 42. To ensure sufficient difference in potential, the electrodes were placed 100 mm apart.

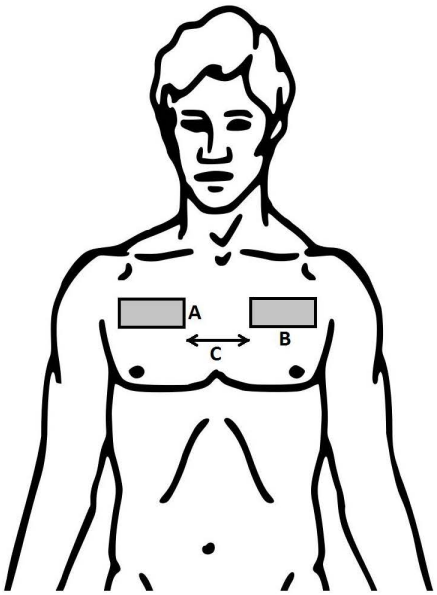

Fig. 42 Placement of textile electrodes (with using [104]).

3.5.3. Experimental Verification

The suitability of the textile electrodes for ECG monitoring was validated with experimental measurements. We compared the ECG data recorded using the textile electrodes with the ECG data obtained using a high-quality reference system.

During the ECG, the subject was lying on the back and was instructed to relax his muscles. This position is known to minimize muscle artifacts and allowed us to obtain clean ECG data.

The signal was first recorded using two metallic electrodes attached to the subject's right and left index fingers; a third electrode was placed on the right middle finger. The system included a noise suppression circuit [105], [106]. The placement of the electrodes is shown in Fig. 43 Electrode placement for three-lead ECG. From our previous experiments, we knew that this method provided a high-quality ECG recording, that's why we used it as the reference for the evaluation of the ECG recordings obtained using the textile electrodes.

Once the reference recording had been obtained, we proceeded with the experiment involving the textile electrodes. For this experiment, we used only 2 leads and no active noise suppression. The electrode placement is shown in Fig. 44.

The electronic system incorporated high-pass and low-pass filters with cut-off frequencies of 0.1 Hz and 200 Hz, respectively. The signals were first digitized (the sampling frequency was 800 Hz) and then filtered with a set of notch filters with centre frequencies at multiples of 50 Hz to eliminate power-line interference.

It is expected that the ECG signal will contain various kinds of movement artifacts (particularly muscle artifacts and baseline wander) if the subject moves. However, these artifacts can be removed using digital signal processing techniques [107].

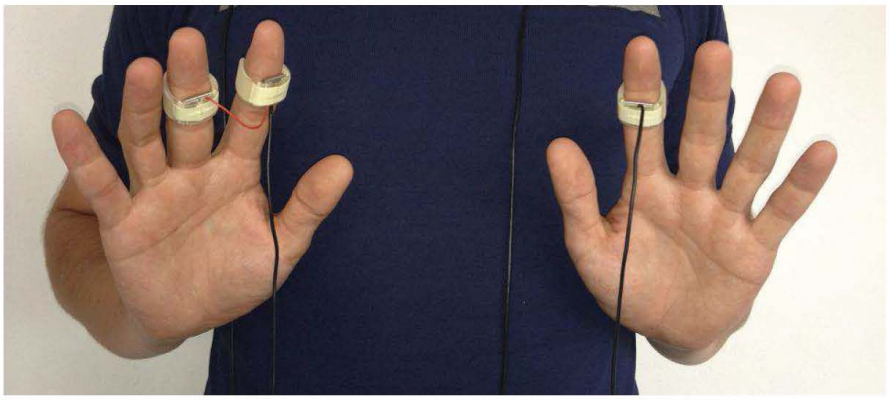

Fig. 43 Electrode placement for three-lead ECG.

Fig. 44 Placement of textile electrodes.

The recording of the reference ECG signal is shown in Fig. 45. The ECG recording shows clearly visible P waves, QRS complexes and T waves.

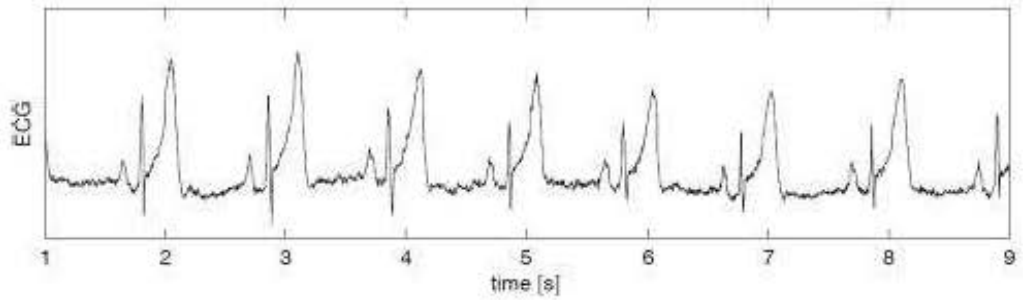

Fig. 45 Three-lead ECG waveform. This recording serves as the reference for the evaluation of the recording made using the textile electrodes.

The ECG recording obtained using the textile electrodes is shown in Fig. 46. As in the reference recording, the signal is clean with clearly discernible P waves, QRS complexes and T waves.

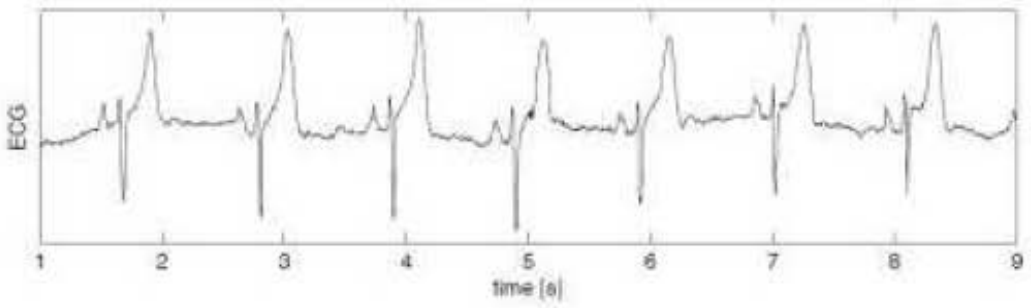

Fig. 46 Two-lead ECG involving the use of textile electrodes.

A clearer comparison of the measured signals is shown in Fig. 47. The amplitude of the individual waves of the ECG signal obtained using the textile electrodes is smaller compared to the reference ECG signal due to the difference in the placement of the electrodes. Both recordings show visible P waves, QRS complexes and T waves. This proves that textile electrodes can be used for ECG applications.

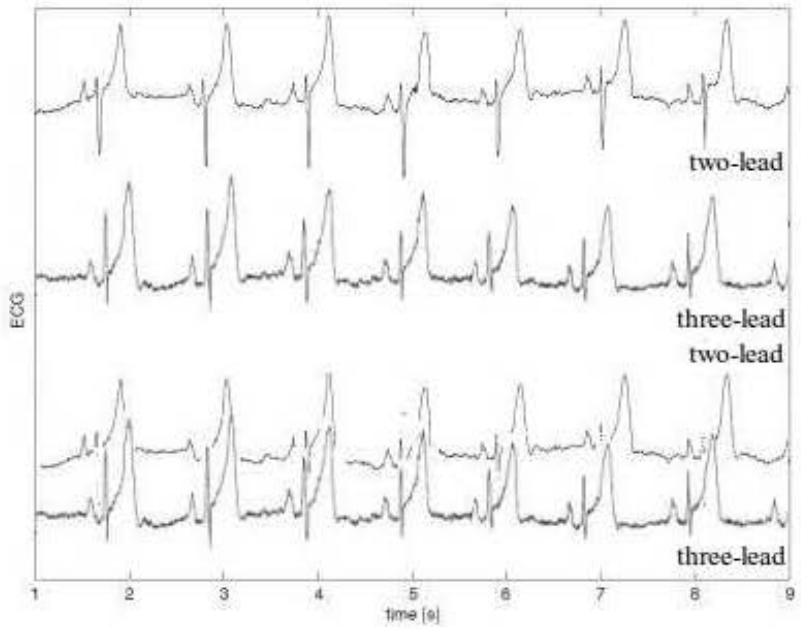

Fig. 47 Comparison of the ECG signal recorded using two-lead (textile electrodes) and three-lead (reference signal) ECG configurations.

3.5.4. Conclusions

As part of a proof-of-concept phase, wearable textile electrodes were shown to be suitable for ECG applications. The P wave, QRS complex and T wave were clearly discernible in the signals recorded and heart rate could be measured. Furthermore, baseline wander was negligible, indicating good contact between the conductive textile electrodes and the skin.

We developed a prototype of a textile product in the form of a T-shirt capable of capturing the ECG signal using two leads that are in direct contact with the person's body without causing any inconvenience. Garments containing these wearable textile electrodes are washable and ironable and comfortable for the wearer, while providing good ECG recordings. As shown, the quality of the recordings made using wearable textile electrodes in a two-lead configuration is comparable to the reference method which uses a third electrode for active noise suppression.

3.6. Application – Proof of Concept - Pure Textile Antenna

New-generation textile materials are both conductive and wearable. One of the possible applications of such materials is an antenna made of wearable parts. Conductivity in textile materials is used to implement wireless functions into clothing. In general, antennas are made of highly conductive metals with a solid structure, resulting in a stable output. Achieving output stability in textile antennas is a challenge because the radiating element, dielectric material and ground are wholly made of a textile, which can be can be folded and twisted. This chapter discusses the design and fabrication of a textile antenna designed to run in a 50 ohm system (such as standard communication systems like Global Positioning System (GPS) or Wireless Local Area Network (WLAN) at 2.45 GHz – our example) [154].

3.6.1. Introduction

The general use of electronic devices is growing every day. Portable devices like mobile phones provide various functions such as internet connectivity, personal digital assistance, and GPS and multimedia functions. With the advent of more advanced technology, a person in the future may have to carry a number of sensors on them, for example sensors that continuously monitor their health and send the data to cloud. Integrating such sensors into garments appears to be a particularly promising path to follow [108].

Going one step further, there's ongoing research into the use of textile materials as antennas. Paper [109] describes the top radiating element layer and the bottom ground plane of antennas made of copper sheets with a thickness of 0.1 mm and 0.5 mm. Paper [110] presents a ground plane and antenna made from thin, flexible and lightweight copper plated nylon fabric. The following experiment is based on a standard microstrip patch antenna design [111]. This chapter describes two 50 ohm antenna designs with a pure textile radiating element, dielectric substrate and ground plane. The first antenna is made from a Cu/Ni-coated non-woven PES fabric. The second antenna is made from a woven fabric containing conductive fibres. Simulation and measurement data are presented as an example of the proposal feasibility.

3.6.2. Design of Rectangular Patch Antenna

A microstrip patch antenna consists of a radiating element, ground, and a dielectric substrate sandwiched between them. The radiating patch consists of finite edges, resulting in fringing. Fringing is a function of the dimensions of the substrate, the height of the dielectric substrate and the dielectric constant [111].

3.6.3. Conductive Textile Materials

Textile materials containing metal elements can conduct an electric current and can be made by weaving metal fibres or applying a metal coating on a fabric [112].

A good textile antenna design has to satisfy several parameters, the most important of which are small electrical resistance, homogenous surface resistivity and fabric flexibility. Two different textile materials, Table XXII, were chosen: the experimental “Betex” fabric (woven) Fig. 47. and Cu/Ni fabric (nonwoven) Fig. 47.

Table XXIII Textile Materials

	Betex	**Cu-Ni**
Material	Shieldex (60%), Polyester (40 %)	Copper & nickel plated non-woven polyamide
Surface Resistivity	1.19 Ω/sq.	0.02 Ω/sq.
Warp/weft Density	20 t/cm	-

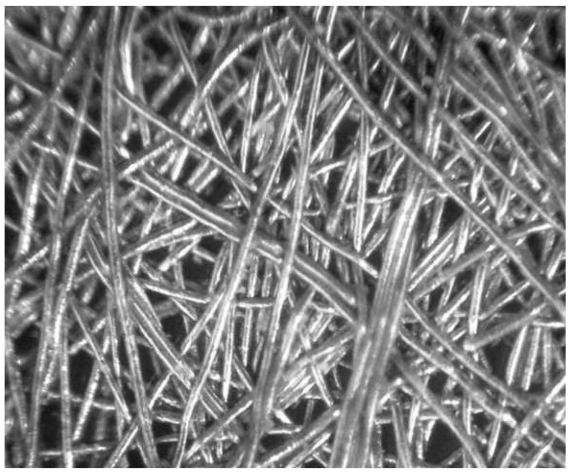

Fig. 48 Copper + nickel plated non-woven polyamide in detail.

Fig. 49 Betex sample.

3.6.4. Simulation of Microstrip Patch Antenna

Microstrip patch antennas are widely used within wireless communications. The bandwidth and efficiency of a microstrip patch increase with the height of the dielectric substrate. However, as the height increases, the polarization property and

radiation pattern degrade. Thus, the height of the dielectric substrate has to be chosen carefully [111].

In order to determine the conductive properties of a textile material, two different antennas were simulated and fabricated, Table XXII. The radiating element and ground plane of one of the antennas are made from Cu/Ni (copper + nickel plated non-woven fabric); a woven fabric is used for the other one.

Table XXIV Antenna Parameters Used in the Simulation of the Two Different Antennas

Sample	Type of fabric	Dielectric Material	Freq. (GHz)	Dielectric constant ε_r (-)	Height of Dielectric substrate (mm)	Surface resistivity (Ω/sq)
Cu/Ni	Nonwoven	Fleece fabric	2.45	1.25	2	0.02
Betex	Woven	Fleece fabric	2.45	1.25	2	1.19

Two conductive textile materials are used in the antenna designs. One of the conductive textiles has a very high conductivity and very low resistivity compared to copper. The other textile material has a low conductivity and very high surface resistivity compared to copper.

Considering the standard formulas [111], the dielectric constant ε_r, the permittivity of free space ε_0, the permeability of free space μ_0, a resonant frequency of 2.45 GHz, the effective dielectric constant of a microstrip antenna, the width of the microstrip patch W and the increase in length ΔL are equal to:

$$W = 0.05\ m, \quad \varepsilon_{reff} = 1.23, \quad \Delta L = 1.1\ m.. \tag{27}$$

The actual length L of the patch is calculated as [111]:

$$L = \frac{1}{2 f_r \sqrt{\varepsilon_{reff}} \sqrt{\mu_0 \varepsilon_0}} - 2\Delta L = 0.06\ m\ . \tag{28}$$

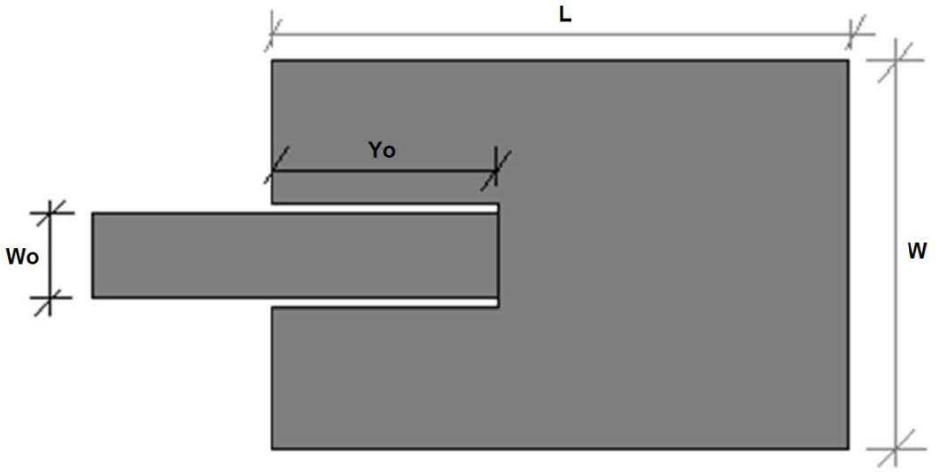

Fig. 50 Inset feed microstrip patch resonating at a distance Yo.

The patch should be connected with a transmission line with an impedance of 50 Ω. Hence, it is required that the patch have a resonance input resistance R_{in} = 50 Ω. This can be achieved by feeding the patch at a distance Y_o from the input point. Thus, Y_o is equal to Y_o =18.5 mm [111].

The calculated data are used for simulation in IE3D software. IE3D contains an optimization tool which we used to optimize the antenna design by finding the right patch length and inset feed position. The goal of the optimization, Table XXII, is to make the real part of the antenna equal to 50 Ω and the imaginary part to be zero. This is because the transmission line has an impedance of 50 Ω.

Table XXV Optimized Dimensions for Two Patch Antennas

Antenna Type	Length of patch [mm]	Width of patch [mm]	Inset feed distance [mm]	Width of feed line [mm]
Cu-Ni	50.4	52.7	34.4	2.2
Betex	54.6	52.7	10.6	11

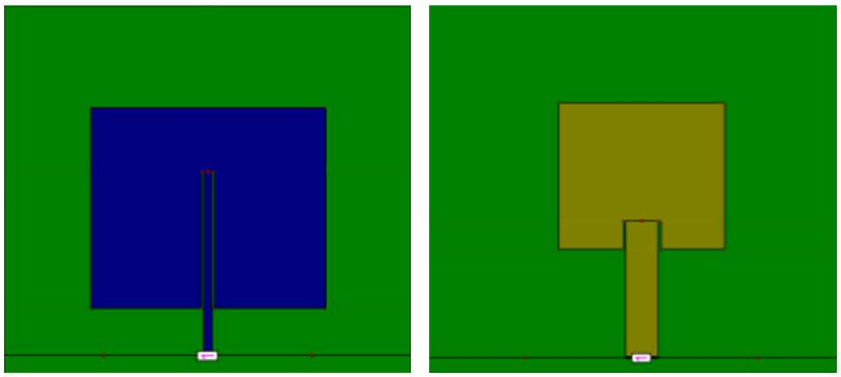

Fig. 51 Microstrip patch antenna resonating at 2.45 GHz with a radiating patch surface resistivity of 0.02 Ω/sq (Cu/Ni) and 1.19 Ω/sq (Betex).

The reflection obtained is -45 dB at 2.45 GHz for the antenna with the Cu-Ni radiating element and -22.5 dB at 2.45 GHz for the antenna with the Betex radiating element, Fig. 52.

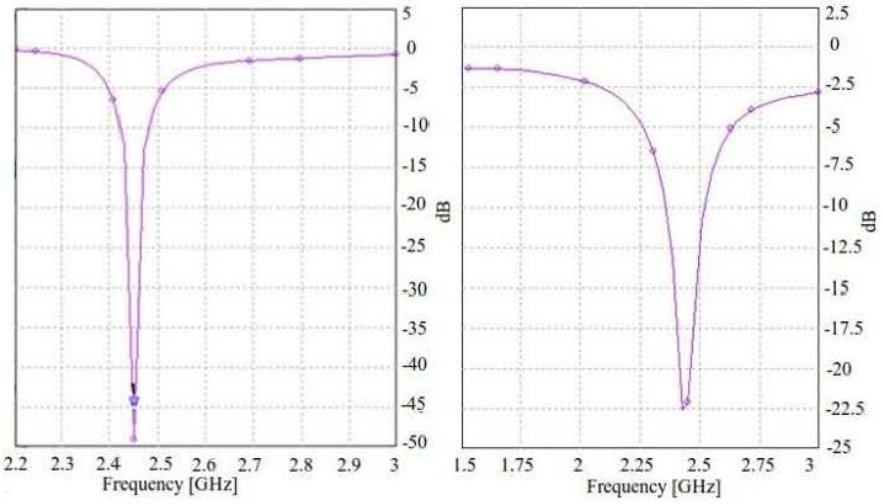

Fig. 52 Simulated reflection coefficient (S_{11}) for Cu/Ni (left) and Betex (right).

In a gain vs. frequency graph, we can see that the gain of the antenna made from a conductive material with a surface resistivity of 0.02 Ω/sq is 8.2 dBi (Cu/Ni) and the gain of the antenna made from a conductive material with a surface resistivity of 1.19 Ω/sq is 4.5 dBi (Betex), Fig. 53.

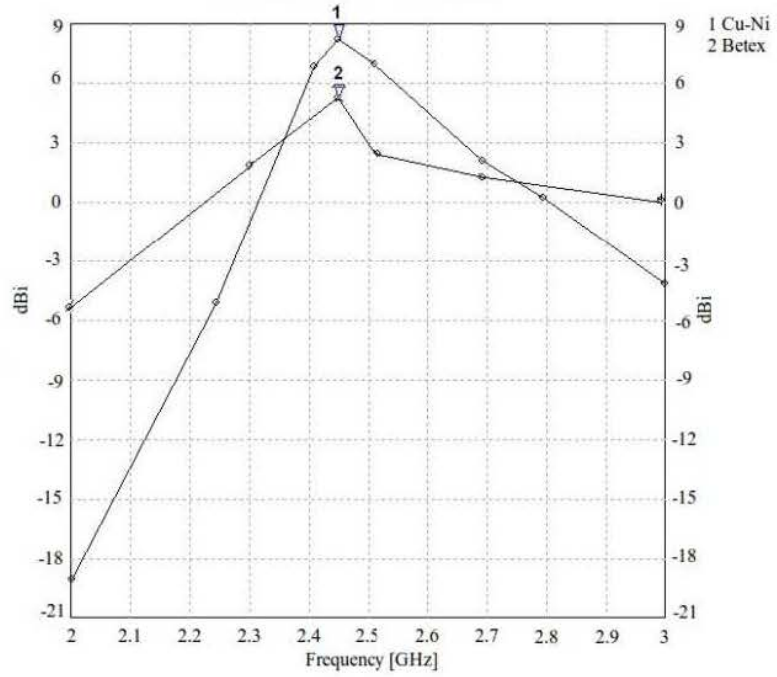

Fig. 53 Gain vs. Frequency for both antenna designs.

3.6.5. Fabrication and Measurements

Two purely rectangular patch antennas were fabricated. The patch radiating elements were made from Betex and Cu/Ni. The dimensions of the ground plane and the patch are obtained by calculation. After optimization, the dielectric substrate and ground plane are cut out using scissors and knife.

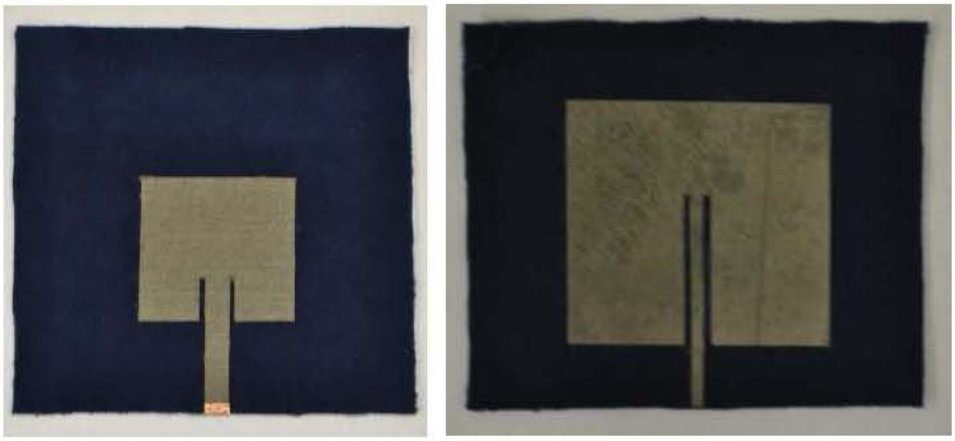

Fig. 54 Betex microstrip patch (left) and Cu/Ni microstrip patch (right).

During fabrication, the dielectric substrate (fleece fabric) is glued to the ground plane and radiating patch. Water-soluble glue is used to join the radiating element, substrate and ground. A 50 Ω cable is connected directly (soldered) to the Cu/Ni material. Betex is not suited for soldering; hence a cable could not be connected directly. Instead, a copper tape with a resistance of 0.005 Ω is connected to the Betex microstrip patch.

A far-field experimental measurement is performed on both antennas in a full anechoic chamber (at the Department of Electromagnetic Field FEE CTU in Prague) and the reflection coefficient (S_{11}) is determined using vector network analyser (VNA), Fig. 55.

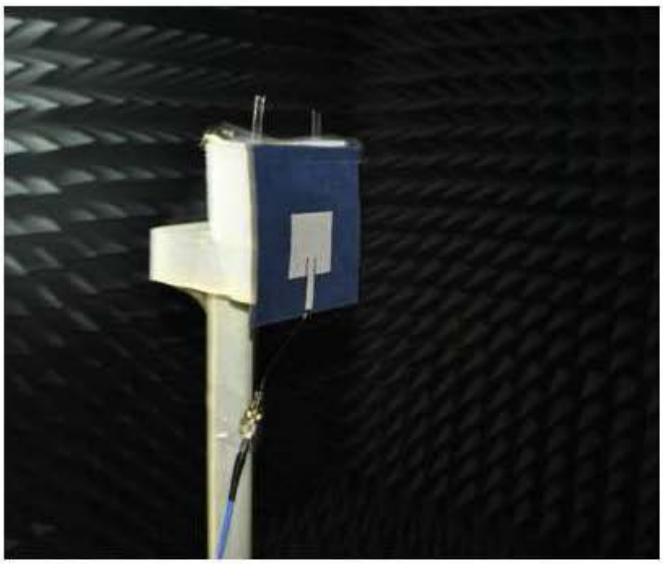

Fig. 55 Radiation pattern measurement of a Betex textile patch antenna in a full anechoic chamber.

The measurement needed for the calculation of gain was performed on a reference antenna. The reference antenna used was DRH 20 (gain was 8.04 dBi). The power received by the reference antenna was -43.8 dBm.

The normalized gain of a test antenna can be determined based on the radiation pattern data obtained in a full anechoic chamber:

$$G_a - G_{ref} = P_{RX} - P_{RXref} \,. \tag{29}$$

where G_a stands for the gain of the test antenna, G_{ref} denotes the gain of the reference antenna (DRH 20), P_{RX} is the power received by the tested antenna and P_{RXref} denotes the power received by the reference antenna.

The maximum power received by the antenna is at an azimuth angle (0 deg), Fig. 56. At this polarization, the maximum power received by an antenna is -46.1 dBm. The power received by the reference antenna is -43.8 dBm and the gain of the reference antenna is G_r = 8.0 dBi. Thus, the maximum gain of the test antenna, based on the measured data, is G_a = -46.1 + 43.8 +8.0= 5.7 dBi.

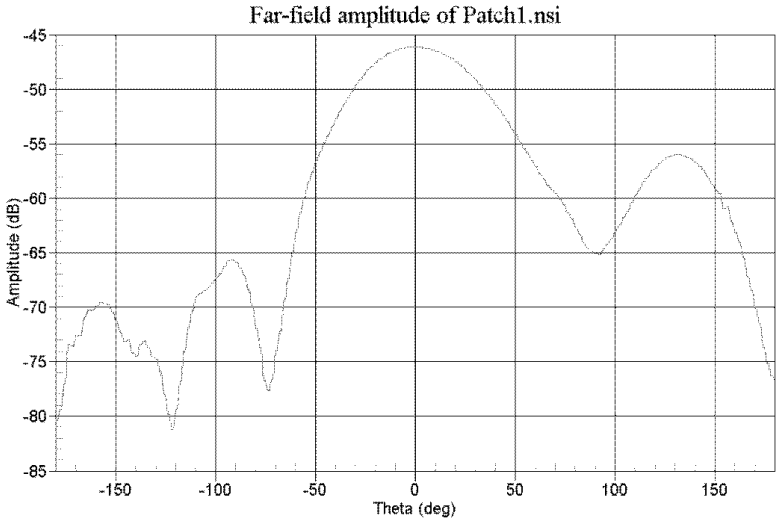

Fig. 56 Non-normalized far-field radiation pattern for Cu/Ni (E-plane).

Fig. 57 shows that at an azimuth angle of 0 degrees, the amplitude of the power received by the test antenna is -58.5 dBm. Using the same reference antenna, the gain of the test antenna can be calculated as G_a=*-58.5 +43.8+ 8.0= -6.6 dBi*.

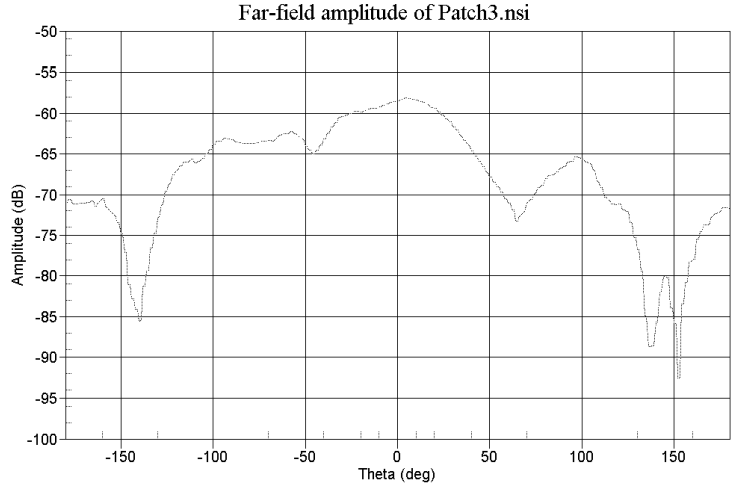

Fig. 57 Non-normalized far-field radiation pattern for Betex (E-plane).

The reflection coefficient of the test antenna is determined using a VNA. One-port calibration is used, and Open, Short and Match calibration is performed to determine the S_{11} of the test antenna, Fig. 58.

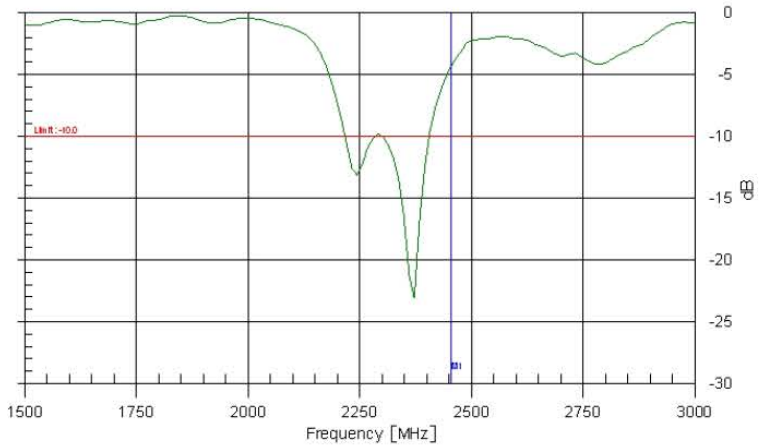

Fig. 58 Reflection coefficient S_{11} plot for a pure textile antenna with a Cu/Ni radiating element.

As expected, the reflection coefficient for Cu/Ni is shifted in frequency due to the inaccuracy of production, used glue between the dielectric substrate and the radiating patch affecting the dielectric parameters. Nevertheless, the resonance is good enough and the bandwidth is also sufficient for this textile material to be used as an antenna. If the antenna is bent, the resonance frequency may change. If it is a wideband antenna and the resonance frequency changes, the reflection will still be below -10 dB at the specified frequency, so the result of the experimental antenna fabrication is sufficient.

The experimental data obtained for Betex differ from the simulation values due to an imprecise determination of the permittivity of the dielectric material, and gluing, Fig. 57 and Fig. 59.

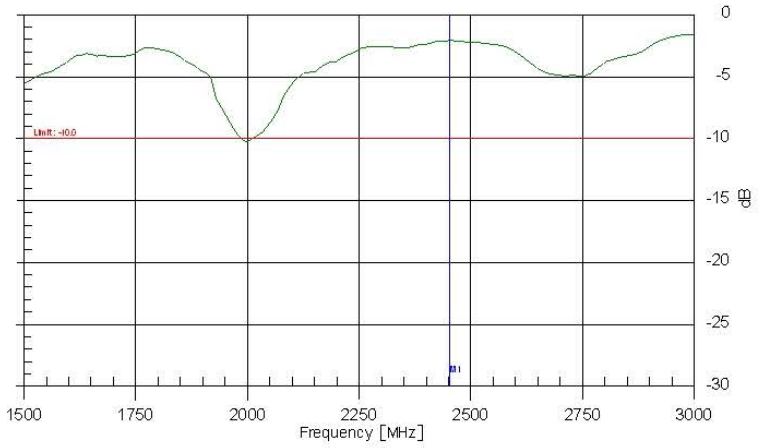

Fig. 59 Reflection coefficient S11 plot for a pure textile antenna with a Betex radiating element.

The shift in frequency and the increased S_{11} value compared to the simulation data are due to the glue applied between the layers (resulting in non-homogeneity), and the cutting process which causes rough edges.

3.6.6. Conclusions

This chapter presented the proof of concept of two patch antenna designs with the radiating element, dielectric substrate and ground wholly made from a textile material. The results show high electrical conductivity and relatively high gain in both antennas (non-woven and woven fabric). The woven antenna is made from an electrically conductive yarn which ensures a high stability of the mechanical and electrical parameters of the textile over time (number of washing cycles). Although the gain of the woven fabric is not very high, research in this area is promising. Future work should be focused on the optimization of the production of composite antennas, in particular the lamination of the composite layers. The antenna could then be used in protective overalls for the communication of personal terminals with a central system gathering real-time data on the physiological load of workers (heavy duty, rescue operation, etc.).

4. Electromagnetic Shielding Efficiency of Woven Fabrics

This chapter focuses on derivation and experimental verification of a numerical model for electromagnetic shielding efficiency of woven fabrics with high electrical conductivity manufactured from mixed and coated yarns. Individual components of electromagnetic shielding efficiency are described and derived for a foil, for a material with one aperture and for a material with multiple apertures, i.e. fabric. A derived numerical model for electromagnetic shielding efficiency calculation of fabrics is compared with measurement of real specimens according to ASTM 4935-10.

To demonstrate the different uses of the materials developed, selected applications of these types of materials are also discussed in this chapter.

4.1. Analysis of Electromagnetic Shielding Efficiency for Woven Textiles

One of the methods for ensuring proper function of these systems is a shielding, expressed by ESE. Primarily, the shielding of electronic systems was performed by metals. Nowadays, the metals can be replaced by electrically conductive textiles in order to obtain a relevant value of the ESE, which has been a highly discussed topic in recent years. The structure of these textile materials can be constituted in the form of coated/metallized fabric, which can be categorized as multi-layered "stack-up" system of composite shielding materials, or particulate-blended shielding textile composites, which are constituted by metallic inclusions like aluminium, copper, silver or nickel particles heterogeneously mixed in a host medium such as polymer/plastic. The main benefits include lower consumption of metals, flexibility of the textile materials, mechanical properties and/or lower weight of the shielding. Woven fabrics with high electrical conductivity are being increasingly utilized in shielding of electromagnetic interference (EMI) and in electrostatic protection in various applications such as the shields for equipment cases, the protective clothing for personnel working under high-voltage magnetic fields and/or in radiofrequency/microwave environment, shielding and grounding curtains, electrostatic discharge wipers, flexible shielded shrouds, smocks, stockings, and boots, etc.

Many research papers describe ESE evaluation from different perspectives. In particular, measurement techniques [113], [114], [115], [116], [117], [118], [119] composition of materials [118], [120], [121], [122], [123], [124], [125], [126], [127], [128], [15], influence of washing/drying cycles on values of ESE of fabrics [129], [130], [131], or calculation of ESE [116], [132], [133], [134], [135], [136], [13], [137].

ESE measurement is commonly performed by a coaxial transmission line method specified in ASTM 4935-10 [113], [114], [115], [116], [118], [120], [121], [122], [124], [126], [15], [129], by measurements of the insertion loss with a dual transverse electromagnetic mode (TEM) cell [115], [117], or by measurement in a free space, shielding box or shielding room with receiving and transmitting antennas [119], [127], [130], [131]. The papers which focus on measurement techniques of various electrically conductive fabrics usually present basic equations for ESE calculation. A final equation for ESE calculation and explanation of relevant equation terms can be found in this work [116], [132], [133], [134], [135], [138], [13], [137], [139] and usually in the following form (SI units are used in all equations unless otherwise stated):

$$ESE = 20 \cdot \log_{10} \left| \frac{E_i}{E_t} \right| = 20 \cdot \log_{10} \left| \frac{H_i}{H_t} \right| = 10 \cdot \log_{10} \left| \frac{P_i}{P_t} \right| = R + A + M. \tag{30}$$

where E_i, H_i, P_i represents electric field intensity, magnetic field intensity and power without the presence of tested material (incident electromagnetic field on the tested material), E_t, H_t, P_t denotes the same physical quantity with the presence of tested material (transmitted electromagnetic field measured behind the tested material), R is reflection loss, A represents absorption loss and M denotes multiple reflections.

Reflection loss R (also called return attenuation R) is a consequence of the electromagnetic wave reflection on the interface. The absorption loss A (also called absorption attenuation A) is produced if the electromagnetic wave is transferred through the shielding barrier. A portion of energy is absorbed in the shielding barrier due to the influence of heat loss. Attenuation caused by multiple reflections M is physically caused by electromagnetic wave propagation in the conducted shielding barrier. The electromagnetic wave is repetitively reflected on the “inner” interfaces of the material.

Numerical models for ESE calculation of fabrics are based either on electrical properties (electrical conductivity) [138], [139] or on transmission line theory, i.e. an analysis of the leakage through apertures in the fabric, [116], [120], [134], [139]. The ESE evaluation of the fabric based on transmission line theory can be expressed as:

$$ESE = A_a + R_a + B_a + K_1 + K_2 + K_3, \tag{31}$$

where A_a represents attenuation introduced by a particular discontinuity, R_a denotes a fabric aperture with single reflection loss, B_a is a multiple reflection correction coefficient, K_1 represents a correction coefficient to account for the number

of like discontinuities, K_2 denotes a low-frequency correction coefficient to account for skin depth and, K_3 is a correction coefficient to account for a coupling between adjacent holes.

The ESE evaluation based on electrical properties of fabrics can be expressed as [138], [139]:

$$ESE_{fabric} = e^{-0{,}129\cdot\ell\cdot\sqrt{f}} \cdot ESE_{foil} + \left(1 - e^{-0{,}129\cdot\ell\cdot\sqrt{f}}\right) \cdot ESE_{aperture}, \tag{32}$$

where ESE_{foil} and $ESE_{aperture}$ are the ESE values for metallic foil (of the same thickness as the fabric) and for the same foil with aperture(s), l represents aperture size of the fabric and, f denotes frequency.

Calculation of the ESE_{foil} is well-known from shielding theory [135], [13], [137], [139], [140], [141] as:

$$ESE_{foil} = \underbrace{20\cdot\log\left|\frac{\left(Z_0 + Z_M\right)^2}{4Z_0 Z_M}\right|}_{R_{foil}} + \underbrace{20\cdot\log\left|e^{t/\delta}e^{-j\beta_0 t}e^{j\beta t}\right|}_{A_{foil}} + \underbrace{20\cdot\log\left|1 - e^{-2t/\delta}e^{-j2\beta t}\left(\frac{Z_0 - Z_M}{Z_0 + Z_M}\right)^2\right|}_{M_{foil}}, \tag{33}$$

where Z_0 represents impedance of free space, Z_M denotes impedance of shielding barrier, t is thickness, δ represents penetration depth, β_0 denotes vacuum phase constant and, β is phase constant.

A complete derivation of (33) is published in our previous research papers [13], [137]. Calculation of $ESE_{aperture}$ is usually expressed similarly to (30) and it is expressed for metallized fabric shields as [138], [139]:

$$ESE_{aperture} = R_{aperture} + A_{aperture} + K_{aperture} = 100 - 20\cdot\log\left(L\cdot f\right) + 20\cdot\log\left(1 + \ln\left(\frac{L}{s}\right)\right) + 30\frac{D}{L}, \tag{34}$$

where L represents the maximum aperture size, f is the frequency of operation, s denotes the minimum aperture size and, D represents the depth of the aperture.

Calculation and derivation of $ESE_{aperture}$ is not present in scientific literature for particulate-blended shielding electrically conductive textile composites. Therefore, the main contribution of this chapter is that the research performed a complete derivation of a numerical model of ESE for woven textile materials manufactured from electrically conductive mixed and coated yarns, i.e. for particulate-blended shielding

electrically conductive textile composites. Basic simplifications, which are valid for metals, are also evaluated for these textile materials. A complete derivation of ESE evaluation is also performed for ESE_{fabric} (32) and $ESE_{aperture}$ of metallized fabric shields (34). A general equation for ESE evaluation for particulate-blended shielding electrically conductive textile composites with electrical conductivity bigger than 244 S/m is derived and compared with measurement of real samples according to ASTM 4935-10.

4.1.1. Material Description

The samples are particulate-blended shielding electrically conductive textile composites manufactured from two types of yarns, mixed and coated, with a plain weave fabric structure, Table XXVI.

The coated yarns SilveR.STAT® (samples #1 – #2) contain a very pure silver layer on the polymer base (Polyamide). The mixed yarns (samples #3 – #7) are blended from the non-conductive textile material, i.e. PES, and the conductive material, i.e. silver in the form of the SilveR.STAT® coated yarns. The plain weave is chosen because of its simple and regular structure.

The samples #1 and #2 and #3 – #5 are made of the same material (the same ratio of conductive and non-conductive textile material in the case of #3 – #5) with the same fabric structure and differ from each other mainly by used warp and weft density in a production process. The samples #6 and #7 are characterized by the same warp and weft density, the same fabric structure and differ from each other by the ration of conductive and non-conductive textile material, i.e. 40%/60% and vice versa. The selected parameters result in a different value of mass per unit area and, more importantly, in the different electrical conductivity value. As a result, the three groups of electrically conductive textile materials can be distinguished by the value of the order of the electrical conductivity, i.e. #1 – #2, #3 – #5 and #6 – #7, which is an important parameter in the ESE calculation as shown in the equations, e.g. (33).

Measurement of electrical conductivity of samples #1 – #7 is based on a four electrode test method described in BS EN 16812:2016 [37]. Mean value (evaluated for five different lengths and five different areas of the sample, 65 % RH, 20 °C) and standard deviation of electrical conductivity are depicted in Table XXVI.

Table XXVI Fabric Specification

No.	Composition	Fabric structure	Mass per unit area [g/m^2]	Warp/weft density d_w [t/cm]	Linear density [tex]	Electrical conductivity [S/m]	Standard deviation [S/m]
1	SilveR.STAT® 240dtex/10F	Plain weave	75	13/13	24	1.71E+04	9.72E+02
2	SilveR.STAT® 240dtex/10F	Plain weave	95	16/16	24	1.77E+04	5.69E+02
3	60% PES / 40% SilveR.STAT® 3.3dtex	Plain weave	92	13/13	29.5	1.07E+03	2.32E+01
4	60% PES / 40% SilveR.STAT® 3.3dtex	Plain weave	115	16/16	29.5	1.00E+03	3.29E+01
5	60% PES / 40% SilveR.STAT® 3.3dtex	Plain weave	135	19/19	29.5	1.37E+03	5.14E+01
6	40% PES / 60% SilveR.STAT® 1.7dtex	Plain weave	115	16/16	29.5	2.44E+02	8.99E+00
7	60% PES / 40% SilveR.STAT® 1.7dtex	Plain weave	117	16/16	29.5	3.9E+01	2.13E+00

4.1.2. Evaluation of Reflection Loss of Foil

Reflection loss R_{foil} is generally expressed in (33). It can be simplified for metals because of its good electrical conductivity, i.e. the inequality $Z_M << Z_0$ is valid. Moreover, the impedance of the material Z_M is further simplified because of the validity $\sigma >> \omega\varepsilon$. The R_{foil} is then calculated as [13], [137]:

$$R_{foil} = 20\cdot\log\left|\frac{(Z_0+Z_M)^2}{4Z_0Z_M}\right| \approx 20\cdot\log\left|\frac{Z_0}{4Z_M}\right| = 20\cdot\log\left|\frac{\sqrt{\frac{\mu_0}{\varepsilon_0}}}{4\sqrt{\frac{j\omega\mu}{\sigma+j\omega\varepsilon}}}\right| \approx 20\cdot\log\left|\frac{\sqrt{\frac{\mu_0}{\varepsilon_0}}}{4\sqrt{\frac{\omega\mu}{\sigma}}}\right| = 20\cdot\log\left(\frac{1}{4}\sqrt{\frac{\sigma}{\omega\mu_r\varepsilon_0}}\right), \quad (35)$$

where μ_0 represents vacuum permeability, μ_r denotes relative permeability, μ is permeability of a specific medium, ω represents angular speed, σ is conductivity, ε_0 denotes vacuum permittivity and, ε represents absolute permittivity.

The conductivity of a material can be expressed as conductivity relative to copper [139]. The value of copper conductivity is equal to σ_{Cu} = 5.8x107 S/m [141], [142]. Material conductivity is described as $\sigma = \sigma_r\sigma_{Cu}$ and R_{foil} is expressed as:

$$R_{foil} = 20 \cdot \log\left(\frac{1}{4}\sqrt{\frac{\sigma_{Cu}}{2\pi\varepsilon_0}}\right) + 20 \cdot \log\left(\sqrt{\frac{\sigma_r}{f\mu_r}}\right) = 168.14 + 20 \cdot \log\left(\sqrt{\frac{\sigma_r}{f\mu_r}}\right), \quad (36)$$

where *f* represents frequency of operation.

A similar equation can be also found in [116], [132], [133], [135]. The calculation of reflection loss R_{foil} corresponds to copper conductivity value, e.g. σ_{Cu} = 5.82x107 S/m [140], 5.7x107 S/m [143] or 5.85x107 S/m [144], which depends on the purity and the production method of copper. Nevertheless, (36) is presented for fabrics. This means the authors presume the validity of presented inequalities, i.e. $Z_M << Z_0$ and $\sigma >> \omega\varepsilon$. This presumption is furthermore verified. Definitions of the impedances Z_M and Z_0 and their simplified versions are described as:

$$Z_0 = \sqrt{\frac{\mu_0}{\varepsilon_0}} = \sqrt{\frac{4 \cdot \pi \cdot 10^{-7}}{8,854 \cdot 10^{-12}}} = 120\ \pi \approx 377, Z_M = \sqrt{\frac{j\omega\mu}{\sigma + j\omega\varepsilon}} \approx \sqrt{\frac{\omega\mu}{\sigma}}. \quad (37)$$

The validity of the $\sigma >> \omega\varepsilon$ can be easily verified for the lowest values of the electrical conductivity of the samples, i.e. #6 and #7. The value of relative permittivity of the used electrically conductive material is considered to be ε_r = 1, because the non-conductive textile material is blended with a conductive material, i.e. silver, Table XXVI.

As a consequence, the resultant textile material is categorized as lossy conductive material, which can be characterized as ε_r = 1. The value of relative permeability is considered to be equal to μ_r = 1. Results for different frequencies are presented in Table XXVII, Fig. 60 and Fig. 61. The condition of $\sigma >> \omega\varepsilon$ is fulfilled for sample #6 in the entire analysed frequency range, i.e. 30 MHz – 10 GHz because of the difference between the values of σ and $\omega\varepsilon$ is at least two orders of magnitude. Sample #7 fulfils the condition up to approx. 6.9 GHz. As a consequence, a simplified version of the Z_M and (36) can be used for #1 – #6 up to 10 GHz and for #7 up to approx. 6.9 GHz. Materials with lower electrical conductivity than #7, i.e. 39 S/m, have to be analysed in order to obtain the frequency limit of validity $\sigma >> \omega\varepsilon$ and (36). It can also be noted the limit of #6 is found to be 43.85 GHz and the ESE measurement is usually performed by a coaxial transmission line method specified in ASTM 4935-10 in the range of 30 MHz – 1.5 GHz.

Table XXVII Results of Ratio of the σ and ωε Evaluation

	Sample #6	Sample #7
Frequency [GHz]	σ/ωε	σ/ωε
1.5	2924	461.4
3	1462	230.7
4	1097	173
10	438.6	69.21

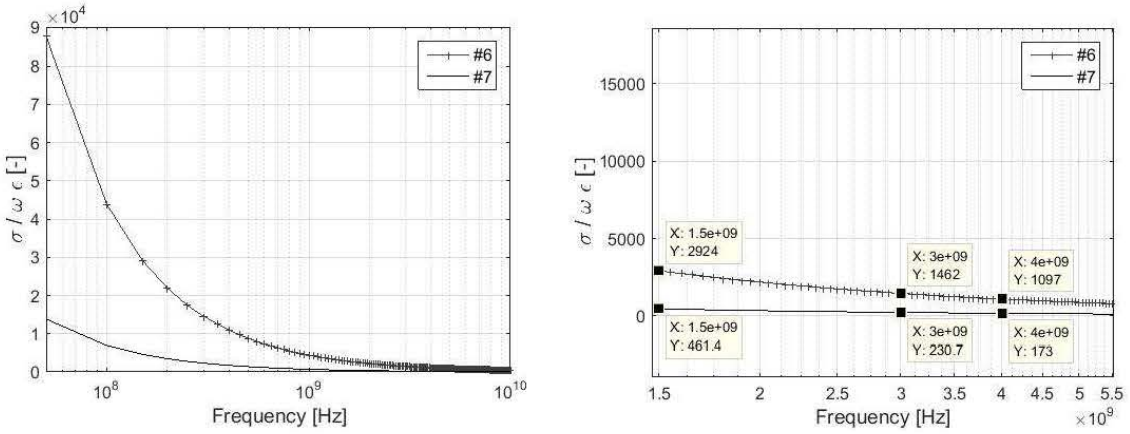

Fig. 60 Ratio σ / ωε for samples #6 and #7 (left) and the details for the 1.5 – 5.5 GHz (right).

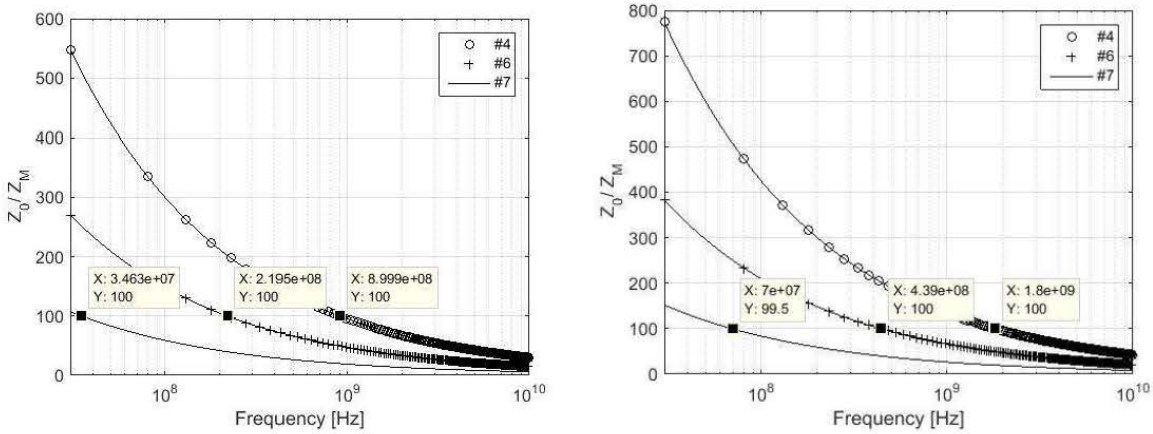

Fig. 61 Ratio Z0 / ZM for samples #4, #6 and #7, σ >> ωε is not assumed (left), σ >> ωε is assumed (right).

The validity of $Z_M << Z_0$ is verified for samples #7, #6 and #4, which are characterized by lower values of electrical conductivity from all described samples, Fig. 61. The validity of $\sigma >> \omega\varepsilon$ is assumed, i.e. a simplified version of Z_M is considered. A difference in values of two orders of magnitude in the frequencies 70 MHz, 439 MHz and 1.8 GHz can be seen for #7, #6 and #4, respectively. If the

validity of $\sigma >> \omega\varepsilon$ is not assumed, the values of two orders of magnitude are in the frequencies 34.6 MHz, 219.5 MHz and 899.9 MHz for #7, #6 and #4, respectively.

The clarity of application of the validity $Z_M << Z_0$ and $\sigma >> \omega\varepsilon$ can be also seen in Fig. 62. It compares the R_{foil} parameter of the four cases, i.e. $Z_M << Z_0$ and $\sigma >> \omega\varepsilon$ are/are not considered (in all four combinations), and also for all samples #1 – #7. All four cases are almost identical to #1 – #5, i.e. the greatest difference is reached for the sample with the lowest electrical conductivity (#4) and it is equal to about 0.5 dB in 10 GHz. The results also show an insignificant difference, i.e. the greatest difference is about a thousandth of a dB, for cases $Z_M << Z_0$ with (dash-dot line) and without (dotted line) consideration of $\sigma >> \omega\varepsilon$ validity for the sample with the lowest electrical conductivity (#7). This difference is nearly undetectable for all samples in Fig. 62. The greatest difference between these four cases is obtained for #7 in the frequency 10 GHz. It is about 2 dB for the cases $Z_M << Z_0$ is not considered and $\sigma >> \omega\varepsilon$ is considered (solid line), $Z_M << Z_0$ is considered and $\sigma >> \omega\varepsilon$ is (dash-dot line) / is not (dotted line) considered (both cases of $\sigma >> \omega\varepsilon$ show similar results as previously mentioned). The same situation is also valid for #6 with a difference not exceeding 1 dB. The results also show higher values of R_{foil} for #7 at 10 GHz, i.e. about 0.5 dB, for the case $Z_M << Z_0$ is not considered and $\sigma >> \omega\varepsilon$ is considered (solid line) in comparison with the case of $Z_M << Z_0$ and $\sigma >> \omega\varepsilon$ are not considered (dashed line), i.e. no simplification is performed.

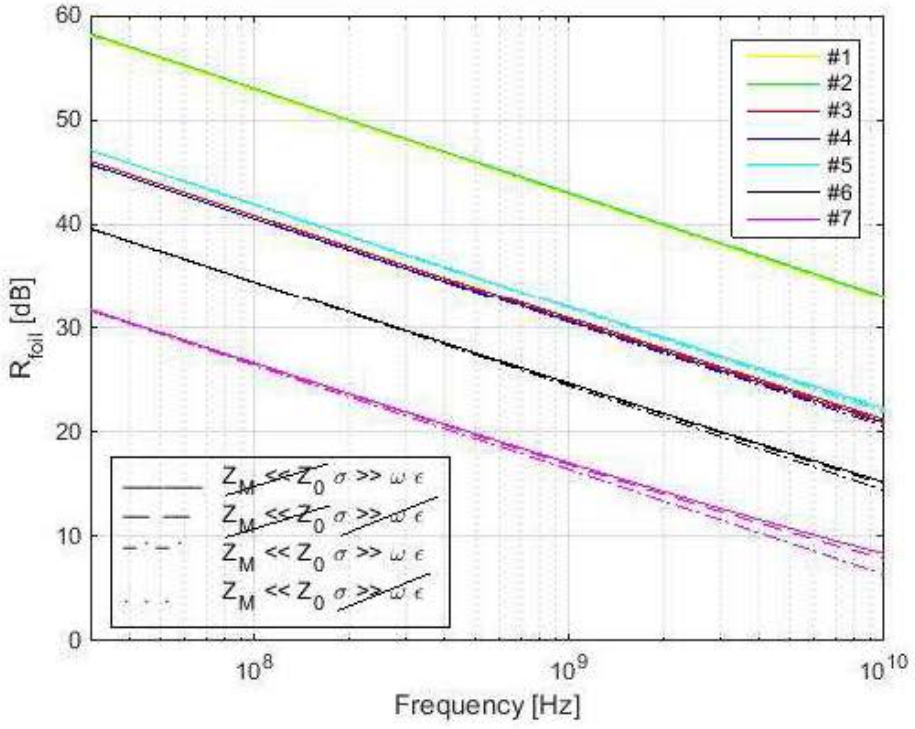

Fig. 62 R_{foil} evaluation for #1 - #7 and $Z_M << Z_0$ and $\sigma >> \omega\varepsilon$ are/are not considered (four combinations).

As a consequence, a simplification of ESE evaluation by $Z_M << Z_0$ and $\sigma >> \omega\varepsilon$ in frequency range up to 10 GHz is valid for samples with electrical conductivity value higher than 1000 S/m with an error up to 0.5 dB, for samples with electrical conductivity value 244 S/m with an error not exceeding 1 dB error and for samples with electrical conductivity value of 39 S/m an error up to 2 dB.

4.1.3. Evaluation of Reflection Loss of Aperture

Reflection loss of aperture $R_{aperture}$ is generally derived from the basic relation between the gain and effective aperture of the antenna. It is described as [141]:

$$A_e = \frac{\lambda^2}{4\pi} \mathrm{G}, \tag{38}$$

where λ is wavelength, A_e is effective aperture and, G is the gain.

The parameter A_e differs for different shapes of antenna loop [145]. Woven textile materials are manufactured by interlacing the yarns at right angles and therefore a rectangular or square shape of the apertures can be considered. Presented samples are manufactured from the same yarn and by the same sett in the warp and weft directions. As a consequence, the aperture is square shaped. For the square shape of antenna loop effective aperture is calculated as:

$$A_e = l^2, \tag{39}$$

where l is the length of the aperture.

The equality of (38) and (39) describes the gain as:

$$G_{aperture\_square} = \frac{4\pi\ell^2}{\lambda^2} = \left(\frac{2\ell\sqrt{\pi}}{\lambda}\right)^2, \tag{40}$$

The equation for G calculation for circular loop antenna and for a slot is commonly mentioned in literature as:

$$G_{aperture\_circular} = \left(\frac{2\pi r}{\lambda}\right)^2, \tag{41}$$

where r is the radius of the circular loop.

$$G_{aperture\_slot} = \left(\frac{2l}{\lambda}\right)^2, \tag{42}$$

where *l* is the length of the slot.

Reflection loss $R_{aperture}$ is then calculated [141], [143] as:

$$R_{aperture\_square} = 10 \cdot \log\left(\frac{1}{G_{aperture\_square}}\right) = 20 \cdot \log\left(\frac{\lambda}{2l\sqrt{\pi}}\right), \tag{43}$$

$$R_{aperture\_circular} = 10 \cdot \log\left(\frac{1}{G_{aperture\_circular}}\right) = 20 \cdot \log\left(\frac{\lambda}{2\pi r}\right), \tag{44}$$

$$R_{aperture\_slot} = 10 \cdot \log\left(\frac{1}{G_{aperture\_slot}}\right) = 20 \cdot \log\left(\frac{\lambda}{2l}\right), \tag{45}$$

Equations (43) – (45) can be also described as:

$$R_{aperture\_square} = 20 \cdot \log\left(\frac{c}{2\sqrt{\pi}}\right) - 20 \cdot \log\left(\ell \cdot f\right) = 158.55 - 20 \cdot \log\left(\ell \cdot f\right), \tag{46}$$

$$R_{aperture\_circular} = 20 \cdot \log\left(\frac{c}{2\pi}\right) - 20 \cdot \log\left(r \cdot f\right) = 153.58 - 20 \cdot \log\left(r \cdot f\right), \tag{47}$$

$$R_{aperture\_slot} = 20 \cdot \log\left(\frac{c}{2}\right) - 20 \cdot \log\left(l \cdot f\right) = 163.52 - 20 \cdot \log\left(l \cdot f\right), \tag{48}$$

where *c* is the speed of light.

Equations (46) – (48) are derived for one aperture in the foil. It can be seen that it is valid for any material with an aperture, because reflection loss of aperture $R_{aperture}$ is dependent on the frequency and dimensions of an aperture.

4.1.4. Evaluation of Reflection Loss of Multiple Apertures

Multiple apertures are discussed in [140], [142], [143]. The equation for multiple apertures is described as:

$$R_{aperture\_multiple} = -20 \cdot \log\sqrt{n}, \tag{49}$$

where *n* is the number of apertures.

Nevertheless, calculation of the number of apertures *n* is not unified in [140], [142], [143]. The conditions for (49) validity follow:

- Reference [140]: linear array of apertures, equal sizes and closely spaced apertures, the total length of linear array of apertures is less than ½ of the wavelength. If the two-dimensional array of holes is considered, (49) can be directly applied only for the first row of apertures (the rest of the apertures are not included in parameter n). This means, if the two-dimensional array is given by 7x12 holes, the n is equal to n=12. This approximation is motivated by experience.
- Reference [142]: equally sized perforations, hole spacing < $\lambda/2$, hole spacing > thickness, n is the number of all apertures
- Reference [143]: thin material, equally sized apertures, n is the number of all apertures

The minimal value of the wavelength can be easily found as depicted in Fig. 63. The results are shown for selected frequencies in Table XXVIII.

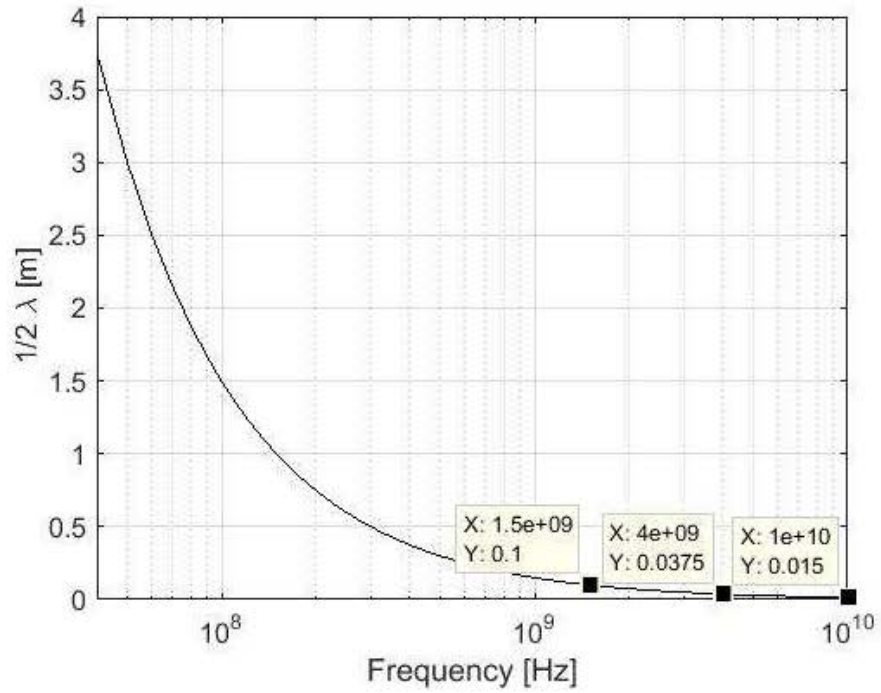

Fig. 63 Calculation of the ½ wavelength.

Table XXVIII Calculation of wavelength λ

Frequency [GHz]	½ λ [m]	½ λ [cm]
1.5	0.1	10
3	0.05	5
4	0.0375	3.75
10	0.015	1.5

The longest linear array of apertures can be determined with respect to ASTM D4935-10. The standard ASTM D4935-99 was withdrawn in 2005, because the committee could not maintain a standard for which the expertise may not lie within the current committee membership [146]. It also describes the dimensions of the measured samples. The longest linear array of apertures that can be found on the sample is the tangent of the inner circle limited by the middle circle, Fig. 64. The distance is equal to l_c = 0.069 m. That means the total length of apertures is less than ½ of the wavelength in the frequency range 30 MHz – 1.5 GHz.

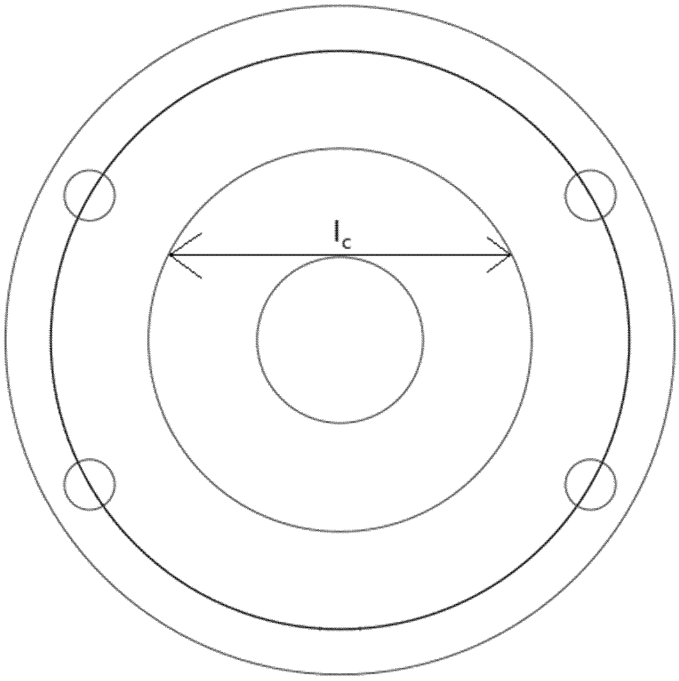

Fig. 64 The longest linear array of apertures according to ASTM 4935-10.

The apertures are equally sized, closely spaced and form a linear array of apertures because of the production process of textiles and parameters used during the production of samples.

The textile structure forms the two-dimensional array of holes and the longest linear array of apertures is equal to l_c = 0.069 m.

Hole spacing is equal to the yarn diameter, which is in the range of 0.220 – 0.251 x 10^{-3} m. It is less than ½ of the wavelength and it is less than the thickness of the material, which is at a minimum equal to 0.295 x 10^{-3} m, Table XXIX.

Table XXIX Material Characterization and Thin Material Evaluation

#	Sett [n/cm]	Fabric thickness [μm]	Yarn diameter [μm]	Aperture length [μm]	Thin material 7δ [GHz]	Thin material 5δ [GHz]	Thin material 3δ [GHz]
1	13	295	251	517	0.03 – 8.34	0.03 – 4.25	0.03 – 1.53
2	16	300	251	373	0.03 – 7.79	0.03 – 3.98	0.03 – 1.43
3	13	469	239	530	0.03 – 52	0.03 – 27	0.03 – 9.69
4	16	537	239	386	0.03 – 43	0.03 – 22	0.03 – 7.93
5	19	533	239	287	0.03 – 31	0.03 – 16	0.03 – 5.85
6	16	476	220	405	0.03 – 228	0.03 – 110	0.03 – 41.3
7	16	491	240	385	0.03 – 1 316	0.03 – 680	0.03 – 243

A difference of the thin and thick material is presented in [142]. The material is considered to be thick when there is no reflection from the "far" interface of the material. This definition can be verified by the equivalent depth of penetration δ (50), which defines a distance of wave penetration to amplitude wave degradation to the value e^{-1}, i.e. amplitude wave degradation of about 36.8 %, in comparison with the thickness of the material. If we consider 3δ, amplitude wave degradation is about 95 %, i.e. 95 % of the current flows within a material. This is the point beyond which current flow is negligible in a material [138]. Nevertheless, comparison for almost 100 % of amplitude wave degradation can be performed. The penetration depth 4δ decreases the amplitude wave to about 98.2 %, 5δ to about 99.3 %, 6δ to about 99.8 % and 7δ to about 99.9 %. If the penetration depth 3δ, 5δ and 7δ are calculated for sample #2 (the sample with the highest value of electrical conductivity, i.e. the value of penetration depth is the lowest), the dependence for the frequency band 30 MHz – 10 GHz is obtained, Fig. 65. The results show the penetration depth 3δ, 5δ and 7δ is lower than the thickness of #2 in the frequency range 1.43 – 10 GHz, 3.98 – 10 GHz and 7.79 – 10 GHz, respectively. This means that in this frequency range there is no reflection from the "far" interface of the material. In other words, the material is considered to be thick. In the frequency range 30 MHz – 1.43 GHz for 3δ, 30 MHz – 3.98 GHz for 5δ and 30 MHz – 7.79 GHz for 7δ, there are reflections from the "far" interface of the material and therefore the material is considered to be thin, Table XXIX.

$$\delta = \sqrt{\frac{2}{\omega\mu\sigma}} = \frac{1}{\sqrt{\pi f \mu\sigma}}, \tag{50}$$

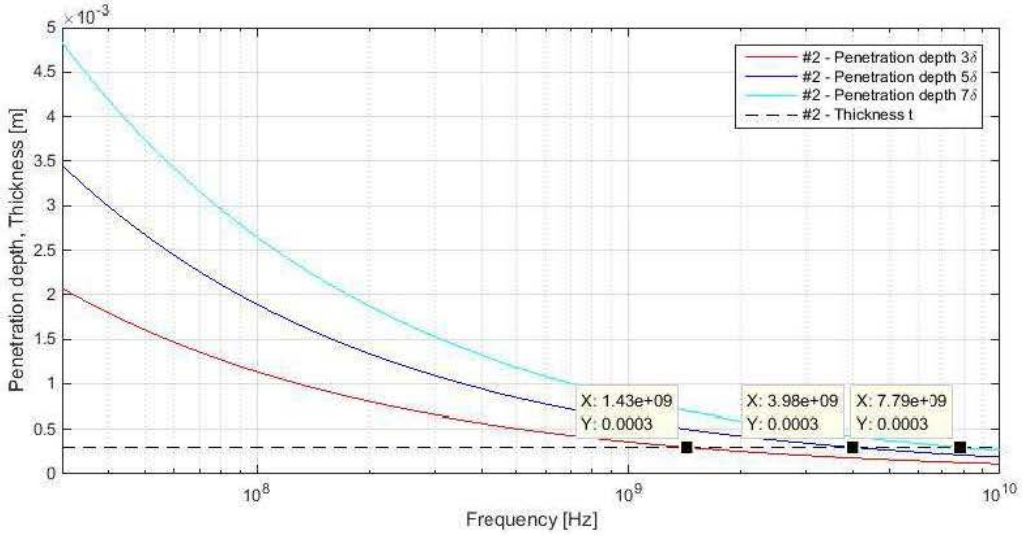

Fig. 65 Penetration depth 3δ, 5δ and 7δ in comparison with thickness for #2.

As a consequence of the reflection loss of multiple apertures discussion, (32) has to be specified for electrically conductive textile samples described, i.e. (49) is added and the values of electrical conductivity of described samples are considered.

4.1.5. Evaluation of ESE Fabric

An expression for ESE calculation of fabric has been developed on the basis of plane wave shielding theory [138], [139]. It is based on linear combination of ESE of compact material f_1 (l, λ) (in lower frequency ranges) and ESE of apertures f_2 (l, λ) (in higher frequency ranges) as shown in (32). It can be written as:

$$f_1(\ell,\lambda) + f_2(\ell,\lambda) = 1; \quad f_2(\ell,\lambda) = 1 - f_1(\ell,\lambda), \tag{51}$$

$$ESE_{fabric} = f_1(\ell,\lambda)\cdot ESE_{foil} + \left(1 - f_1(\ell,\lambda)\right)\cdot ESE_{aperture}, \tag{52}$$

A one dimensional base of the solution f_1 (l, λ), i.e. f_1 (l, λ) with respect to λ calculation $\lambda = c / f$, can be written as [138]:

$$f_1(\ell, f) = e^{-C\ell\sqrt{f}}, \tag{53}$$

where C is the constant.

An assumption of the equality of components, which correspond to reflection loss R of compact material R_{foil} and material with apertures $R_{aperture}$, is used for f_1 (l, λ) derivation:

$$R_{foil} = R_{aperture}, \tag{54}$$

The parameter R_{foil} can be used in its simplified version because the R_{foil} evaluation shows the difference is not significant for samples #1 – 6#, especially for the frequency range up to 3 GHz, i.e. error does not exceed 0.5 dB, Fig. 62. Then (35) and (36) for material with electrical conductivity σ are valid. $R_{aperture}$ is used from (46) and (49). It is written as:

$$20 \cdot \log\left(\frac{1}{4}\sqrt{\frac{\sigma}{\omega\mu_r\varepsilon_0}}\right) = 20 \cdot \log\left(\frac{c}{2\sqrt{\pi}}\right) - 20 \cdot \log(\ell f) - 20 \cdot \log\left(\sqrt{n}\right), \tag{55}$$

(55) can be modified as:

$$\log\left(\frac{\sigma}{16\omega\mu_r\varepsilon_0}\right) = \log\left(\frac{c^2}{4\pi}\right) - \log\left(\ell^2 f^2\right) - \log(n), \tag{56}$$

$$\log\left(\frac{\sigma}{32\pi f\mu_r\varepsilon_0}\right) = \log\left(\frac{c^2}{4\pi\ell^2 f^2 n}\right), \tag{57}$$

$$\frac{\sigma n}{8c^2\mu_r\varepsilon_0} = \frac{1}{\ell^2 f}, \tag{58}$$

$$l\sqrt{f} = \sqrt{\frac{8c^2\mu_r\varepsilon_0}{\sigma n}}, \tag{59}$$

A boundary condition, which defines a decrease of the amplitude about 95 % in specific material [138], i.e. equivalent of 3 depth of penetration (3δ decrease of the amplitude on the multiple $e^{-1} \cdot e^{-1} \cdot e^{-1} = e^{-3}$ of original value) can be used in:

$$Cl\sqrt{f} = e^{-3} = C\sqrt{\frac{8c^2\mu_r\varepsilon_0}{\sigma n}}, \tag{60}$$

$$C = \frac{e^{-3}}{l\sqrt{f}} = e^{-3}\sqrt{\frac{\sigma n}{8c^2\mu_r\varepsilon_0}} = 1.972 \cdot 10^{-5}\sqrt{\sigma n}, \tag{61}$$

Evaluation of the constant *C* and *n* are shown for samples #1 – #7 in Table XXX. The number of apertures *n* is calculated with respect to the longest linear array of apertures of ASTM 4935-10, i.e. l_c = 0.069 m and sett of each sample d_w as:

$$n = l_c \cdot d_w, \tag{62}$$

Table XXX Calculation of the *C* Constant

#	σ [S/m]	d_w [n/cm]	*n*	*C*
1	1.71E+04	13	89	2.44E-02
2	1.77E+04	16	110	2.76 E-02
3	1.07E+03	13	89	6.1 E-03
4	1.00E+03	16	110	6.6 E-03
5	1.37E+03	19	131	8.4 E-03
6	2.44E+02	16	110	3.2 E-03
7	3.9E+01	16	110	1.3 E-03

As a consequence, (52) is specified for sample #1 as:

$$ESE_{fabric} = e^{-0.0244 \cdot \ell \cdot \sqrt{f}} \cdot ESE_{foil} + \left(1 - e^{-0.0244 \cdot \ell \cdot \sqrt{f}}\right) \cdot ESE_{aperture}, \tag{63}$$

It is obvious ESE calculation has to be specified for each sample with regards to its electrical conductivity, sett and number of apertures. Therefore an equation for ESE calculation of woven fabrics manufactured from the electrically conductive mixed and coated yarns with square apertures can be written generally with respect to C constant calculation (61) as:

$$ESE_{fabric} = e^{-C \cdot \ell \cdot \sqrt{f}} \cdot ESE_{foil} + \left(1 - e^{-C \cdot \ell \cdot \sqrt{f}}\right) \cdot ESE_{aperture}, \tag{64}$$

The calculation of ESE_{foil} is performed according to (33), (36) and (37) and it is also described in depth in [13], [137], [139], [140], [141] as:

$$ESE_{foil} = 168.14 + 20 \cdot \log\left(\sqrt{\frac{\sigma_r}{f \mu_r}}\right) + 8.6859 \frac{t}{\delta} + 20 \cdot \log\left|1 - e^{-2t/\delta} e^{-j2\beta t} \left(\frac{Z_0 - Z_M}{Z_0 + Z_M}\right)^2\right|, \tag{65}$$

4.1.6. Evaluation of ESE of Apertures

$ESE_{aperture}$ is calculated as a sum of $R_{aperture}$, $A_{aperture}$ and $K_{aperture}$. $R_{aperture}$ is derived in this chapter and expressed in (46) and (49) as:

$$R_{aperture} = 158.55 - 20 \cdot \log(\ell \cdot f) - 20 \cdot \log(\sqrt{n}), \quad (66)$$

The absorption loss $A_{aperture}$ is included in $ESE_{aperture}$ if the fabric is considered to be a thick material, Table XXIX. It is calculated for a subcritical rectangular waveguide as [140], [143]:

$$A_{aperture} = 27.2 \frac{t_a}{l_a}, \quad (67)$$

where l_a is the largest linear dimension of the cross-section of the aperture and, t_a is the depth of the aperture (length of "waveguide").

As shown in Table XXIX, samples #1 – #7 are considered to be thin in a specific analysed frequency range 30 MHz – 1.5 GHz for 7δ, 5δ and also 3δ (with the exception of the most electrically conductive sample #2 in the frequency range 1.43 – 1.5 GHz) and therefore $A_{aperture}$ is not included in $ESE_{aperture}$ calculation. $K_{aperture}$ takes into account the geometrical dimensions of the aperture in a shielding barrier. It is described as [139]:

$$K_{aperture} = 20 \cdot \log\left(1 + \ln\left(\frac{\ell}{s}\right)\right), \quad (68)$$

(68) clearly shows the square apertures, i.e. $l = s$, do not influence $ESE_{aperture}$. Therefore the resultant $ESE_{aperture}$ is calculated for #1 – #7 characterized as thin material as:

$$ESE_{aperture} = R_{aperture} = 158.55 - 20 \cdot \log(\ell \cdot f) - 20 \cdot \log(\sqrt{n}), \quad (69)$$

4.1.7. Comparison of Equations for ESE Fabric

As previously mentioned, the ESE_{fabric} is calculated as (64), e.g. (63) for #1. A similar equation was also previously mentioned as (32) for metallized fabric shields as published in [25, 28]. (32) is furthermore derived in order to compare (32) and (63) for specific samples. The constant $C = 0.129$ is obtained as:

$$Cl\sqrt{f} = e^{-3} \Rightarrow C = \frac{e^{-3}}{l\sqrt{f}} = \frac{2.71^{-3}}{0.389} = 0.129, \quad (70)$$

The authors in [138] use the value 2.71 for the mathematical constant e, which is approximately equal to e = 2.718 828. Moreover, the value of $l\sqrt{f}$ is equal to

$l\sqrt{f}$ = 0.389, which is written as $l\sqrt{f}$ = 0.398 in [138] (and obviously calculated as $l\sqrt{f}$ = 0.389). The value of $l\sqrt{f}$ = 0.389 is calculated with respect to the description of (55) from:

$$20\cdot\log\left(\frac{1}{4}\sqrt{\frac{\sigma}{\omega\mu_r\varepsilon_0}}\right)=100-20\cdot\log\left(\ell f\right), \tag{71}$$

$$\log\left(\frac{\sigma}{32\pi f\mu_r\varepsilon_0}\right)=10-\log\left(\ell^2 f^2\right), \tag{72}$$

$$\log\left(\frac{\sigma}{32\pi\mu_r\varepsilon_0}\right)-10=-\log\left(\frac{1}{f}\right)-\log\left(\ell^2 f^2\right), \tag{73}$$

Considering the electrical conductivity of copper, i.e. σ = 5.85 x 10^7 S/m [144], the material used for electrically conductive textile material production in [138], (73) is rewritten as:

$$16.818-10=\log\left(\frac{1}{\ell^2 f}\right), \tag{74}$$

$$10^{-6.818}=\ell^2 f, \tag{75}$$

$$\ell\sqrt{f}=10^{\frac{-6.818}{2}}=10^{-3.409}=389.9\cdot10^{-6}, \tag{76}$$

The order of the value $l\sqrt{f}$ = 389.9 x 10^{-6} is multiplied by 1000 because of used units [mm] and [MHz] in [138], i.e. 10^{-3} [m] and 10^6 [Hz].

Equations (71) – (73) show no apertures are considered and the condition $Z_M << Z_0$ is applied. The value 100 is derived from the $R_{aperture}$ equation, e.g. (43) – (48), as:

$$R_{aperture}=20\cdot\log\left(\frac{c}{x}\right)-20\cdot\log\left(\ell\cdot f\right)=100-20\cdot\log\left(\ell\cdot f\right), \tag{77}$$

$$20\cdot\log\left(\frac{c}{x}\right)=100\Rightarrow10^5=\frac{c}{x}, \tag{78}$$

$$x=\frac{c}{10^5}, \tag{79}$$

The equations (46) – (48) show the value of parameter x is equal to 2 (slot aperture), $2\sqrt{\pi}$ (circular aperture) or $2\sqrt{\square}$ (square aperture). If the speed of light c = 3 x 10^8 m/s is considered, the x is equal to x = 3000. Nevertheless, if the speed of

light is equal to c = 186 000 miles/s, the x = 1.86. This result is close to the value, which is valid for the slot aperture. If the value x = 2 is used, (48) is described as:

$$R_{aperture} = 20 \cdot \log\left(\frac{186000}{2}\right) - 20 \cdot \log(\ell \cdot f) = 99.4 - 20 \cdot \log(\ell \cdot f), \quad (80)$$

The value 99.4 presented in (80) is further rounded to the value 100.

The derivation of (32) clearly shows the used equation is valid for copper metallized fabric, i.e. fabric without apertures, as the authors present in [138] and [139], and not valid for electrically conductive woven textile materials manufactured from the electrically conductive mixed and coated yarns.

4.1.8. Results and Discussion

The presumption of validity of $Z_M << Z_0$ and $\sigma >> \omega\varepsilon$ for reflection loss of foil evaluation is previously mentioned in detail. It is also shown in Fig. 60, Fig. 61, Fig. 62, and Table XXVII. The validity of presented inequalities is based on a ratio of magnitudes of individual values, i.e. at least two orders of values of magnitudes are required. As a result, a simplified version of the Z_M, i.e. $\sigma >> \omega\varepsilon$ is valid, and (36) can be used for #1 – #6 up to 10 GHz and for #7 up to approx. 6.9 GHz. The presumption of $Z_M << Z_0$ is valid for #7, #6 and #4 up to 70 MHz, 439 MHz and 1.8 GHz, respectively, if the validity of $\sigma >> \omega\varepsilon$ is assumed and up to 34.6 MHz, 219.5 MHz and 899.9 MHz, respectively, if the validity of $\sigma >> \omega\varepsilon$ is not assumed. It can be seen, the greater value of electrical conductivity of samples is, the greater frequency limit is obtained. As a result, #1 – #3 and #5 fulfil this validity up to frequency limit, which is greater than 1.8 GHz (#4, i.e., σ = 1000 S/m). This frequency limit is chosen with respect to the limits of ASTM D4935-10, i.e., 0.03 – 1.5 GHz. The presumption of validity of $Z_M << Z_0$ and $\sigma >> \omega\varepsilon$ is also verified for R_{foil} parameter, i.e. $Z_M << Z_0$ and $\sigma >> \omega\varepsilon$ are/are not considered (in all four combinations), and also for all samples #1 – #7, Fig. 62. It shows the greatest difference is reached for the sample with the lowest electrical conductivity from #1 – # 5, i.e. #4, and it is equal to about 0.5 dB in 10 GHz. The similar results are obtained for #6 and #7, i.e. 1 dB and 2 dB, respectively, in 10 GHz. As a consequence, the presented limits for $Z_M << Z_0$, e.g., 70 MHz, 439 MHz and 1.8 GHz for #7, #6 and #4, respectively, can be ignored and the relevant error has to be taken into account.

Derivation of reflection loss of one aperture shows an importance of determination of the effective aperture A_e for different shapes of aperture. It is obvious knitted fabrics require different calculation of reflection loss of one aperture in comparison with woven fabrics.

Calculation of reflection loss of multiple apertures is not unified in scientific literature [140], [142], [143], because different conditions for calculation of number of apertures n are presented. It is for instance the calculation of total length of linear array of apertures l_c. Obviously, different size of samples results in different value of total length of linear array of apertures l_c. We consider standard ASTM D4935-10, which is one of the most used standards for ESE evaluation, and l_c = 0.069 m, Fig. 64. This parameter has to be also less than ½ of the wavelength, and it fulfils this condition in the frequency range defined in ASTM D4935-10, i.e., 30 MHz – 1.5 GHz, Fig. 63 and Table XXVIII. One of the conditions is also that the material has to be thin, which is verified by comparison of the equivalent depth of penetration δ, usually 3δ, and the thickness of the material t, i.e., material is considered to be thin if inequality $3\delta > t$ is valid. The results show the penetration depth 3δ is greater than the thickness of #2 (the sample with the highest value of electrical conductivity, i.e., the value of penetration depth is the lowest from all samples) in the frequency range 30 MHz – 1.43 GHz, Fig. 65 and Table XXIX.

The penetration depth for 5δ and 7δ is also analysed in order to verify whether there are any reflections from the "far" interface of the material for the frequency beyond 1.43 GHz, i.e., the material can be considered to be thin. The results show it is valid for 5δ and 7δ in frequency range 30 MHz – 3.98 GHz, and 30 MHz – 7.79 GHz, respectively, Fig. 65 and Table XXIX.

The results of reflection loss of multiple apertures evaluation show (49) has to be considered in reflection loss calculation and the values of electrical conductivity and thickness of samples have to be considered because of thin/thick material evaluation.

Evaluation of ESE fabric considers simplified version of reflection loss of foil, i.e., $Z_M << Z_0$ and $\sigma >> \omega\varepsilon$ are valid, a boundary condition, which defines a decrease of the amplitude about 95 % in specific material, i.e., equivalent of 3 depth of penetration e^{-3}, and number of apertures, which is calculated with respect to the longest linear array of apertures of ASTM 4935-10, i.e., l_c = 0.069 m. As a result, constant C, the value in the exponent of Euler's number in the equation of ESE fabric calculation, is derived (61), Table XXX. It clearly shows ESE fabric evaluation depends on sett, number of the longest linear array of apertures and electric conductivity of each sample. As a consequence, the equation for ESE calculation of woven fabrics manufactured from the electrically conductive mixed and coated yarns with square apertures is generally derived (64) with respect to (61).

Individual components of ESE fabric evaluation are ESE_{foil}, i.e., the ESE values for metallic foil of the same thickness as the fabric (33), (65), which is derived and described in many research papers [135], [13], [137], [139], [140], [141], and $ESE_{aperture}$, i.e., the ESE values for metallic foil of the same thickness as the fabric

with aperture(s), which is derived in this chapter for particulate-blended shielding electrically conductive textile composites, i.e., woven fabrics manufactured from the electrically conductive mixed and coated yarns with square apertures, samples #1 – #7. Calculation of reflection loss of aperture $R_{aperture}$ is a sum of reflection loss of one aperture $R_{aperture\_square}$ (46) and reflection loss of multiple apertures $R_{aperture\_multiple}$ (49), i.e., (66). The absorption loss $A_{aperture}$ is neglected because the material is considered to be thin. A correction of geometrical dimensions of the aperture $K_{aperture}$ does not influence $ESE_{aperture}$ because of square apertures. As a result, the resultant $ESE_{aperture}$ is equal to $R_{aperture}$.

Derivation of $ESE_{aperture}$ (69) and ESE_{fabric} (64) clearly shows many factors have to be considered, i.e., shape of apertures, thickness of fabric in comparison with penetration depth (in order to determine conditions for thin/thick material), values of electrical conductivity, validation of $Z_M << Z_0$ and $\sigma >> \omega\varepsilon$, total length of linear array of apertures and sett of the fabric. It also shows (32) is valid for copper metallized fabric, i.e., fabric without apertures, and not valid for electrically conductive woven textile materials manufactured from the electrically conductive mixed and coated yarns.

Modelling of the ESE_{fabric} (64) with respect to used textile material, i.e. electrical conductivity of samples described in Table XXVI, evaluation of the constant C (61) and n (62) shown in Table XXX, calculation of the ESE_{foil} presented in (33) and specified in (36) and $ESE_{aperture}$ derived in (69) can be performed and compared with measurement results, Fig. 66.

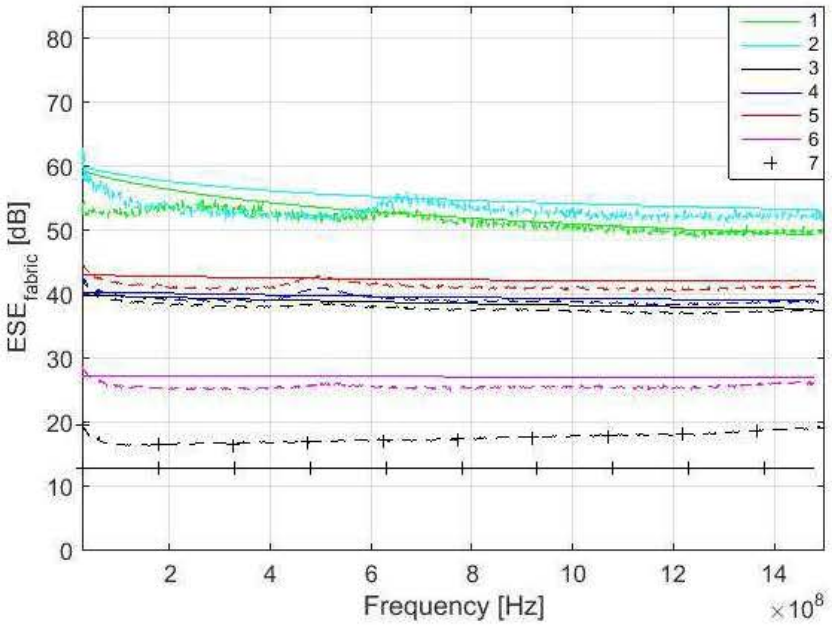

Fig. 66 Comparison of the modelling (solid line) and measurement results for #1 – #7 in 30 MHz – 1.5 GHz.

Measurement is performed according to ASTM D4935-10 [22] (22 °C, RH 48 %). The results show the presented equations are valid for electrically conductive textile materials with a value of electrical conductivity equal to and higher than σ = 244 S/m, i.e., samples #1 – #6. The maximal difference between modelling and measurement results is obtained for #1 and #2 in the frequency range 30 MHz – 280 MHz. This is in the range of 2 – 6 dB. Nevertheless, it is within the random error of the used measurement method, which is defined in ASTM D4935-10 as ±5 dB. It is also within an observed standard deviation based on measurements by five laboratories on five samples presented in ASTM D4935-10 as 6 dB [22]. It is important to note that the measurement results are evaluated with respect to ASTM D4935-10, which defines test procedure in the frequency range 30 MHz – 1.5 GHz. The measurement results are therefore only informative in the frequency range 1.5 GHz – 3 GHz, i.e., increasing value of the measured ESE is caused by the excitation of modes other than the TEM [22], Fig. 67. The results for sample #7, show these equations have to be modified for these materials (σ = 39 S/m). The frequency range of the model can be also extended, Fig. 68. It shows increasing and decreasing trend of the ESE_{fabric} of samples.

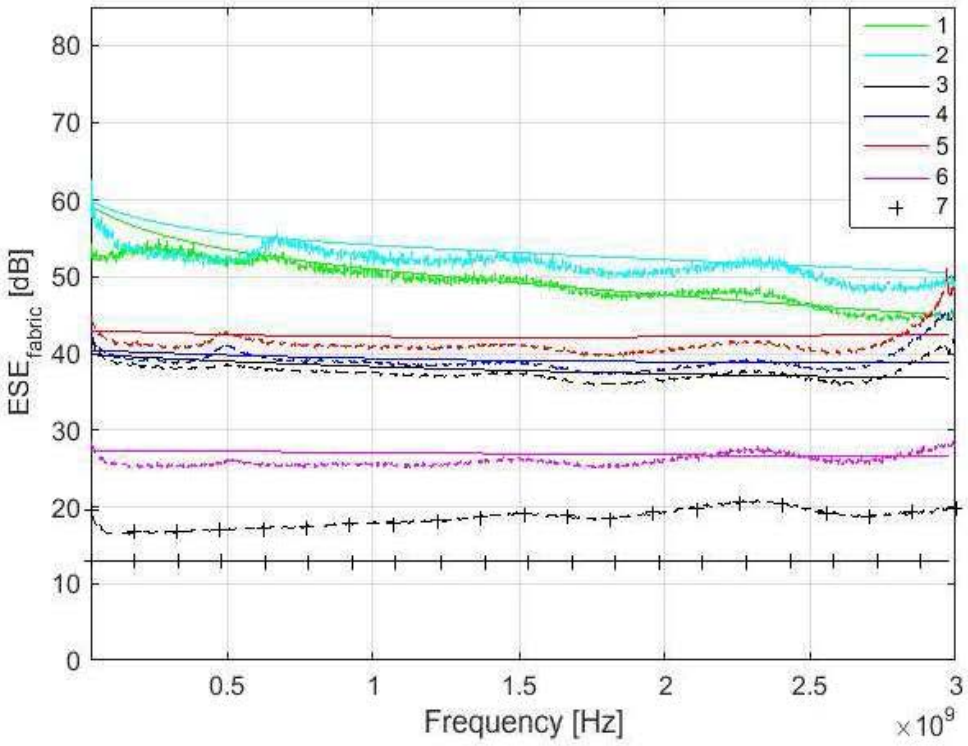

Fig. 67 Comparison of the modelling (solid line) and measurement results for #1 – #7 in 30 MHz – 3 GHz.

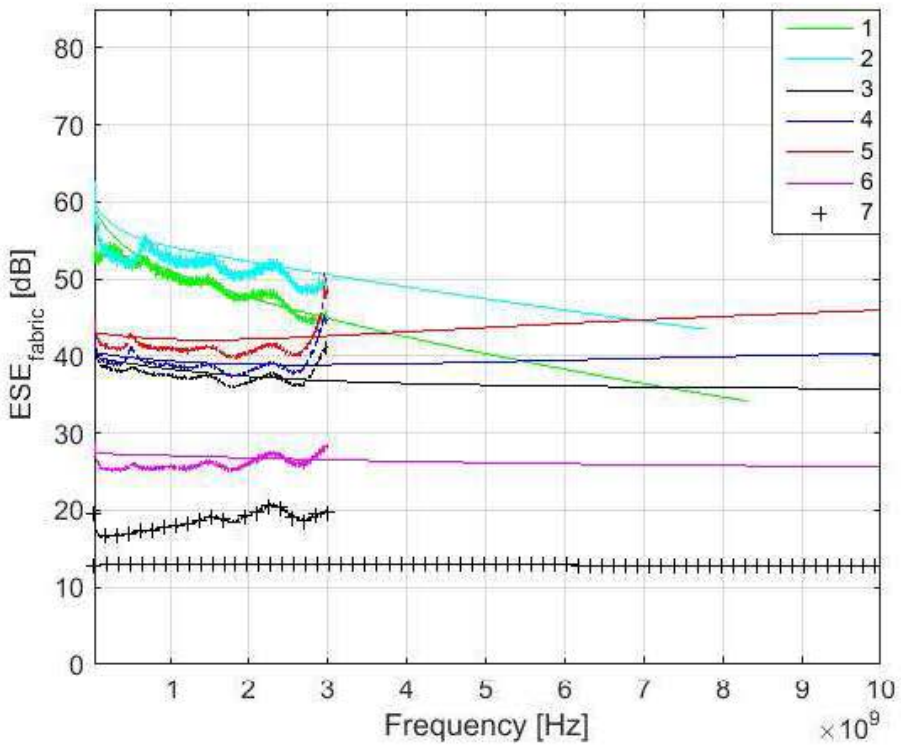

Fig. 68 Comparison of the modelling (solid line) and measurement results for #1 – #7 in 30 MHz – 3 GHz (7δ) and modelling (solid line) results in 3 GHz – 10 GHz.

4.1.9. Conclusions

The chapter is focused on a derivation of a numerical model of electromagnetic shielding efficiency for woven fabrics manufactured from the electrically conductive mixed and coated yarns. Commonly used measurement techniques are mentioned. Basic equations of electromagnetic shielding efficiency calculation are presented.

An evaluation of reflection loss of foil is described in depth and verifies the assumption of $Z_M << Z_0$ and $\sigma >> \omega\varepsilon$ in frequency range up to 10 GHz is valid for specimens with electrical conductivity higher than 1000 *S*/m with an error up to 0.5 dB, for a specimen with electrical conductivity 244 *S*/m with an error not exceeding 1 dB error and for a specimen with electrical conductivity 39 *S*/m an error up to 2 dB.

A derivation of reflection loss of one aperture is performed for a slot, square aperture and circular aperture. The evaluation of reflection loss of multiple apertures describes the different calculation of the number of apertures in a shielding barrier and verifies presented conditions for its calculation. The longest linear array of apertures is used for the numerical model.

A complete derivation of electromagnetic shielding efficiency of woven fabrics manufactured from the electrically conductive mixed and coated yarns is presented in detail. It shows the equations for electromagnetic shielding efficiency evaluation differ

for a material, which is considered to be thin or thick (based on penetration depth and thickness comparison), for different values of electrical conductivity and for different sett of used manufacturing process.

A comparison of modelling and measurement results of electromagnetic shielding efficiency fabric is performed in frequency range 30 MHz – 1.5 GHz according to ASTM D4935-10. It clearly shows a numerical model is valid for electrically conductive woven textile materials with a value of electrical conductivity equal to and higher than σ = 244 S/m. The results of the numerical mode are also extended up to 10 GHz in order to show the trend of electromagnetic shielding efficiency.

4.2. Application - Shielding Textiles for Increasing Safety Airborne Systems (Limitation of GSM Interference)

The continued growth in air travel requires a strict adherence to safety regulations, including such that seek to minimize interference from mobile devices. Aviation regulations include restrictions on the use of portable electronic devices that may affect airplane systems and equipment. These regulations are binding for all operators of commercial airplanes. Most airlines issue verbal or graphic warnings. This chapter discusses the use of shielding textiles and the development of a special shielding textile that protects aircraft electronic systems from interference by Global System for Mobile Communications (GSM) mobile terminals [5].

4.2.1. Rationale

The use of Portable Electronic Devices (PEDs) aboard aircraft is a source of electromagnetic radiation that interferes with aircraft electrical systems. PEDs are divided into several groups based on the risks they pose to airplane systems. The largest group of PEDs includes radio transmitters such as mobile phones. These devices have to be switched off in flight, especially during landing and take-off [147].

These devices are considered as transmitters. A mobile station (MS) transmits user and control data when communicating with the GSM network. Mobile stations operate in frequency ranges of 450 up to 2690 MHz, depending on the transmission technology and area of use.

Random impulse interference occurs. Measurements were performed under continuous power conditions, transforming impulse interference to continuous interference.

The present research was spurred by the findings of a study [148] that assessed the impact of a continuous high-frequency signal in the GSM frequency range on an aeronautical on-board system consisting of:

- Very high frequency (VHF) communication transceiver
- VHF omni directional radio range / Instrument Landing System (VOR/ILS) navigation receiver
- Gyro-stabilized distant-reading compass

The types and numbers of anomalies are summarized in a report. The measurement data confirm the need to restrict the use of mobile phones aboard airplanes. Compliance with this restriction must be enforced to ensure the reliable

function of the avionics. The severest effects of interference observed are shown in Table XXXI.

Table XXXI Interference Effect

Aircraft system	Defect
Compass	Stiff azimuth, sudden changes in azimuth values
Indicators	Unstable data
VOR	5-degree error
VOR	"From" – "To" changes
VOR and ILS	Error data without warnings
ILS Localiser	Impaired sensitivity
Audio device	Background noise

The study above is only one of the many initiatives undertaken worldwide that concluded that the use of mobile phones must be restricted during critical phases of flight. Verbal warnings are used in civil aviation, e.g. "Please switch off your mobile phones". Printed instructions to the same effect are found at various locations in the aircraft.

The critical phases of flight include taxiing (when device calibration occurs), take off, landing and any nonstandard situations. Erroneous information can divert the attention of the crew during these critical periods and lead to an incorrect crew response.

There is no evidence of the role of interference from PEDs in airplane accidents; however, the effects of interference were demonstrated multiple times and not only in laboratory conditions. One of the effective ways of preventing accidents is the use of shielding cases which block communication between mobile phones and base stations, thereby reducing the impact that mobile phones have on avionics or other airplane communication systems.

4.2.2. Mobile Terminals and Signal Quality

In general, signal quality is defined by Signal-to-Noise Ratio (SNR), which is the ratio of useful signal P_s and noise P_n:

$$SNR = \log \frac{P_S}{P_n} \quad [dB]. \tag{81}$$

A decrease in SNR (decrease in P_s) leads to an increase in Bit Error Rate (BER).

This is due to P_s attenuation in the communication channel. LPATH is defined as the attenuation of an electromagnetic wave with the wave length λ propagated through the air over the distance d (wireless data transmission) [149].

$$L_{PATH} = \left(\frac{\lambda}{4 \cdot \pi \cdot d} \right)^2 \quad [dB]. \tag{82}$$

If our aim is to block communication between the base station and the mobile terminal, attenuation in the communication channel must be increased by introducing additional losses. This leads to a decrease in SNR and increase in BER whereby the mobile terminal is disconnected from the network.

The new attenuation L^*_{PATH} adds another source of signal attenuation to the L_{PATH} by introducing an $ESE_{ABSORBER}$.

$$L^*_{PATH} = \left(\frac{\lambda}{4 \cdot \pi \cdot d} \right)^2 + ESE_{ABSORBER} \quad [dB]. \tag{83}$$

In EMC, undesirable electromagnetic signals are attenuated by electromagnetic shielding or absorbers.

4.2.3. Absorber DEMO Proposal

The ability of specific materials to reduce the intensity of electromagnetic radiation is related to their electrical conductivity [146] or ESE. Fabrics can be made with continuous carbon fibres instead of glass fibres using in laminated fabric production techniques.

An absorber consists of three layers of planar textiles. The external layers are made of a polyester fabric. The core is made of a special textile that provides shielding from electromagnetic radiation in the frequency range from several tens of MHz to several GHz. This textile was developed as part of the Be-Tex project.

Samples of the cloth were made from a composite carbon yarn with a rectangular cross-section and a fineness of 220 tex in both weft and warp directions. The thread count is 10 threads per cm. A macro picture of the carbon textile is shown in Fig. 69.

The physical-mechanical parameters of this new shielding fabric can be adjusted by modifying the production parameters.

An example of an absorber and mobile station is shown in Fig. 70 and Fig. 71.

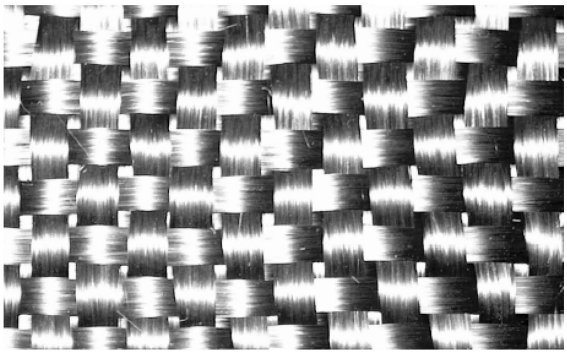

Fig. 69 Macro picture of a carbon fabric.

Fig. 70 Example of absorber and mobile station.

Fig. 71 Example of absorber and mobile station inside the absorber.

4.2.4. Prototyping, Measurement, Discussion

To measure attenuation, we placed a source of electromagnetic radiation in a case made of the tested material (shielding fabric). The attenuation value was obtained by comparing the difference in field strength inside and outside the case. For this type of measurement we can also use an EMC test chamber of the type used for mobile phone testing.

A NOKIA 3310 mobile phone with network monitor activated was used for the measurements, as it allowed us to read the signal strength (indicated in dBm) directly. Measurements were performed with the phone outside and inside the case.

To record the measurement data, we used the GSMcables-developed BTS SCAN v 2.00 freeware solution [150] which reads data from the mobile station via RS-232. The measurement data for the 900 MHz and 1800 MHz GSM frequency bands are shown in Fig. 72 and Fig. 73.

The signal strength of a given GSM radio channel can be measured with an accuracy of 0.5 dB. The software is only used for remote communication with and control of the mobile phone's network monitor via AT commands (AT stands for attention).

The experiment led to the creation of a working prototype of textile absorber capable of blocking communication between a mobile phone and a base station. The textile material achieves an attenuation of over 37 dB in the 900 MHz frequency band and over 30 dB in the 1800 MHz frequency band.

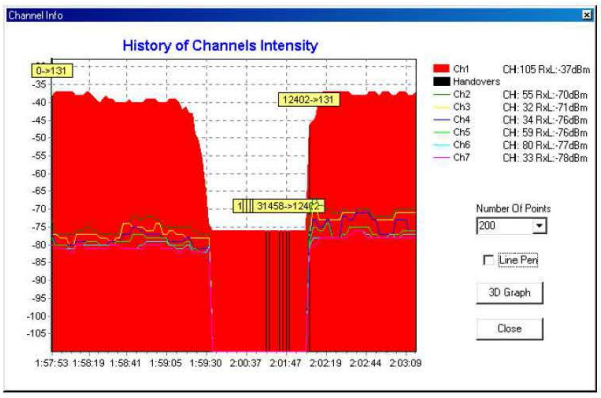

Fig. 72 Attenuation of mobile phone signal in the 900 MHz frequency band, the mobile phone is placed inside the case.

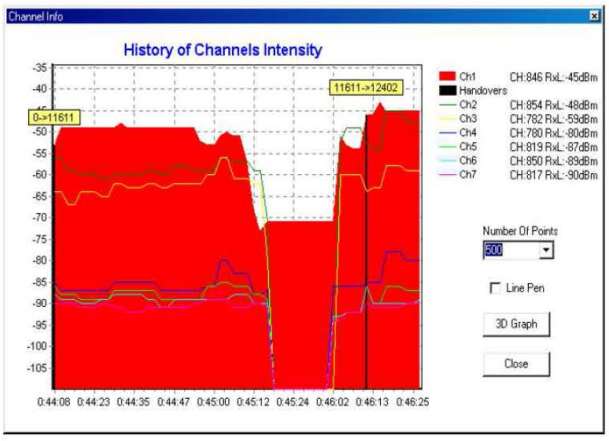

Fig. 73 Attenuation of mobile phone signal in the 1800 MHz frequency band, the mobile phone is placed inside the case.

4.2.5. Conclusions

This chapter describes the development of a textile absorber that blocks communication between a mobile phone and a base station, preventing any instrument errors in avionics equipment and other aircraft communication systems that might result from impulse interference. The goal, which we managed to achieve, was to stop mobile phones from interfering with other sensitive devices. The absorber we have developed achieves an attenuation of over 37 dB in the 900 MHz frequency band and over 30 dB in 1800 MHz frequency band. These attenuation values ensure that the mobile phone is unable to communicate with any GSM base station.

4.3. Application - Data Hardware Protection of Electronic Identifiers, Especially RFID Proximity Cards

Contactless personal and object identification systems and contactless payment systems are susceptible to tampering, theft or fraud. An increasing number of scientific publications have dealt with various non-invasive (i.e., from the owner's point of view) attacks on electronic identification systems. In a non-invasive attack, the attacker does not come into physical possession of the identifier, but can read the data stored in the identifier over a long range. Methods of preventing such attacks are dealt with in the field of cryptography.

This chapter is focused on data hardware protection of electronic identifiers based on RFID technology [157]. The use of new shielding fabrics prevents unauthorized reading of data from electronic identifiers.

4.3.1. Working principle

RFID technology is based on the well-known principle of the radar. RFID tags can be active or passive. This chapter focuses mainly on passive RFID tags, Fig. 74.

The reader generates an electromagnetic wave at the carrier frequency which is received by the RFID tag antenna. The induced voltage produces an electric current which is then rectified and used to charge a capacitor. The capacitor serves as an electric power supply for the RFID tag's logic and radio circuits.

When the capacitor receives a certain minimum voltage, the logic controller or microprocessor (i.e., the control circuits in the tag) is activated and the tag responds to the reader. The transmission of data is based on mainly Amplitude Shift Keying (ASK) modulation which involves changes in the terminating impedance of the RFID tag antenna (antenna matching or short-circuit termination). The reflections caused by changes in the antenna's impedance are detected and interpreted as logical "1" and logical "0" values. The communication control and communication circuit parameters are defined in an International Organization for Standardization (ISO) standard [151].

There has to be enough energy for the RFID tag capacitor to charge and the reader must be able to detect and receive a response from the tag. The quality of the signal decreases with distance between the reader and the tag. Noise in the signal may make it impossible for the reader to detect the message. The reader can also write information to the tag by modulating the waves.

An external reader must supply enough energy to the RFID tag for identification to occur.

There are two main methods of energizing RFID tags:

- Near-field communication – involves the inductive coupling of the RFID reader antenna (coil) and the tag (low and high frequency ranges)
- Far-field communication – involves the use of antenna systems with dimensions comparable to the wavelength of the carrier wave (very high and ultra-high frequency ranges)

A decrease in the useful signal power affects the read range. In the worst-case scenario, communication between the RFID tag and the reader may become impossible.

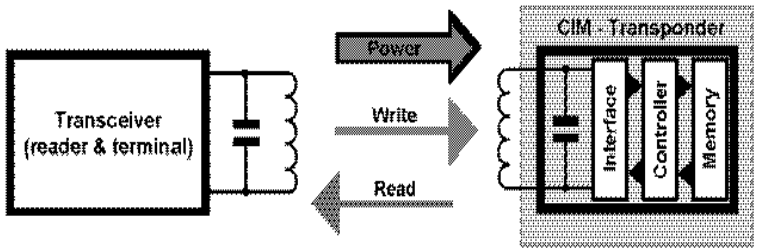

Fig. 74 Principle of RFID communication.

The power collected by an RFID tag can be calculated as [152]:

$$P_{CHIP} = P_{READER} \cdot C \cdot \tau \quad [W], \tag{84}$$

where P_{CHIP} is the power collected by an RFID tag, P_{READER} is the power generated by an RFID reader, C is the coupling coefficient (power loss) between the reader and the tag antenna, and τ is the matching coefficient.

In the ideal case, the coupling coefficient is equal to 1. The RFID chip is wired to the reader and an impedance match is maintained. In practice, the coupling coefficient is calculated as:

$$C = L_{PATH} \cdot G_t \cdot G_r \cdot p \quad [-], \tag{85}$$

where L_{PATH} denotes loss in the communication channel due to a mismatch in polarization in the reader and RFID tag antennas. G_t is the reader antenna gain, G_r is the receiving tag's antenna gain and p is the polarization loss factor.

L_{PATH} is defined in (82) and a principle of reduction of the read range is shown in (83).

4.3.2. Absorber Testing in RFID System

We tested three absorber prototypes (single-layer and double-layer configurations) in the three most common RFID frequency ranges. Table XXXII shows the results of testing the readability of tags placed in absorbers. Our RFID-blocking credit card holder sample is shown in Fig. 75.

Fig. 75 RFID-blocking credit card holder.

The absorbers were tested using a testing workbench which consisted of a standard RFID reader with the desired operational frequency range (Elatec TWN3 OEM PCB Multi 125 and TWN3 OEM PCB Multi ISO), RFID tag and absorber. The RFID tag was placed in the absorber. The RFID reader and tag were placed close to each other and a control computer evaluated the individual detection operations.

The best results were achieved using the Be-Tex Anticoro shielding material in a single-layer configuration. The RFID tag could not be identified in any of the 50 test iterations.

Table XXXII RFID Absorbers Tested

Material / Frequency	125 kHz	13. 56 MHz	868 MHz
Be-Tex nr. 38, single	signal	signal	no signal
Be-Tex nr. 38, double	signal	no signal	no signal
Be-Tex nr. 39, single	signal	signal	no signal
Be-Tex nr. 39, double	signal	no signal	no signal
Be-Tex Anticoro, single	no signal	no signal	no signal

4.3.3. Conclusions

This chapter describes the prototyping of a data protection of RFID electronic identifiers. We developed and fabricated a prototype and performed ESE tests of specific materials in the RFID frequency ranges. We confirmed that a textile case with silver nanoparticles provided the desired level of NFC credit card protection.

4.4. Application – EM Shielding Textile Materials in Electric Vehicles

This chapter is focused on the use of conductive textiles for electromagnetic shielding in electric vehicles [156]. The research was conducted under the project EUREKA LF13011 – Electromagnetic Reliability (EMR) of Electronic Systems for Electro Mobility (2013-2015, MSM/LF). The chapter presents a suitable measurement setup involving a shielding fabric designed to protect the device under test. The results show that electrically conductive textiles can mitigate electromagnetic interference affecting data transmission.

4.4.1. Shielding Design

The purpose of ESE description is the ability to present the main principles in the design of shielding. It can be summarized as follows:

- A decrease in aperture dimensions leads to an increase in ESE.
- Attenuation by reflection can be increased by using highly electrically conductive materials.
- Return loss is not dependent on the thickness of the material. This means that shielding can be made of thin, highly electrically conductive materials.
- Attenuation by absorption (heat loss) can be increased by using materials with greater thickness.
- Greater aperture dimensions mean lower return loss.
- Multiple reflections can be neglected if the thickness of the material is much greater than the equivalent penetration depth (otherwise, multiple reflections lead to a decrease in ESE).
- Attenuation caused by multiple reflections leads to a decrease in ESE in the lower frequency range.

4.4.2. Device Under Test

The device under test (DUT) is a BBCU_MB IDEAS electronic control unit designed for use in electric vehicles, Fig. 76.

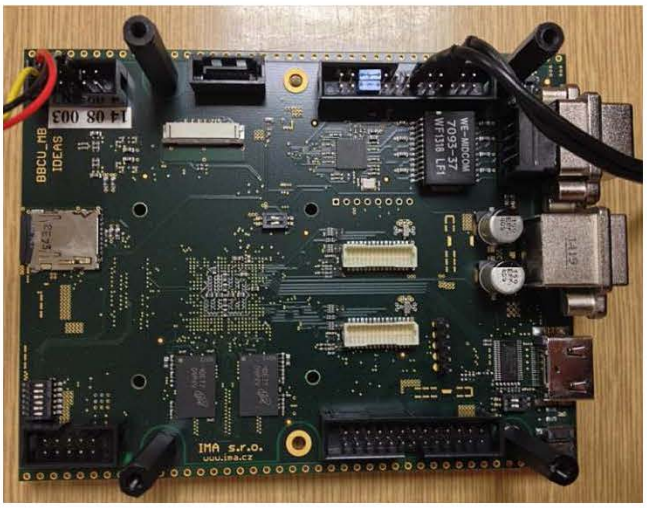

Fig. 76 Device under test.

According to the principles of shielding design, a highly conductive textile material is required. Copper-coated polyester was chosen due to its low resistivity ρ = 0.0352 Ω/square.

4.4.3. Experimental Setup

The experimental setup is shown in Fig. 77 and includes a TRIAC generator of broadband noise, SMV 11 selective microvoltmeter, the device under test and two lines. The line carrying noise (disturbing line) is connected to the TRIAC generator which is powered by an RFT NNB18 artificial mains network. The tested line (a data cable) is placed near the disturbing line. The data cable connects the control unit to a USB port of a laptop running special control software that transmits and receives signal to/from the control unit to evaluate the transmission efficiency.

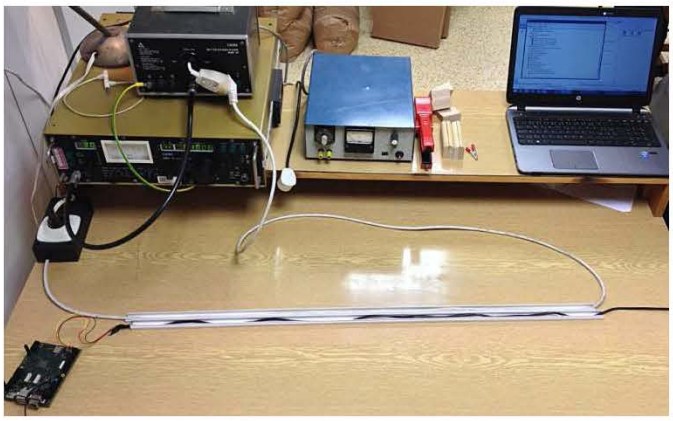

Fig. 77 Experimental setup - Configuration I.

The performance criteria (PEC) were defined as follows:

- A – the control application and DUT are operational, interference symbols may appear in the control application
- B – the control application is unavailable (it has to be restarted by the user), the DUT is operational
- C – the control application and DUT are not operational

Disturbing signal (TRIAC noise-generator) was measured at four frequencies, Table XXXIII. Influence of the interference was measured in three configurations:

- Configuration I: A data cable without additional shielding
- Configuration II: A data cable surrounded by a shielding fabric without grounding
- Configuration III: A data cable surrounded by a shielding fabric with grounding

In configuration I, which is described in the previous section and shown in Fig. 77, we evaluated the noise arising from the parallel placement of the power and data cables. Configuration II, where the data cable under examination was surrounded by a shielding fabric, is shown in Fig. 78. Data transmission efficiency was determined using control software, where performance criteria A represented 100% efficiency with the occasional presence of interference symbols, Fig. 79. We can see that messages 39 – 50 were transferred correctly despite the presence of interference symbols and messages numbered 900 and 901. The grounding of the shielding fabric is shown in Fig. 80.

A summary of the results is given in Table XXXIV. We can see that the shielding fabric was able to protect the data cable from interference. Performance criteria C were observed once and the DUT had to be reset. Performance criteria B which involve a failure of the control software to respond to user commands were observed twice. Performance criteria A were observed when using the shielding fabric with grounding.

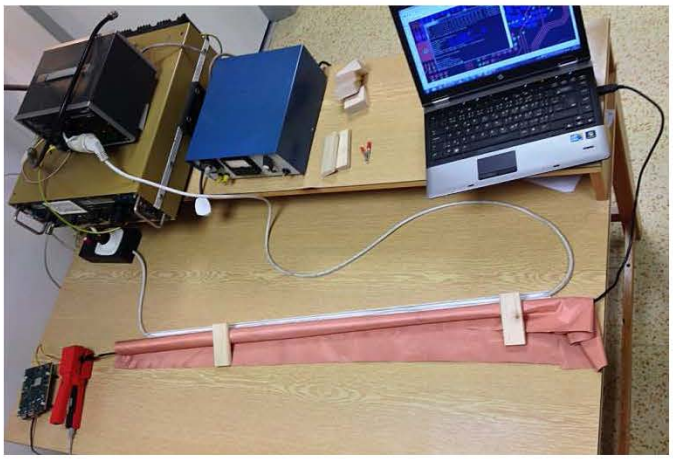

Fig. 78 Configuration II.

Fig. 79 Noise in the data cable recorded by the control software.

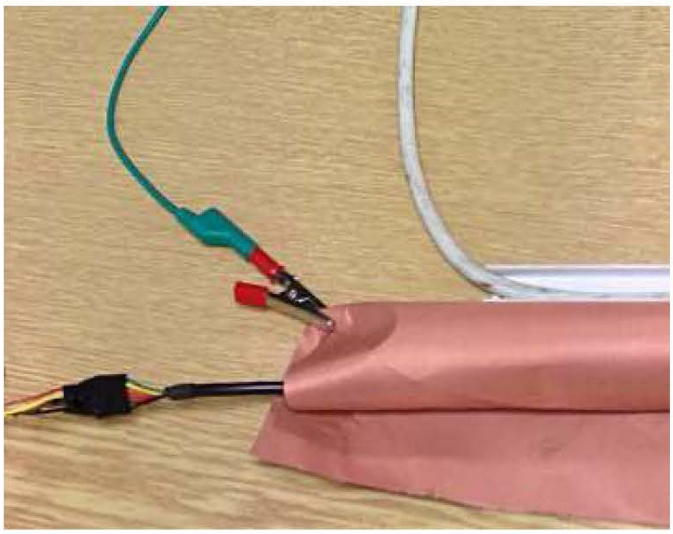

Fig. 80 Configuration III – the shielding fabric is grounded.

Table XXXIII Triac Generator of Broadband Noise - Values

Frequency [kHz]	Voltage [dBμV]
25	112
50	107
100	102
400	80

Table XXXIV Measurement Data

Configuration I		Configuration II		Configuration III	
Meas. no.	PEC	Meas. no.	PEC	Meas. no.	PEC
1	A	1	A	1	A
2	B	2	B	2	A
3	A	3	A	3	A
4	C	4	A	4	A
5	A	5	A	5	A

4.4.4. Conclusions

In this chapter, we have demonstrated that electrically conductive textiles are able to mitigate undesirable electromagnetic interference affecting the transmission of data over CAN buses in electric vehicles. The conclusions we have drawn in line with shielding theory support the use of electrically conductive textiles for electromagnetic shielding not only in electric vehicles. A number of measurements were performed to assess the electromagnetic shielding capability of electrically conductive textiles (these measurements were performed with an unshielded cable, with a cable with ungrounded shielding, and with a cable with grounded shielding). The results confirm that shielding textiles, which are characterized by high electrical conductivity and elasticity, can mitigate electromagnetic interference and can therefore be used as additional shielding for cables with low weight (electric vehicles, aircrafts, space probes...).

5. References

[1] "GREEN PAPER: From Challenges to Opportunities: Towa rds a Common Strategic Framework for EU Research and Innovation funding," 2011. [Online]. Available: http://ec.europa.eu/research/horizon2020/pdf/com_2011_0048_csf_green_paper_en.pdf#page=2. [Accessed 2013-08-09].

[2] "Towards Green Electronics in Europe: Strategic Research Agenda Organic & Large Area Electronics," 2009. [Online]. Available: http://cordis.europa.eu/fp7/ict/photonics/docs/reports/olae-sra_en.pdf. [Accessed 2017-07-27].

[3] L. Ji and X. Zhang, "Fabrication of porous carbon/Si composite nanofibers as high-capacity battery electrodes," *Electrochemistry Communications*, vol. 11, no. 6, pp. 1146-1149, 2009.

[4] M. Neruda and L. Vojtech, "Verification of Surface Conductance Model of Textile Materials," *Journal of Applied Research and Technology*, vol. 10, no. 4, p. 579–585, 2012.

[5] L. Vojtech and M. Neruda, "Application of Shielding Textiles for Increasing Safety Airborne Systems - Limitation of GSM Interference," in *2010 Ninth International Conference on Networks*, Piscataway, 2010.

[6] EN 1149-1:2006, *Protective clothing - Electrostatic properties - Part 1: Test method for measurement of surface resistivity*, Brussels: CEN, 2006.

[7] ASTM D4496 - 13, *Standard Test Method for D-C Resistance or Conductance of Moderately Conductive Materials*, West Conshohocken: ASTM International, 2013.

[8] S. Greco, A. Tamburrano and M. S. Sarto, "Experimental characterization and modeling of metallized textiles for electromagnetic shielding," in *Electromagnetic Compatibility (EMC EUROPE), 2013 International Symposium on*, Piscataway, 2013.

[9] B. Ivšić, D. Bonefačić and J. Bartolić, "Textile antennas for on-body sensors," in *2015 IEEE Sensors Applications Symposium (SAS)*, Piscataway, 2015.

[10] M. Neruda and L. Vojtech, "Modelling of Conductive Textile Materials for Shielding Purposes and RFID Textile Antennas," *ELEKTRONIKA IR ELEKTROTECHNIKA*, vol. 20, no. 8, 2014.

[11] V. Préault, R. Corcolle, L. Daniel and L. Pichon, "Shielding Effectiveness of Composite Materials: Effect of Inclusion Shape," *IEEE Transactions on Magnetics*, vol. 49, no. 5, pp. 1941-1944, 2013.

[12] Z. Yildiz, I. Usta and A. Gungor, "Electrical properties and electromagnetic shielding effectiveness of polyester yarns with polypyrrole deposition," *Textile Research Journal*, vol. 82, no. 20, pp. 2137-2148, 2012.

[13] L. Vojtech, M. Neruda and J. Hajek, "Planar Materials Electromagnetic Shielding Efficiency Derivation," *International Journal on Communications Antenna and Propagation*, vol. 1, no. 1, pp. 21-28, 2011.

[14] M. S. Ozen, E. Sancak and M. Akalin, "The effect of needle-punched nonwoven fabric thickness on electromagnetic shielding effectiveness," *Textile Research Journal*, vol. 85, no. 8, pp. 804-815, 2014.

[15] V. Safarova and J. Militky, "Electromagnetic shielding properties of woven fabrics made from high-performance fibers," *Textile Research Journal*, vol. 84, no. 12, pp. 1255-1267, 2014.

[16] K. Yang, G. I. Song, L. Zhang and L. w. Li, "Modelling the Electrical Property of 1×1 Rib Knitted Fabrics Made from Conductive Yarns," in *2009 Second International Conference on Information and Computing Science*, Piscataway, 2009.

[17] H. Zhang, X. Tao, S. Wang and T. Yu, "Electro-Mechanical Properties of Knitted Fabric Made From Conductive Multi-Filament Yarn Under Unidirectional Extension," *Textile Research Journal,* vol. 75, no. 8, pp. 598-606, 2005.

[18] M. Neruda and L. Vojtech, "Modeling of smart textile materials for ESD applications," in *Proceedings ELMAR-2012*, Piscataway, 2012.

[19] L. Vojtech and M. Neruda, "Modelling of Surface and Bulk Resistance for Wearable Textile Antenna Design," *Przegląd Elektrotechniczny,* vol. 89, no. 2b, pp. 217--222, 2013.

[20] *MILITARY STANDARD: Attenuation Measurements for Enclosures, Electromagnetic Shielding, For Electronic Test Purposes, Method Of,* Piscataway: IEEE, 1956.

[21] *IEEE Standard Method for Measuring the Effectiveness of Electromagnetic Shielding Enclosures,* 2 ed., Piscataway: IEEE, 2006.

[22] ASTM D4935 - 10, *Standard Test Method for Measuring the Electromagnetic Shielding Effectiveness of Planar Materials*, West Conshohocken, PA: ASTM International, 2010.

[23] Y. K. Hong, C. Y. Lee, C. K. Jeong, D. E. Lee, K. Kim and J. Joo, "Method and apparatus to measure electromagnetic interference shielding efficiency and its shielding characteristics in broadband frequency ranges," *Review of Scientific Instruments,* vol. 74, no. 2, pp. 1098-1102, 2003.

[24] V. Safarova, M. Tunak and J. Militky, "Prediction of hybrid woven fabric electromagnetic shielding effectiveness," *Textile Research Journal,* vol. 85, no. 7, pp. 673-686, 2014.

[25] J. Mueller, "Cable Shielding Test Methods: A Comparison of Different Test Methods," in *2007 IEEE International Symposium on Electromagnetic Compatibility*, Piscataway, 2007.

[26] Establishing a dialogue on risks from electromagnetic fields, Geneva: World Health Organization, Radiation and Environmental Health, Dept. of Protection of the Human Environment, 2002.

[27] D. Schröder, Leistungselektronische Schaltungen: Funktion, Auslegung und Anwendung, Berlin: Springer Berlin Heidelberg, 2012.

[28] S. Jeschke, M. Maarleveld and H. Hirsch, "Investigation on the influence of the shielding concept on the disturbances from the propulsion system of an electric vehicle," in *2013 International Symposium on Electromagnetic Compatibility*, Piscataway, 2013.

[29] Y. Wang, X. Zhao, Q. Wen and J. Cai, "The research of vehicle electromagnetic shielding effectiveness in high power electromagnetic pulse," in *2010 2nd IEEE International Conference on Information Management and Engineering*, Piscataway, 2010.

[30] K. Feldhues, M. Diebig and S. Frei, "Analysis of the low frequency shielding behavior of high voltage cables in electric vehicles," in *2014 International Symposium on Electromagnetic Compatibility*, Piscataway, 2014.

[31] *ICNIRP GUIDELINES: For limiting exposure to time-varying electric, magnetic and electromagneitc fields (up to 300 GHz),* vol. 74, HEALTH PHYSICS, 1998.

[32] ASTM D257 - 14, *Standard Test Methods for DC Resistance or Conductance of Insulating Materials,* West Conshohocken, PA: ASTM International, 2014.

[33] ANSI/ESD STM11.11, *Surface Resistance Measurement of Static Dissipative Planar Materials,* New York: EOS/ESD Association, Inc., 2006.

[34] ISO 10965:2011, *Textile floor coverings -- Determination of electrical resistance,* Geneva: ISO, 2011.

[35] EN 1149-2:2007, *Electrostatic properties. Test methods for measurement of the electrical resistance through a material (vertical resistance),* Brussels: CEN, 2007.

[36] ASTM D991 - 89(2014), *Standard Test Method for Rubber Property—Volume Resistivity Of Electrically Conductive and Antistatic Products,* West Conshohocken, PA: ASTM International, 2014.

[37] CEN - EN 16812, *Textiles and textile products. Electrically conductive textiles. Determination of the linear electrical resistance of conductive tracks.,* Brussels: CEN, 2016.

[38] ESD ADV1.0-2014, *ESD Association Advisory for Electrostatic Discharge Terminology – Glossary,* New York: EOS/ESD Association, Inc., 2014.

[39] ASTM D257 - 07, *Standard Test Methods for DC Resistance or Conductance of Insulating Materials,* West Conshohocken, PA: ASTM International, 2007.

[40] J. G. Webster, Electrical Measurement, Signal Processing, and Displays, London: CRC Press, 2003.

[41] L. J. van der Pauw, "A Method of Measuring Specific Resistivity and Hall Effect of Discs of Arbitrary Shapes," *Philips Res. Repts.,* vol. 13, pp. 1-9, 1958.

[42] F. Wenner, *A method of measuring earth resistivity,* Washington, D.C.: U.S. Dept. of Commerce, Bureau of Standards, 1916.

[43] M. Tokarska, "Measuring resistance of textile materials based on Van der Pauw method," *Indian Journal of Fibre & Textile Research,* vol. 38, no. 2, pp. 198-201, 2013.

[44] M. Tokarska, "Evaluation of Measurement Uncertainty of Fabric Surface Resistance Implied by the Van der Pauw Equation," *IEEE Transactions on Instrumentation and Measurement,* vol. 63, no. 6, pp. 1593-1599, 2014.

[45] J. Banaszczyk, A. Schwarz, G. De Mey and L. Van Langenhove, "The Van der Pauw method for sheet resistance measurements of polypyrrole-coated para-aramide woven fabrics," *Journal of Applied Polymer Science,* vol. 117, no. 5, pp. 2553-2558, 2010.

[46] I. Kazani, G. De Mey, C. Hertleer, J. Banaszczyk, A. Schwarz, G. Guxho and L. Van Langenhove, "Van Der Pauw method for measuring resistivities of anisotropic layers printed on textile substrates," *Textile Research Journal,* vol. 81, no. 20, pp. 2117-2124, 2011.

[47] H. C. Montgomery, "Method for Measuring Electrical Resistivity of Anisotropic Materials," *Journal of Applied Physics,* vol. 42, no. 7, pp. 2971-2975, 1971.

[48] C. A. M. dos Santos, A. de Campos, M. S. da Luz, B. D. White, J. J. Neumeier, B. S. de Lima and C. Y. Shigue, "Procedure for measuring electrical resistivity of anisotropic materials: A revision of the Montgomery method," *Journal of Applied Physics,* vol. 110, no. 8, p. 083703, 2011.

[49] D. Knittel and E. Schollmeyer, "Electrically high-conductive textiles," *Synthetic Metals,* vol. 159, no. 14, pp. 1433-1437, 2009.

[50] M. Åkerfeldt, M. Strååt and P. Walkenström, "Influence of coating parameters on textile and electrical properties of a poly(3,4-ethylene dioxythiophene):poly(styrene sulfonate)/polyurethane-coated textile: poly(styrene sulfonate)/polyurethane-coated textile," *Textile Research Journal,* vol. 83, no. 20, pp. 2164-2176, 2013.

[51] AATCC 76, *Electrical Surface Resistivity of Fabrics,* Research Triangle Park: American Association of Textile Chemists and Colorists (AATCC), Developed in 1954 by AATCC Committee RA32, 2011.

[52] "Technical Data Sheet: Conductive Metallized Nylon Fabric (Zell)," 2010. [Online]. Available: http://www.hitek-ltd.co.uk/media/downloads/77/HITEK%20Zell%20-%20Woven%20%282010%29.pdf. [Accessed 2017-08-07].

[53] "Electrical Conductivity and Resistivity," in *The measurement, instrumentation, and sensors handbook*, 2 ed., Boca Raton, Fla., CRC Press published in cooperation with IEEE Press, 1999, pp. 26-1-26-15.

[54] "Four Point Probe Equations," 2013. [Online]. Available: http://four-point-probes.com/four-point-probe-equations/. [Accessed 2017-03-27].

[55] F. Smits, "Measurements of Sheet Resistivity with the Four-Point Probe," *Bell System Technical Journal,* vol. 37, no. 3, p. 711–718, 1958.

[56] I. Kazani, G. De Mey, C. Hertleer, J. Banaszczyk, A. Schwarz, G. Guxho and L. Van Langenhove, "About the collinear four-point probe technique´s inability to measure the resistivity of anisotropic electroconductive fabrics," *Textile Research Journal,* vol. 83, no. 15, pp. 1587-1593, 2013.

[57] D. Kincal, A. Kumar, A. D. Child and J. R. Reynolds, "Conductivity switching in polypyrrole-coated textile fabrics as gas sensors," *Synthetic Metals,* vol. 92, no. 1, pp. 53-56, 1998.

[58] Y. Ouyang and W. Chappell, "Measurement of electrotextiles for high frequency applications," in *IEEE MTT-S International Microwave Symposium Digest, 2005*, Piscataway, 2005.

[59] H. Shimasaki, T. Nakagawa and M. Akiyama, "Measurement of the surface resistance of conductive textiles at microwave frequency," in *2009 Asia Pacific Microwave Conference*, Piscataway, 2009.

[60] "Resistance and resistivity," in *Duke, Department of Physics*, Durham, 2013.

[61] DIN IEC 60093, *Methods of test for volume resistivity and surface resistivity of solid electrical insulating materials,* Berlin: DIN-adopted IEC Standard, 1993.

[62] V. Safarova and J. Militky, "A Study of Electrical Conductivity of Hybrid Yarns Containing Metal Fibers," *Journal of Materials Science & Engineering B,* vol. 2, no. 2b, pp. 197-202, 2012.

[63] W. A. Maryniak, T. Uehara and M. A. Noras, "Surface Resistivity and Surface Resistance Measurements Using a Concentric Ring Probe Technique," 2003. [Online]. Available: http://www.trekinc.com/Download/App_note/1005_Resistivity_Resistance.pdf. [Accessed 2017-10-03].

[64] R. Kacprzyk, "Measurements of the Volume and Surface Resistance of Textile Materials," *FIBRES & TEXTILES in Eastern Europe*, vol. 19, no. 1(84), pp. 47-49, 2011.

[65] "Volume and Surface Resistivity Measurements of Insulating Materials Using the Model 6517A Electrometer/High Resistance Meter," 2001. [Online]. Available: www.keithley.com/data?asset=6069. [Accessed 2017-08-07].

[66] "oregano - an electrical engineering tool," 2012. [Online]. Available: https://github.com/drahnr/oregano. [Accessed 2017-03-27].

[67] J. Čajka and J. Kvasil, Teorie lineárních obvodů: Analýza lineárních a linearizovaných elektrických obvodů, 1. vyd. ed., Praha: Státní nakladatelství technické literatury, 1979.

[68] "chol: Cholesky factorization," c1994-2017. [Online]. Available: https://www.mathworks.com/help/matlab/ref/chol.html. [Accessed 2017-08-07].

[69] ISO 2062:2009, *Textiles — Yarns from packages — Determination of single-end breaking force and elongation at break using constant rate of extension (CRE) tester,* 3 ed., Geneva: International Organization for Standardization (ISO), 2009.

[70] ISO 13934-1:2013, *Textiles -- Tensile properties of fabrics -- Part 1: Determination of maximum force and elongation at maximum force using the strip method,* 2 ed., Geneva: International Organization for Standardization (ISO), 2013.

[71] T. R. Kuphaldt, Lessons in Electric Circuits, First edition ed., Boise: EETech Media, LLC., 2012.

[72] R. Malaric, Instrumentation and measurement in electrical engineering, Florida: Brown Walker Press, 2011.

[73] P. S. Horn, "Some Easy t Statistics," *Journal of the American Statistical Association,* vol. 78, no. 384, pp. 930-936, 1983.

[74] "Innovative conductivity solutions to boost your textile and industrial product's performance with conductive speciality filament yarns and monofilaments," 2015. [Online]. Available: http://www.swicofil.com/innovationconductivitysynfilament.html. [Accessed 2017-08-07].

[75] "Products : silveR.STAT® fibres: silveR.STAT® fibres," 2013. [Online]. Available: http://www.r-stat.fr/uk/silveRstat-fibre.php. [Accessed 2017-03-27].

[76] "SHIELDEX® Yarns," 2016. [Online]. Available: http://statex.de/index.php/en/fibres-and-yarns/item/153-shieldex%C2%AE-garne. [Accessed 2017-03-27].

[77] L. Yunhong, S. Xiaogang, L. Jihong and L. Sa, "Research on Heat Conduction Performance of Carbon-Fibre Fabric based on Infrared Thermal Imaging Technology," in *2008 IEEE International Symposium on Knowledge Acquisition and Modeling Workshop*, Piscataway, 2008.

[78] "Heating Textile," 2014. [Online]. Available: http://www.gerster-techtex.com/content.php?page_id=896. [Accessed 2017-03-27].

[79] "Stainless steel fibers for heatable textiles - Bekinox®," 2014. [Online]. Available: http://www.bekaert.com/en/Product%20Catalog/Products/B/Stainless%20steel%20fibres%20for%20heatable%20textiles%20-%20Bekinox.aspx?Industry={F4EFD0BC-A1FB-4B5E-9923-B5241DCF01F7}&ProductCategory={2DDBEBF8-6AA8-4A2B-818F-E3712FFB524F}. [Accessed 2017-03-27].

[80] "Non- Carbon Fiber Electrical Heating Textile," 2014. [Online]. Available: http://www.adafruit.com/datasheets/HEATING%20TEXTILE.PDF. [Accessed 2015-08-09].

[81] "SEFAR PowerHeat," 2015. [Online]. Available: http://www.sefar.com/en/609/Product-Detail.htm?Folder=1484711. [Accessed 2015-08-09].

[82] L. Vojtech and M. Neruda, "Self-drying planar textile materials with electrically conductive structures," in *Proceedings of 15th International Conference MECHATRONIKA*, Piscataway, 2012.

[83] M. Neruda and L. Vojtech, "Heating Ability of Electrically Conductive Textile Materials," in *Proceedings of the 16th International Conference on Mechatronics - Mechatronika 2014*, Piscataway, 2014.

[84] IEC 60364-4-41:2005, *Low-voltage electrical installations - Part 4-41: Protection for safety - Protection against electric shock*, 5 ed., Geneva: International Electrotechnical Commission (IEC), 2005.

[85] "HOOK & LOOP FASTENER," 2014. [Online]. Available: http://www.lessemf.com/fabric.html#207. [Accessed 2017-03-27].

[86] "Microwave Drying," 2017. [Online]. Available: http://www.romill.cz/en/microwave-drying. [Accessed 2017-08-09].

[87] "How to Dry Textile without Over-Drying," 2017. [Online]. Available: http://www.conservationphysics.org/wetstuff/wetstuff.pdf. [Accessed 2017-08-09].

[88] HD 60364-1:2008 en, *Low-voltage electrical installations - Part 1: Fundamental principles, assessment of general characteristics, definitions*, Delft: NEN, 2008.

[89] "Battery separators," 2017. [Online]. Available: http://www.elmarco.com/application-areas/battery-separators. [Accessed 2017-08-09].

[90] "Chemical Resistance Chart PVDF," 2013. [Online]. Available: http://www.zeusinc.com/technicalservices/technicalbulletins/chemicalresistanceofpolymers/chemicalresistancechartpvdf.aspx. [Accessed 2017-08-09].

[91] Y. Kojima, Y. Mototani and J. Asaoka, "Alkaline battery having a gelled negative electrode".

[92] V. Krejčík, Technologie pro II. a III. ročník učební obor galvanizér, Praha: Práce, 1963.

[93] D. K. Hamilton and T. Wilson, "Three-dimensional surface measurement using the confocal scanning microscope," *Applied Physics B*, vol. 27, no. 4, pp. 211-213, 1982.

[94] B. P. Artamonov, M. S. Grilikhes, F. S. Kontorovich and B. K. Filanovskii, "Electrodes with burned-in platinum for contact conductometry," *Biomedical Engineering*, vol. 5, no. 6, pp. 377-378, 1971.

[95] G. Prati, L. Pietrantoni and E. Cicognani, "Self-efficacy moderates the relationship between stress appraisal and quality of life among rescue workers," *Anxiety, Stress, & Coping*, vol. 23, no. 4, pp. 463-470, 2010.

[96] E. Varnauskas, P. Björntorp, M. Fahlén, I. Přerovský and J. Stenberg, "Effects of physical training on exercise blood flow and enzymatic activity in skeletal muscle1," *Cardiovascular Research*, vol. 4, no. 4, pp. 418-422, 1970.

[97] A. Achilli, M. Sassara, S. Ficili, D. Pontillo, P. Achilli, C. Alessi, S. De Spirito, R. Guerra, N. Patruno and F. Serra, "Long-term effectiveness of cardiac resynchronization therapy in patients with refractory heart failure and "narrow" QRS," *Journal of the American College of Cardiology*, vol. 42, no. 12, pp. 2117-2124, 2003.

[98] Y.-D. Lee and W.-Y. Chung, "Wireless sensor network based wearable smart shirt for ubiquitous health and activity monitoring," *Sensors and Actuators B: Chemical*, vol. 140, no. 2, pp. 390-395, 2009.

[99] G. López, V. Custodio and J. I. Moreno, "LOBIN: E-Textile and Wireless-Sensor-Network-Based Platform for Healthcare Monitoring in Future Hospital Environments," *IEEE Transactions on Information Technology in Biomedicine*, vol. 14, no. 6, pp. 1446-1458, 2010.

[100] J. Yoo, L. Yan, S. Lee, H. Kim and H. J. Yoo, "A Wearable ECG Acquisition System With Compact Planar-Fashionable Circuit Board-Based Shirt," *IEEE Transactions on Information Technology in Biomedicine*, vol. 13, no. 6, pp. 897-902, 2009.

[101] C. R. Merritt, H. T. Nagle and E. Grant, "Fabric-Based Active Electrode Design and Fabrication for Health Monitoring Clothing," *IEEE Transactions on Information Technology in Biomedicine,* vol. 13, no. 2, pp. 274-280, 2009.

[102] L. Pollonini, N. O. Rajan, S. Xu, S. Madala and C. C. Dacso, "A Novel Handheld Device for Use in Remote Patient Monitoring of Heart Failure Patients—Design and Preliminary Validation on Healthy Subjects," *Journal of Medical Systems,* vol. 36, no. 2, pp. 653-659, 2012.

[103] J. Ottenbacher, L. Jatoba, U. Großmann, W. Stork and K. Müller-Glaser, "ECG electrodes for a context-aware cardiac permanent monitoring system," Berlin, Heidelberg, Springer Berlin Heidelberg, 2007, pp. 672-675.

[104] M. Häggström, "Pioneer plaque man upper body as diagram template," in *Wikimedia Commons*, San Francisco, 2009.

[105] J. Hospodka and R. Bortel, "Amplifier for Biological Signal Sensing with Efficient Common Mode Rejection," in *International Conference on Applied Electronics*, Plzeň, 2011.

[106] J. Hospodka and R. Bortel, "System for measuring biological signals with suppression of interference".

[107] R. Bortel and P. Sovka, "Real-Time Robust Heart Rate Estimation Based on Bayesian Framework and Grid Filters," in *Medical Applications of Intelligent Data Analysis: Research Advancements*, Hershey, IGI Global, 2012, pp. 67-90.

[108] S. Coyle, E. Mitchell, T. Ward, G. May, N. O'Connor and D. Diamond, "Textile sensors for personalized feedback," in *IAPMA2010 - ECIR2010 workshop on information access for personal media archives*, Milton Keynes, 2010.

[109] S. Sankaralingam and B. Gupta, "Development of textile antennas for body wearable applications and investigations on their performance under bent conditions," *Progress In Electromagnetics Research B,* vol. 22, pp. 53-71, 2010.

[110] A. Tronquo, H. Rogier, C. Hertleer and L. V. Langenhove, "Robust planar textile antenna for wireless body LANs operating in 2.45 GHz ISM band," *Electronics Letters,* vol. 42, no. 3, pp. 142-143, 2006.

[111] C. A. Balanis, Antenna theory: analysis and design, 2nd ed. ed., New York: Wiley, 1997.

[112] H. Aniołczyk, J. Koprowska, P. Mamrot and J. Lichawska, "Application of electrically conductive textiles as electromagnetic shields in physiotherapy," *Fibers and Textiles in Eastern Europe*, vol. 12, no. 4, pp. 47-50, 2004.

[113] V. Safarova, M. Tunak, M. Truhlar and J. Militky, "A new method and apparatus for evaluating the electromagnetic shielding effectiveness of textiles," *Textile Research Journal,* vol. 86, no. 1, pp. 44-56, 2015.

[114] B. S. Villacorta, T. H. Hubing and A. A. Ogale, "Influence of composite electrical properties on the VHF–UHF electromagnetic shielding characteristics of polyethylene–carbon nanoparticle composites," *Composites Science and Technology,* vol. 89, no. Supplement C, pp. 158-166, 2013.

[115] H. Chen, K. Lee, J. Lin and M. Koch, "Comparison of electromagnetic shielding effectiveness properties of diverse conductive textiles via various measurement techniques," *Journal of Materials Processing Technology,* vol. 192, no. -, pp. 549-554, 2007.

[116] V. Safarova and J. Militky, "Comparison of methods for evaluating the electromagnetic shielding of textiles," *Vlakna a Textil,* vol. 19, no. 3, pp. 50-56, 2012.

[117] J. Avloni, M. Ouyang, L. Florio, A. R. Henn and A. Sparavigna, "Shielding Effectiveness Evaluation of Metallized and Polypyrrole-coated Fabrics," *Journal of Thermoplastic Composite Materials,* vol. 20, no. 3, pp. 241-254, 2007.

[118] J.-S. Roh, Y.-S. Chi, T. J. Kang and S.-w. Nam, "Electromagnetic Shielding Effectiveness of Multifunctional Metal Composite Fabrics," *Textile Research Journal,* vol. 78, no. 9, pp. 825-835, 2008.

[119] H. Özdemir, Ş. S. Uğurlu and A. Özkurt, "The electromagnetic shielding of textured steel yarn based woven fabrics used for clothing," *Journal of Industrial Textiles,* vol. 45, no. 3, pp. 416-436, 2015.

[120] H. Chen, K. Lee, J. Lin and M. Koch, "Fabrication of conductive woven fabric and analysis of electromagnetic shielding via measurement and empirical equation," *Journal of Materials Processing Technology,* vol. 184, no. 1, pp. 124-130, 2007.

[121] K. B. Cheng, T. W. Cheng, R. N. Nadaraj, V. R. G. Dev and R. Neelakandan, "Electromagnetic Shielding Effectiveness of the Twill Copper Woven Fabrics," *Journal of Reinforced Plastics and Composites,* vol. 25, no. 7, pp. 699-709, 2006.

[122] J. A. King, W. A. Pisani, D. R. Klimek-McDonald, W. F. Perger, G. M. Odegard and D. G. Turpeinen, "Shielding effectiveness of carbon-filled polypropylene composites," *Journal of Composite Materials,* vol. 50, no. 16, pp. 2177-2189, 2015.

[123] F. Y. Manesh, H. Hasani and S. M. Mortazavi, "Analyzing the effect of yarn and fabrics parameters on electromagnetic shielding of metalized fabrics coated with polyaniline," *Journal of Industrial Textiles,* vol. 44, no. 3, pp. 434-446, 2013.

[124] Y. Lu and L. Xue, "Electromagnetic interference shielding, mechanical properties and water absorption of copper/bamboo fabric (Cu/BF) composites," *Composites Science and Technology,* vol. 72, no. 7, pp. 828-834, 2012.

[125] S. Maity and A. Chatterjee, "Conductive polymer-based electro-conductive textile composites for electromagnetic interference shielding: A review: A review," *Journal of Industrial Textiles,* p. 1528083716670310, 2016.

[126] V. Tunáková, J. Grégr, M. Tunák and G. Dohnal, "Functional polyester fabric/polypyrrole polymer composites for electromagnetic shielding: Optimization of process parameters: Optimization of process parameters," *Journal of Industrial Textiles,* p. 1528083716667262, 2016.

[127] D. Duran and H. Kadoğlu, "Electromagnetic shielding characterization of conductive woven fabrics produced with silver-containing yarns," *Textile Research Journal,* vol. 85, no. 10, pp. 1009-1021, 2014.

[128] H. G. Ortlek, T. Alpyildiz and G. Kilic, "Determination of electromagnetic shielding performance of hybrid yarn knitted fabrics with anechoic chamber method," *Textile Research Journal,* vol. 83, no. 1, pp. 90-99, 2012.

[129] V. Tunáková, L. Techniková and J. Militký, "Influence of washing/drying cycles on fundamental properties of metal fiber-containing fabrics designed for electromagnetic shielding purposes," *Textile Research Journal,* vol. 87, no. 2, pp. 175-192, 2016.

[130] B. Saravanja, K. Malric, T. Pusic and D. Ujevic, "Impact of dry cleaning on the electromagnetic shield characteristics of interlining fabric," *Fibres & Textiles in Eastern Europe,* vol. 23, no. 1(109), p. 104–108, 2015.

[131] Ö. Kayacan, "The Effect of Washing Process on the Electromagnetic Shielding of Knitted Fabrics," *Journal of Textile & Apparel / Tekstil ve Konfeksiyon,* vol. 24, no. 4, pp. 356-362, 2014.

[132] X. Wang, Z. Liu and M. Jiao, "Computation model of shielding effectiveness of symmetric partial for anti-electromagnetic radiation garment," *Progress In Electromagnetics Research B*, vol. 47, no. -, pp. 19-35, 2013.

[133] Z. Liu, X. Wang and Z. Zhou, "Computation of shielding effectiveness for electromagnetic shielding blended fabric," *Przegląd Elektrotechniczny*, vol. 89, no. 3a, pp. 228-230, 2013.

[134] R. Perumalraj, B. S. Dasaradan, R. Anbarasu, P. Arokiaraj and S. L. Harish, "Electromagnetic shielding effectiveness of copper core-woven fabrics," *The Journal of The Textile Institute*, vol. 100, no. 6, pp. 512-524, 2009.

[135] H. Xiao, M. W. Shi, Q. Wang and Q. Liu, "The electromagnetic shielding and reflective properties of electromagnetic textiles with pores, planar periodic units and space structures," *Textile Research Journal*, vol. 84, no. 16, pp. 1679-1691, 2014.

[136] A. R. Henn and R. M. Cribb, "Modeling the shielding effectiveness of metallized fabrics," in *International Symposium on Electromagnetic Compatibility*, Piscataway, 1992.

[137] L. Vojtech, M. Neruda and J. Hajek, "Modelling of Electromagnetic Parameters of Planar Textile Materials," in *New Trends in the Field of Materials and Technologies Engineering*, Czestochowa, Oficyna Wydawnicza Stowarzyszenia Menedżerów Jakości i Produkcji, 2012, pp. 123-159.

[138] A. R. Henn and R. M. Cribb, "Modeling the shielding effectiveness of metallized fabrics," in *International Symposium on Electromagnetic Compatibility*, 1992.

[139] P. S. Neelakanta, Handbook of electromagnetic materials: monolithic and composite versions and their applications, Boca Raton: CRC Press, 1995.

[140] H. W. Ott, Electromagnetic compatibility engineering, Hoboken, N.J.: John Wiley & Sons, 2009.

[141] C. Christopoulos, Principles and techniques of electromagnetic compatibility, 2nd ed. ed., Boca Raton: CRC Press, 2007.

[142] T. Williams, EMC for product designers, 4th ed. ed., Oxford: Newnes, 2007.

[143] J. Svacina, "Elektromagnetická kompatibilita," Brno, 2002.

[144] "Properties table of Stainless steel, Metals and other Conductive materials: Electrical or thermal condutivity, resistivity, density and melting point," 2011. [Online]. Available: www.tibtech.com/conductivity.php. [Accessed 2017-08-09].

[145] W. Payne, "Sensitivity of Multi Turn Receiving Loops," 2001. [Online]. Available: http://www.vlf.it/octoloop/rlt-n4ywk.htm. [Accessed 2017-08-09].

[146] T. Więckowski and J. Janukiewicz, "Methods for Evaluating the Shielding Effectiveness of Textiles," *Fibres & Textiles in Eastern Europe*, vol. 14, no. 5(59), p. 18–22, 2006.

[147] "Terms and Conditions, Article 12.2 Conduct Aboard Aircraft," 2010. [Online]. Available: https://www.easyjet.com/en/book/conditions.html. [Accessed 2017-08-09].

[148] *CAA PAPER 2003/3: Effects of Interference from Cellular Telephones on Aircraft Avionic Equipment*, Aviation House, Gatwick Airport South, West Sussex, RH6 0YR: Civil Aviation Authority, 2003.

[149] H. T. Friis, "A Note on a Simple Transmission Formula," *Proceedings of the IRE*, vol. 34, no. 5, pp. 254-256, 1946.

[150] “BTSScan v 2.00,” 2010. [Online]. Available: http://www.gsmcables.cz/btssc202.zip. [Accessed 2010-01-09].

[151] K. Finkenzeller, RFID Handbook: Fundamentals and Applications in Contactless Smart Cards, Radio Frequency Identification and Near-Field Communication, 3 ed., Chichester: John Wiley & Sons, 2010.

[152] P. V. Nikitin, K. V. S. Rao and S. Lazar, “An Overview of Near Field UHF RFID,” in *2007 IEEE International Conference on RFID*, Piscataway, 2007.

[153] L. Vojtěch, J. Hájek, M. Neruda, M. Zatloukal, Monometallic Textile Electrodes for “Green” Batteries. Elektronika ir Elektrotechnika. 2014, 20(9), s. 25-28. ISSN 1392-1215. [cit. 2017-03-27]. Available: http://www.eejournal.ktu.lt/index.php/elt/article/view/8434

[154] R. Dahal, R., D.Mercan, L.Vojtěch, Textile Antenna for 50 Ohm Applications. Advances in Electrical and Electronic Engineering. 2012, 10.(4), s. 229-234. ISSN 1336-1376. [cit. 2017-03-27]. Available: http://advances.utc.sk/index.php/AEEE/article/view/725

[155] L. Vojtěch, R. Bortel, M. Neruda, M. Kozák, Wearable Textile Electrodes for ECG Measurement. Advances in Electrical and Electronic Engineering. 2013, 11(5), s. 410-414. ISSN 1336-1376. [cit. 2017-03-27]. Available: http://advances.utc.sk/index.php/AEEE/article/view/889

[156] M. Neruda, L. Vojtěch, M. Rohlík, J. Hájek, R. Holý, M. Kalika, Application of Shielding Textile Materials in Electric Vehicles. In: 2015 24th Wireless and Optical Communication Conference (WOCC). 24th Wireless and Optical Communication Conference. Taipei, 23.10.2015 - 24.10.2015. Piscataway: IEEE. 2015, s. 113-117. ISSN 2379-1268. ISBN 978-1-4799-8854-9. [cit. 2017-03-27]. Available: http://ieeexplore.ieee.org/stamp/stamp.jsp?tp=&arnumber=7346188

[157] L. Vojtěch, M. Neruda, J. Hájek, Data Hardware Protection of Electronic Identifiers In: IWSSIP 2010 Proceedings. Rio de Janeiro: EdUFF - Editora da Universidade Federal Fluminense, 2010, pp. 162-165. ISBN 978-85-228-0565-5. Available from: http://www.ic.uff.br/iwssip2010/Proceedings/nav/papers/paper_50.pdf

6. The applicant contribution

The author's R&D output presented in this habilitation thesis and his other scientific publications currently includes 14 papers in indexed journals, 3 chapters in a book published in English, more than 60 papers presented at significant conferences, 11 utility models, 1 patent and 6 patent applications. This body of published results can help the scientific community to achieve progress in research and development and has potential to be applied in industry and in the teaching of undergraduate, graduate and doctoral students.

The research results presented in this thesis indicate that electrically conductive textiles must be divided into several groups based on volume conductivity. This must also be reflected in the modelling methods we choose. This is because of the effects of the various mechanisms of electrical conduction in the textile structures under investigation. There was found and formulated a theoretical approach to modelling electrical conductivity in woven textiles and carried out an experimental validation of the model with woven textile samples.

Using the modified approaches to assess the electromagnetic shielding capability of nonhomogeneous 3D structures, a new analytical description of the electromagnetic shielding efficiency of selected conductive woven textiles has been successfully found. The observation is based on research of the structural similarity between woven textiles and metallic grids. The proposed modelling method was analytically validated for the different conductivity values of the yarns used; experimental validation was performed as well. This led to the identification of a set of suitable conductivity values for yarns, for which these approaches are valid within a given error.

Considering the novel approaches to modelling the electrical conductivity and electromagnetic shielding efficiency of electrically conductive textiles presented in the thesis, the findings contribute significantly to the existing body of interdisciplinary research and applications at the boundary between electrical engineering and materials science.

The thesis contains examples of the experiments undertaken and the results of the development of applications of the proposed types of materials. The examples of uses span multiple branches of electronics and communications technologies and have great application potential. The examples and experiments presented here will certainly help the reader grasp the breadth of these applications in the context of interdisciplinary collaboration.

The research team led by the author of the thesis has been successful in the long term in exploring and exploiting these perhaps non-traditional spaces between disciplines. This has led to strong links with industrial and research partners and across various departments of the Faculty of Electrical Engineering, CTU in Prague. The interdisciplinary RFID locator project, which was led by the author of the thesis, was recognized in 2015 by the CTU's leadership with the Rector's Prize for the application of scientific, research and creative work in practice.

The thesis draws on more than eight years of research in the modelling, measurement and industrial applications of electrically conductive textiles. It is based on two research and development projects supported by the Ministry of Industry and Trade of the Czech Republic, namely the 2008-2010 FI-IM5/202 (BE-TEX) "Humans and Equipment Protection Against High-Frequency Electromagnetic Radiation – Research and Development of New Textiles" project and the 2012-2015 FR-TI4/202 (KOMPOZITEX) "Composite Textile Materials for Protection of Humans and Devices Against the Effects of Electromagnetic and Electrostatic Fields" project. The work was also supported by the international LF13005 – "RFID Technology in Logistic Networks of Automotive Industry" (2013-2016, MSM/LF) project and the award-winning EUREKA LF13011 – "Electromagnetic Reliability (EMR) of Electronic Systems for Electro Mobility" (2013-2015, MSM/LF) project.

The results are being applied in ongoing scientific activities and industrial applications related to the design of manufacturing processes and preparation for the production of electrically conductive technical textiles with an electromagnetic shielding capability. This work is carried out by the companies VÚB a.s. Ústí nad Orlicí and Nyklíček a spol. s r.o. Nové Město nad Metují.

The interdisciplinary nature of the work is likely to stimulate cooperation between the departments of the FEE CTU in Prague. Recently, selected research results have served as the basis of a new joint project of FEE CTU and HE3DA s.r.o. focused on the development of new types of lithium batteries and the control for those.

7. Upcoming challenges

When it comes to opportunities, I have identified two suitable areas of focus for future science and research.

The first area is the application of the findings in the production of electrically conductive textiles, electrically conductive applications, the manufacture of sensors, and electromagnetic shielding applications.

Within this area, the presented models can be used within production planning and optimization to minimize the amount of raw material needed to manufacture electrically conductive yarns, while meeting the desired parameters.

The presented procedures will also make it possible to manufacture different planar textiles (fabrics) using existing stocks of yarn and make various types of products to order.

Drawing on the proposed models, it will be possible to build new types of materials as early as the production planning stage, or modify, in real time, the production process at the mass production stage.

Such an approach will enable the automation of textile manufacturing as we know it and will reduce human labour intensity, thus increasing production efficiency.

As well, the added value of the production technologies currently in use, which is very low, will increase. System-wise, the application of the proposed models will make it possible to apply the Industry 4.0 philosophy in the industrial production of electrically conductive technical textiles thanks to, among other things, the ability to modify, in real time, the parameters of the material produced.

In the second area, new types of applications of the materials produced with the aid of the proposed models will be devised. Selected results have already been exploited in a joint project of FEE CTU and HE3DA s.r.o. focused on the development of new types of electrode materials for lithium batteries.

The results can also be applied in developing new types of textile sensors using existing textile materials or materials fabricated with the aid of the proposed models. These ideas are being explored in joint research projects with the companies Nyklíček a spol. s.r.o. Nové Město nad Metují and VÚB, a.s. Ústí nad Orlicí currently in preparation.

The experiments undertaken have indicated a possibility to use these new types of materials in healthcare, as evidenced by interest from the company PROMA REHA, s.r.o. Česká Skalice.

As an alternative electromagnetic shielding technology, conductive textiles can be used to reduce the weight and amount of non-ferrous metals in power and communication cables.

These materials will find use as functional electromagnetic shielding elements in many industrial sectors. Promising areas, aside from electronics and communications technologies, include aviation and aerospace engineering where performance parameters (electrical conductivity and electromagnetic shielding efficiency) need to be matched by low weight. It is precisely the low weight, which is achieved while meeting the desired electrical parameters that can play an important role in the future development of new and promising textile applications.

Only the future, and whether we succeed in exploiting the presented models through original approaches, will tell how realistic these expectations were.

8. List of research project

- VOJTĚCH, L.: NANOTROTEX - Composite nanostructured electrode materials with textile matrix 2018-2021, FV30171
- VOJTĚCH, L.: Auto-id technology and the internet of things to enhance the quality of health services 2017 - 2020, LTE117005, EUREKA
- VOJTĚCH, L.: The Multichannel Communication Platform for the Internet of Things (IoT) 2017 - 2019, TH02010568
- VOJTĚCH, L.: Security in Internet of Things and Industry 4.0 2016 - 2017, SGS16/159/OHK3/2T/13
- VOJTĚCH, L.: RFID Technology in Logistic Networks of Automotive Industry 2013-2016, LF13005, EUREKA
- VOJTĚCH, L.: RFID locator 2013-2015, VG20132015125
- VOJTĚCH, L.: KOMPOZITEX - Composite Textile Materials for Protection of Humans and Devices Against the Effects of Electromagnetic and Electrostatic Fields2012-2015, FR-TI4/202
- VOJTĚCH, L.: BE-TEX Humans and Equipment Protection Against High-frequency Electromagnetic Radiation - Research and Development of New Textiles. MPO-IMPULS, 2008-2010, FI-IM5/202

9. Summarized list of the applicant published papers

- VOJTĚCH, L. a NERUDA, M. Design of Radiofrequency Protective Clothing Containing Silver Nanoparticles [online]. Fibres & Textiles in Eastern Europe. 2013, 21(5), s. 141-147. ISSN 1230-3666. Available: http://www.fibtex.lodz.pl/article1002.html

- NERUDA, M. a VOJTĚCH, L. Modelling of Conductive Textile Materials for Shielding Purposes and RFID Textile Antennas. Elektronika ir Elektrotechnika. 2014, 20(8), s. 63-67. ISSN 1392-1215.

- NERUDA, M. a VOJTĚCH, L. Verification of Surface Conductance Model of Textile Materials [online]. Journal of Applied Research and Technology. 2012, 10(4), s. 579-585. ISSN 1665-6423.

- VOJTĚCH, L., et al. Monometallic Textile Electrodes for "Green" Batteries. Elektronika ir Elektrotechnika. 2014, 20(9), s. 25-28. ISSN 1392-1215. Available: http://www.eejournal.ktu.lt/index.php/elt/article/view/8434

- KYPUS, L. a VOJTĚCH, L. Comparative Method for Indirect Sensitivity Measurement of UHF RFID Reader with Respect to Interoperability and Conformance Requirements. Advances in Electrical and Electronic Engineering. 2014, 12(4), s. 319-324. ISSN 1336-1376. Available: http://advances.utc.sk/index.php/AEEE/article/view/1211/991

- VOJTĚCH, L. a NERUDA, M. Modelling of Surface and Bulk Resistance for Wearable Textile Antenna Design. Przeglad Elektrotechniczny. 2013, 89(2b/2013), s. 217-222. ISSN 0033-2097. Available: http://pe.org.pl/articles/2013/2b/54.pdf

- DAHAL, R., et al. Textile Antenna for 50 Ohm Applications. Advances in Electrical and Electronic Engineering. 2012, 10.(4), s. 229-234. ISSN 1336-1376. Available: http://advances.utc.sk/index.php/AEEE/article/view/725

- VOJTĚCH, L., et al. GNSS/RFID Active Transponder Design. Advances in Electrical and Electronic Engineering. 2015, 13(5), s. 484-490. ISSN 1336-1376. Available: http://advances.utc.sk/index.php/AEEE/article/view/1384

- VOJTĚCH, L., et al. Wearable Textile Electrodes for ECG Measurement. Advances in Electrical and Electronic Engineering. 2013, 11(5), s. 410-414. ISSN 1336-1376. Available: http://advances.utc.sk/index.php/AEEE/article/view/889

- LOPEZ, A., VOJTĚCH, L., a NERUDA, M. Comparison Among Models to Estimate the Shielding Effectiveness Applied to Conductive Textiles. Advances in Electrical and Electronic Engineering. 2013, 11(5), s. 387-391. ISSN 1336-1376. Available: http://advances.utc.sk/index.php/AEEE/article/view/902

- KVARDA, L., et al. Software Implementation of a Secure Firmware Update Solution in an IOT Context. Advances in Electrical and Electronic Engineering. 2016, 14(4), s. 389-396. ISSN 1336-1376. Available: http://advances.utc.sk/index.php/AEEE/article/view/1858

- VALENTINE, G., VOJTĚCH, L., a NERUDA, M. Design of Solar Harvested Semi Active RFID Transponder with Supercapacitor Storage. Advances in Electrical and Electronic Engineering. 2015, 13(4), s. 344-349. ISSN 1336-1376. Available: http://advances.uniza.sk/index.php/AEEE/article/view/1485/1090

- KYPUS, L., et al. RFID Platform as a Service, Containerized Ecosystem, Feasibility and Security Impact Analysis. Advances in Electrical and Electronic Engineering. 2015, 13(5), s. 502-507. ISSN 1336-1376. Available: http://advances.utc.sk/index.php/AEEE/article/view/1499

- STASA, P, et al. Ensuring the Visibility and Traceability of Items Through Logistics Chain of Automotive Industry Based on AutoEPCNet Usage. Advances in Electrical and Electronic Engineering. 2016, 14(4), s. 378-388. ISSN 1336-1376.

- NERUDA, M. a VOJTĚCH, L. Heating Ability of Electrically Conductive Textile Materials. In: BŘEZINA, T., MAGA, D., a ŠTEFEK, A., eds. 16th Mechatronika 2014. Mechatronika. Brno, 03.12.2014 - 05.12.2014. Brno: Brno University of Technology. 2014, s. 631-634. ISBN 978-80-214-4816-2.

- PARTILA, P., et al. Impact of Human Emotions on Physiological Characteristics [online]. In: Proceedings of SPIE, Volume 9118. Independent Component Analyses, Compressive Sampling, Wavelets, Neural Net, Biosystems, and Nanoengineering XII. Batlimore, 05.05.2014. Washington: SPIE. 2014, Proceedings of SPIE. ISSN 0277-786X. ISBN 9781628410556. Available: http://proceedings.spiedigitallibrary.org/proceeding.aspx?articleid=1876157

- VOJTĚCH, L., et al. Quality of Service and Experience – Business Driven Standardisation for Interoperability in Internet of Things. In: VODRÁŽKA, J. a NEVOSAD, M., eds. RTT 2014 Conference Proceedings. 16th International Conference on Research in Telecommunication Technologies. Frymburk, 10.09.2014 - 12.09.2014. Praha: Czech Technical University in Prague. 2014, s. 66-70. ISBN 978-80-01-05540-3.

- KYPUS, L., VOJTĚCH, L., a HRAD, J. Security of ONS Service For Applications of the Internet of Things and Their Pilot Implementation in Academic Network. In: VÁSÁRHELYI, J., et al., eds. Proceedings of the 16th International Carpathian Control Conference (ICCC). 16th International Carpathian Control Conference. Szilvásvárad, 27.05.2015 - 30.05.2015. Piscataway: IEEE. 2015, s. 271-276. ISBN 978-1-4799-7370-5.

- VOJTĚCH, L., et al. Outdoor Localization Technique Using Active RFID Technology Aimed for Security and Disaster Management Applications. In:

VÁSÁRHELYI, J., et al., eds. Proceedings of the 16th International Carpathian Control Conference (ICCC). 16th International Carpathian Control Conference. Szilvásvárad, 27.05.2015 - 30.05.2015. Piscataway: IEEE. 2015, s. 586-589. ISBN 978-1-4799-7370-5. Available: http://ieeexplore.ieee.org/xpls/abs_all.jsp?arnumber=7145148

- NERUDA, M., et al. Application of Shielding Textile Materials in Electric Vehicles. In: 2015 24th Wireless and Optical Communication Conference (WOCC). 24th Wireless and Optical Communication Conference. Taipei, 23.10.2015 - 24.10.2015. Piscataway: IEEE. 2015, s. 113-117. ISSN 2379-1268. ISBN 978-1-4799-8854-9. Available: http://ieeexplore.ieee.org/stamp/stamp.jsp?tp=&arnumber=7346188

- VOJTĚCH, L., et al. Design of RFID Outdoor Localization System - RFID Locator for Disaster Management. In: 5th International Conference on Internet of Things - Conference Proceedings. 5th International Conference on the Internet of Things. Seoul, 26.10.2015 - 28.10.2015. Piscataway: IEEE. 2015, s. 4-11. ISBN 978-1-4673-8056-0. Available: http://ieeexplore.ieee.org/xpls/abs_all.jsp?arnumber=7356542

- VOJTĚCH, L., et al. UHF RFID Tag Design for Disaster Management. In: 38th International Conference on Telecommunications and Signal Processing. 38th International Conference on Telecommunications and Signal Processing. Prague, 09.07.2015 - 11.07.2015. Piscataway: IEEE. 2015, s. 168-171. ISSN 1805-5435. ISBN 978-1-4799-8498-5. Available: http://ieeexplore.ieee.org/xpls/abs_all.jsp?arnumber=7296245

- KYPUS, L., VOJTĚCH, L., a KVARDA, L. Qualitative And Security Parameters Inside Middleware Centric Heterogeneous RFID/IoT Networks, On-Tag Approach. In: 38th International Conference on Telecommunications and Signal Processing. 38th International Conference on Telecommunications and Signal Processing. Prague, 09.07.2015 - 11.07.2015. Piscataway: IEEE. 2015, s. 21-25. ISSN 1805-5435. ISBN 978-1-4799-8498-5.

- GREGORA, L., VOJTĚCH, L., a NERUDA, M. Indoor Signal Propagation of LoRa Technology. In: MAGA, D., ŠTEFEK, A., a BŘEZINA, T., eds. Proceedings of the 2016 17th International Conference on Mechatronics - Mechatronika (ME) 2016. Mechatronika. Praha, 07.12.2016 - 09.12.2016. Prague: Czech Technical University in Prague, Faculty of Electrical Engineering. 2016, s. 476-479. ISBN 978-80-01-05883-1.

- KRUPKA, L., VOJTĚCH, L., a NERUDA, M. The Issue of LPWAN Technology Coexistence in IoT Environment. In: MAGA, D., ŠTEFEK, A., a BŘEZINA, T., eds. Proceedings of the 2016 17th International Conference on Mechatronics - Mechatronika (ME) 2016. Mechatronika. Praha, 07.12.2016 - 09.12.2016. Prague: Czech Technical University in Prague, Faculty of Electrical Engineering. 2016, s. 480-487. ISBN 978-80-01-05883-1.

- ZITTA, T., NERUDA, M., a VOJTĚCH, L. Mobile Application for Controlling UHF RFID Reader. In: ŠTEFEK, A., MAGA, D., a BŘEZINA, T., eds.

Proceedings of the 2016 17th International Conference on Mechatronics - Mechatronika (ME) 2016. Mechatronika. Praha, 07.12.2016 - 09.12.2016. Prague: Czech Technical University in Prague, Faculty of Electrical Engineering. 2016, s. 471-475. ISBN 978-80-01-05883-1.

- VOJTĚCH, L., et al. DoA Outdoor RFID Locator - System Verification Report. In: Proceedings of the 2016 International Symposium on Information Theory and Its Applications (ISITA). 2016 International Symposium on Information Theory and Its Applications (ISITA). Monterey, California, USA, 30.10.2016 - 02.11.2016. IEEE (Institute of Electrical and Electronics Engineers). 2016, s. 772-776. ISBN 9781509019175.

- VOJTĚCH, L., et al. Solar and Wireless Energy Harvesting Semi-active UHF RFID Tag Design and Prototyping. In: ŠTEFEK, A., BŘEZINA, T., a MAGA, D., eds. 16th Mechatronika 2014. Mechatronika. Brno, 03.12.2014 - 05.12.2014. Brno: Brno University of Technology. 2014, s. 188-193. ISBN 978-80-214-4816-2.

- SVUB, J., et al. Radio Frequency Identification of Metal Objects and RF Transparent Containers Filled Up with Liquids. In: Proceedings of International Symposium on Earth Science and Technology 2013. International Symposium on Earth Science and Technology 2013. Fukuoka, 03.12.2013 - 04.12.2013. Kyoto: Kyoto University. 2013, s. 139-142. ISBN 978-4-9902356-2-8.

- NERUDA, M., et al. Control Procedure of Emergency Calls for Femtocells. In: KŘIVÁNEK, V. a ŠTEFEK, A., eds. ICMT'13 - Proceedings of the International Conference on Military Technologies. International Conference on Military Technologies. Brno, 22.05.2013 - 23.05.2013. Brno: Univerzita obrany. 2013, s. 1331-1338. ISBN 978-80-7231-917-6.

- VOJTĚCH, L., et al. Embedded System with RFID Technology and Inductive Proximity Sensor. In: HERENCSÁR, N. a MOLNÁR, K., eds. 36th International Conference on Telecommunications and Signal Processing. 36th International Conference on Telecommunications and Signal Processing. Rome, 02.07.2013 - 04.07.2013. Piscataway: IEEE. 2013, s. 213-217. ISSN 1805-5435. ISBN 978-1-4799-0404-4.

- KOCUR, Z., et al. Measurement of Mobile Communication Devices on the Testing Railway Ring. In: KLUČIK, S. a CHROMÝ, E., eds. 15th International Conference on Research in Telecommunication Technologies. 15th International Conference on Research in Telecommunication Technologies. Senec, 11.09.2013 - 13.09.2013. Bratislava: Slovak University of Technology in Bratislava. 2013, s. 34-37. ISBN 978-80-227-4026-5.

- NERUDA, M. a VOJTĚCH, L. Modeling of Smart Textile Materials for ESD Applications. In: BOŽEK, J. a GRGIĆ, M., eds. Proceedings ELMAR-2012. 54th International Symposium ELMAR-2012. Zadar, 12.09.2012 - 14.09.2012. Zadar: Croatian Society Electronics in Marine - ELMAR. 2012, s. 145-148. ISBN 978-953-7044-13-8.

- VOJTĚCH, L. a NERUDA, M. Self-drying Planar Textile Materials with Electrically Conductive Structures. In: MAGA, D., ŠTEFEK, A., a BŘEZINA, T., eds. Proceedings of 15th Mechatronika 2012. Mechatronika. Praha, 05.12.2012 - 07.12.2012. Praha: Czech Technical University in Prague. 2012, s. 69-73. ISBN 978-80-01-04987-7.

- MAGA, D., et al. FE Model of EM Shielding Textile Materials. In: BŘEZINA, T., MAGA, D., a ŠTEFEK, A., eds. 16th Mechatronika 2014. Mechatronika. Brno, 03.12.2014 - 05.12.2014. Brno: Brno University of Technology. 2014, s. 499-502. ISBN 978-80-214-4816-2.